Bioorganic & Medicinal Chemistry 24 (2016) 2887–2896

Contents lists available at ScienceDirect

Bioorganic & Medicinal Chemistry

journal homepage: www.elsevier.com/locate/bmc

Dihydrochelerythrine and its derivatives: Synthesis and their application as potential G-quadruplex DNA stabilizing agents

Rajesh Malhotra [a,†], Chhanda Rarhi [a,b,†], K. V. Diveshkumar [c,†], Rajib Barik [b], Ruhee D'cunha [c], Pranab Dhar [b], Mrinalkanti Kundu [b,*], Subrata Chattopadhyay [b], Subho Roy [b], Sourav Basu [b], P. I. Pradeepkumar [c,*], Saumen Hajra [d,*]

[a] Department of Chemistry, Guru Jambheshwar University of Science and Technology, Hisar, Haryana 125001, India
[b] TCG Lifesciences Pvt. Ltd., BN-7, Salt Lake, Kolkata 700091, India
[c] Department of Chemistry, Indian Institute of Technology Bombay, Mumbai 400076, India
[d] Centre of Biomedical Research, SGPGIMS Campus, Lucknow 226014, India

ARTICLE INFO

Article history:
Received 20 January 2016
Revised 25 April 2016
Accepted 28 April 2016
Available online 29 April 2016

Keywords:
Dihydrochelerythrine
6-Acetonyldihydrochelerythrine
Suzuki coupling
G-quadruplex
Anti-cancer

ABSTRACT

A convenient route was envisaged toward the synthesis of dihydrochelerythrine (**DHCHL**), **4** by intramolecular Suzuki coupling of 2-bromo-*N*-(2-bromobenzyl)-naphthalen-1-amine derivative **5** via in situ generated arylborane. This compound was converted to (±)-6-acetonyldihydrochelerythrine (**ADC**), **3** which was then resolved by chiral prep-HPLC. Efficiency of **DHCHL** for the stabilization of promoter quadruplex DNA structures and a comparison study with the parent natural alkaloid chelerythrine (**CHL**), **1** was performed. A thorough investigation was carried out to assess the quadruplex binding affinity by using various biophysical and biochemical studies and the binding mode was explained by using molecular modeling and dynamics studies. Results clearly indicate that **DHCHL** is a strong G-quadruplex stabilizer with affinity similar to that of the parent alkaloid **CHL**. Compounds **ADC** and **DHCHL** were also screened against different human cancer cell lines. Among the cancer cells, (±)-**ADC** and its enantiomers showed varied (15–48%) inhibition against human colorectal cell line HCT116 and breast cancer cell line MDA-MB-231 albeit low enantio-specificity in the inhibitory effect; whereas **DHCHL** showed 30% inhibition against A431 cell line only, suggesting the compounds are indeed cancer tissue specific.

1. Introduction

Benzo[*c*]phenanthridines are fused tetracyclic skeletons, which constitute a small class of isoquinoline alkaloids. These are widely distributed in the higher plant families and used as a traditional medicine for the treatment of fever, pain, diarrhea and cancer.[1] Among these alkaloids, **CHL** and sanguinarine **2** are the most common and have received extensive attention due to their important biological properties (Fig. 1). Sanguinarine shows the inhibition of lipoxygenase and mediates chemical defence against virus and microorganisms in plants.[2] **CHL** is known to inhibit protein kinase C and DNA topoisomerase I.[3] Since, stabilization of G-quadruplex DNAs in the genome has become an attractive strategy for anticancer drug development,[4] **CHL** was also reported to bind selectively with human telomeric DNA and RNA G-quadruplexes over duplex DNAs.[5] Recently, it was reported that **CHL** stabilizes *c-MYC* and *c-KIT* quadruplex DNAs as well.[6] Overexpression of *c-MYC* and *c-KIT* genes has been associated with numerous cancers.[7]

6-Substituted dihydro-derivatives of **CHL** are also known to exhibit important biological activities.[8] Among these, **ADC** is a natural product (Fig. 1). Significant anti-HIV activity of (±)-**ADC** (isolated from Argemone Mexicana) in H9 lymphocytes with EC_{50} of 1.77 μg/mL is reported by Chang et al.[9] During our investigation, Ferreira et al. reported **ADC** (isolated from methanol extract of Zanthoxylumcapense) as a potent inducer of apoptosis in HCT116 and SW620 colon cancers cells.[10] Most of the biological studies were done with isolated **ADC** from natural source. The aim of the present investigation is the synthesis of **DHCHL** and **ADC** via a convenient route, to investigate the G-quadruplex binding activity and anticancer studies.

Several synthetic routes to benzo[*c*]phenanthridine alkaloids have earlier been reported and most of the syntheses utilize linear approaches.[11] Recently, some elegant convergent routes are reported based on (i) intramolecular Suzuki coupling of in situ generated imines of 2-bromo-1-naphthyl amines and 2-formyl

* Corresponding authors.
E-mail addresses: mrinal.kundu@tcgls.com (M. Kundu), pradeep@chem.iitb.ac.in (P.I. Pradeepkumar), saumen.hajra@cbmr.res.in (S. Hajra).
† R.M., C.R. and K.V.D. equally contributed to this work.

http://dx.doi.org/10.1016/j.bmc.2016.04.059
0968-0896/

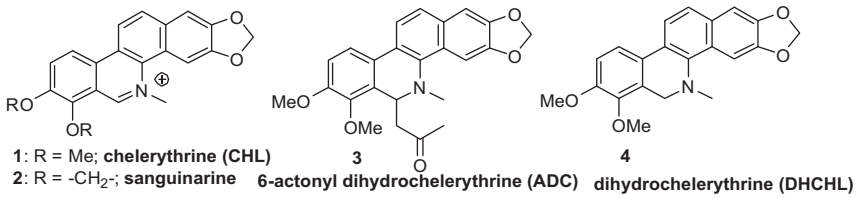

Figure 1.

arylboronic acid;[12] (ii) palladium catalyzed ring-opening coupling of azabicyclic alkenes with 2-iodobenzoates, followed by tandem cyclization;[13] (iii) nickel-catalyzed annulation of *o*-halobenzaldimine with alkyne;[14] (iv) base mediated addition-annulation of electron-rich benzaldhyde and *o*-methyl benzonitriles;[15] (v) *tert*-BuOK mediated intramolecular biaryl coupling;[16] and (vi) aryne aza-Diels–Alder reaction.[17] Herein, we report an efficient synthesis of **DHCHL** followed by (±)-**ADC** utilizing intramolecular Suzuki coupling reaction of dibromo amine **5** via in situ generated organo-borane and their application as G-quadruplex stabilizing ligands. Also, we report the anticancer activities of these compounds in different cell lines.

2. Results and discussion

2.1. Synthesis of DHCHL, CHL and ADC

Retrosynthetic analysis reveals that both **ADC** and **CHL** can be synthesized from **DHCHL**, which might be obtained by intramolecular Ullmann coupling of compound **5** or Suzuki coupling via in situ generated boronic acid, similar to Geen's approach[12] (Scheme 1). In turn, compound **5** could be obtained from 2-bromo-1-naphthyl-amine **6** and benzyl bromide **7**. 2,3-Dimethoxy-6-bromobenzyl bromide **7** was prepared from 1,2-dimethoxy benzene **8** in three steps (Scheme 2). Regioselective methylation of 1,2-dimethoxy benzene **8** via *ortho*-lithiation with *n*-BuLi in diethylether produced 1,2-dimethoxy-3-methyl benzene **9** in very good yield. Successive regioselective aromatic ring bromination of compound **9** and benzylic bromination gave 2,3-dimethoxy-6-bromobenzyl bromide **7** in good yield.

2-Bromo-1-naphthylamine **6** was prepared from tetralone **11** in five steps (Scheme 3).[12] It was achieved with bromination of tetralone **11** with bromine in $CHCl_3$ at rt and gave 2,2-dibromo tetralone **12**. Reaction of dibromide **12** with DBU in warm acetonitrile afforded the 2-bromo-1-naphthol **13**. The bromo-naphthol **13** can be transformed to 2-bromo-1-naphthyl amine **6** via Smiles rearrangement.[18] For this purpose, ether **14** was prepared from bromonaphthol **13** on alkylation with 2-bromo-2-methyl propanamide and sodium hydroxide in DMPU and gave ether **14** in 81% yields. It underwent smooth Smiles rearrangement on heating with NaH in DMF–DMPU (4:1) at 100 °C and gave *N*-acyl-2-bromo-1-naphthyl amine **15** in very good yield. Alkaline hydrolysis of compound **15** on prolong heating in 80% sodium hydroxide in aqueous methanol yielded 6-bromo-2,3-methylenedioxy-5-naphthyl amine **6**.

N-Benzylation of bromonaphthyl amine **6** with 6-bromo-2,3-dimetnoxybenzyl bromide **7** in presence of NaH in DMF gave desired compound **16** (Scheme 4). Weaker bases like DIPEA and K_2CO_3 with or without TBAI showed traces of product. Attempt was made for the Ullman coupling of the dibromo amine **16** and its *N*-methyl derivative **5**. But, both did not give any desired Ullman product under different reaction conditions.[19] Then dibromo-substrate **5** was subjected to Pd-catalyzed cyclization in presence of bispinacolatodiborane, where it was presumed that one of the arene bromides would be transformed to arylborane

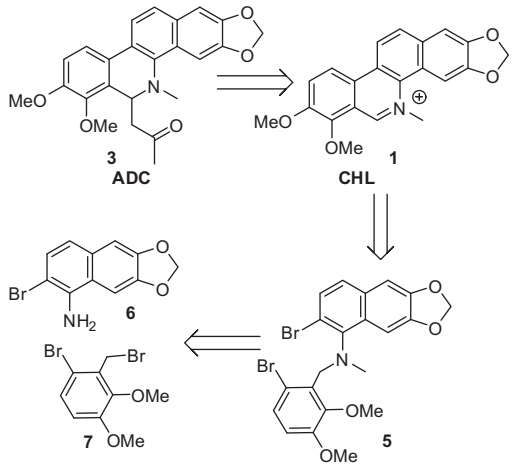

Scheme 1. Retrosynthesis of **DHCHL**, **CHL** and **ADC**.

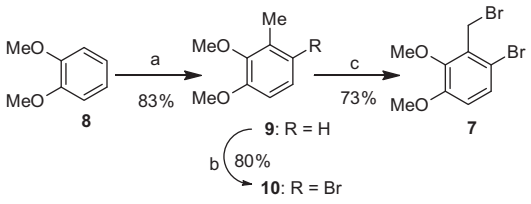

Scheme 2. Reagents & conditions: (a) *n*-BuLi, Me_2SO_4, Et_2O, 40 °C, 6 h; (b) NBS, CH_3CN, rt, 24 h; (c) NBS, AIBN, CH_3CO_2Et, reflux, 16 h.

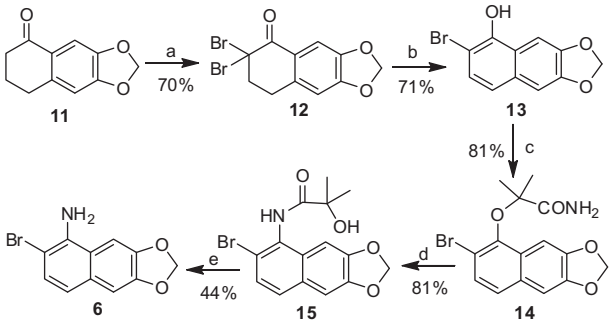

Scheme 3. Reagents & conditions: (a) Br_2, $CHCl_3$, rt; (b) DBU, CH_3CN, 45 °C, 30 min; (c) $Me_2CBrCONH_2$, NaOH, DMPU, rt, 5 h; (d) NaH, DMF–DMPU (4:1), 100 °C, 2 h; (e) 80% aq NaOH, MeOH, reflux, 2 d.

and subsequently undergoes intramolecular Suzuki coupling. We delighted to report that it provided desired **DHCHL** in 79% of yield. **DHCHL** on refluxing with iodine and sodium acetate in ethanol afforded **CHL**. Acetonylation of **CHL** on refluxing in aqueous acetone in the presence of sodium carbonate accomplished the synthesis of **ADC**. The racemic compound **ADC** was then resolved with >99% ee by chiral prep-HPLC using Chiralpak AD-H column.

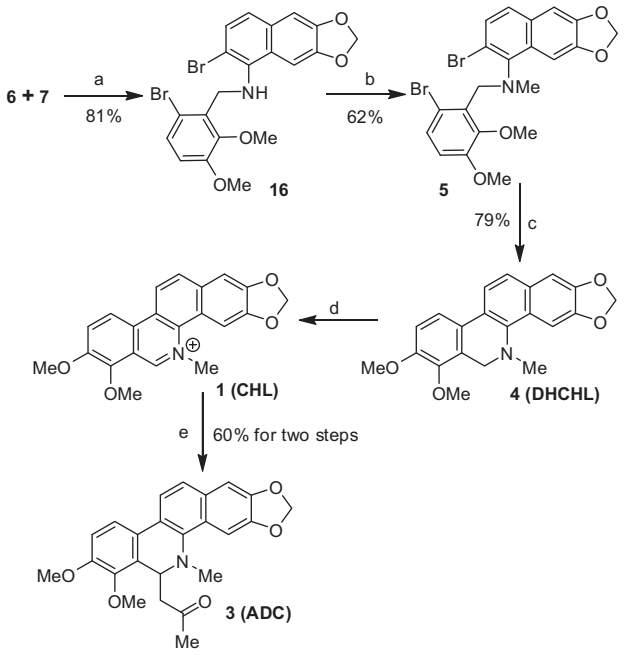

Scheme 4. Reagents & conditions: (a) NaH, DMF, 0 °C to rt, 5 h; (b) NaH, MeI, DMF, 0 °C to rt, 5 h; (c) $Pd(dppf)_2Cl_2$, BPDB, KOAc, DMSO, 110 °C, 16 h; (d) I_2, AcONa, EtOH, 2 h, reflux; (e) CH_3COCH_3, Na_2CO_3, H_2O, reflux.

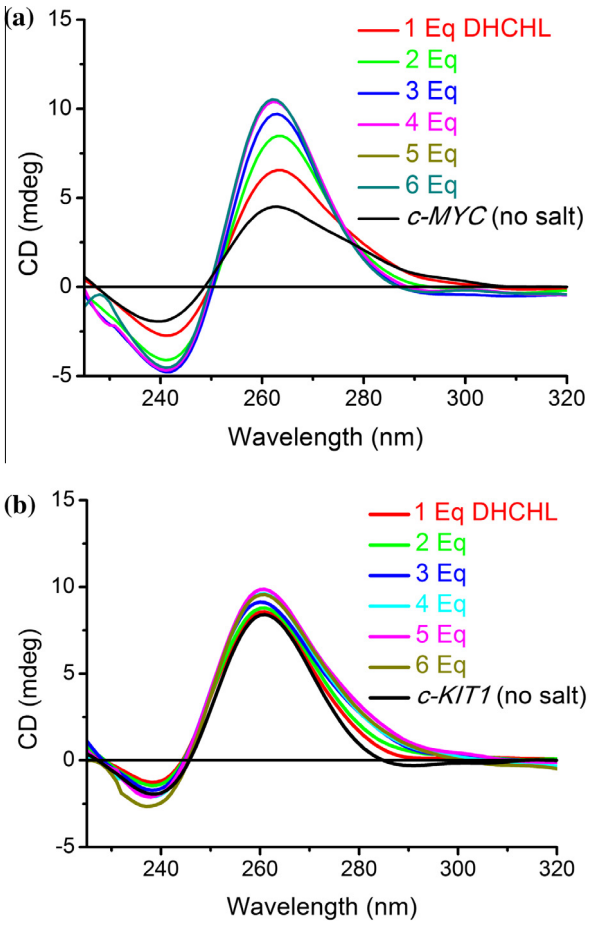

Figure 2. CD titration spectra of promoter quadruplex DNAs (12.5 μM in 50 mM Tris–HCl, pH 7.2) with compound **DHCHL**. (a) *c-MYC* DNA; (b) *c-KIT1* DNA.

2.2. Biophysical studies with promoter quadruplex DNAs

2.2.1. Circular dichroism studies (CD spectroscopy)

CD spectroscopy can be wisely used to assess the efficiency of the ligands to induce a particular topology of quadruplex DNAs. G-quadruplex structures exhibits various topologies and those can be well analyzed by using CD spectroscopy and can be confirmed with other spectroscopic techniques like NMR.[20] CD titration spectra for the natural product **CHL** with telomeric DNA were reported to show an induction of hybrid topologies under K^+ conditions.[5] We have performed CD titration experiments with promoter *c-MYC* and *c-KIT1* quadruplex DNAs which are reported to adopt parallel topologies (Fig. 2).

For the *c-MYC* DNA strong positive peak around 260 nm and a negative peak around 240 nm indicating preformed parallel topology of the quadruplex DNA was observed even in the absence of any added monovalent cations (Fig. 2). Upon titration with **DHCHL** as well as with **CHL** ellipticity for both the peaks were significantly increased and saturation was attained after the addition of 5 equiv of ligands (Figs. 2a and S1, Supporting information). Intense increase in the ellipticity clearly indicates the strong induction and stabilization of the existing preformed parallel topology for *c-MYC* quadruplex DNAs. Similarly, CD spectra of *c-KIT1* quadruplex DNA with ligands showed moderate induction of the preformed parallel topology (Figs. 2b and S1, Supporting information). CD spectra of **ADC** with *c-MYC* DNA showed weak induction of the pre-folded parallel topology of *c-MYC* DNA, whereas there was no further induction of parallel topology for *c-KIT1* DNA upon titration with **ADC** (Fig. S1, Supporting information).

2.2.2. CD melting studies

Ligand induced thermal stabilization was studied by using CD spectroscopy with *c-MYC* and *c-KIT1* promoter quadruplex DNAs. Salt and buffer conditions were adjusted according to the reported procedure to get a melting temperature in the range of 40–60 °C.[21]

Melting experiments for the promoter quadruplex DNAs were conducted by measuring the molar ellipticity at 263 nm in the presence and absence of 5 equiv of ligands. For *c-MYC* DNA, melting experiment was performed with 1 mM KCl and yielded a melting temperature of 57 °C (Fig. 3). As expected, there was a significant increase in the melting temperature with 5 equiv of ligands, $\Delta T_m \sim 24$ °C for **DHCHL** and $\Delta T_m \sim 19$ °C for **CHL**, respectively (Fig. 3a and Table 1). Similarly, melting experiment for *c-KIT1* quadruplex DNA was performed with 10 mM KCl giving a melting temperature of 46 °C. Addition of 5 equiv of ligands resulted in the increase of melting temperature of *c-KIT1* DNA, $\Delta T_m \sim 17$ °C for **DHCHL** and $\Delta T_m \sim 24$ °C for **CHL**, respectively (Fig. 3b and Table 1). For both the promoter quadruplex DNAs, very high thermal stabilization was obtained with both **CHL** and **DHCHL**. Thermal stabilization of **DHCHL** was slightly greater than the **CHL** with *c-MYC* quadruplex DNA, whereas for *c-KIT1* DNA it was found to be in the reverse order. As expected, ligands were not able to show any significant increase in the melting temperature of duplex DNA (Fig. S2, Supporting information and Table 1). Moreover, we have performed CD melting experiment for the ligand **ADC** with telomeric as well as with *c-MYC* quadruplex DNA (Fig. S2, Supporting information). Surprisingly, there was no considerable increase in the melting temperature for **ADC** with both the quadruplex DNAs ($\Delta T_m \sim 1$ °C for telomeric and $\Delta T_m \sim 2.6$ °C for *c-MYC* DNA).

2.2.3. UV–Visible absorption spectroscopic studies

Determination of binding constants of the ligands with *c-MYC* quadruplex DNA carried out by using UV–Visible absorption spectroscopy. Concentration dependent increase or decrease in the

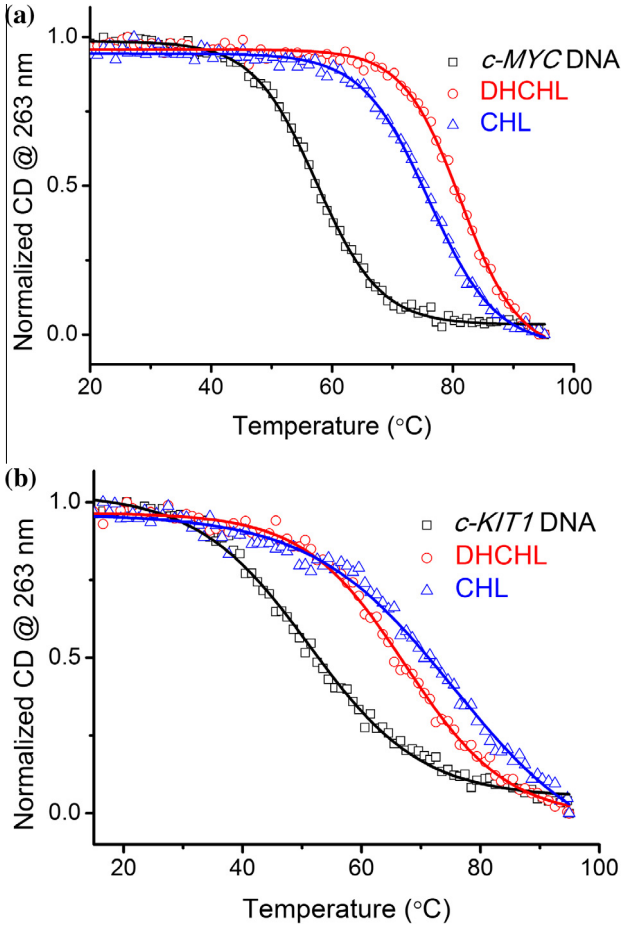

Figure 3. CD melting curves for promoter quadruplex DNAs (10 μM in 10 mM lithium cacodylate buffer, pH 7.2) with ligands. (a) *c-MYC* DNA (1 mM KCl and 99 mM LiCl); (b) *c-KIT1* DNA (10 mM KCl, 90 mM LiCl).

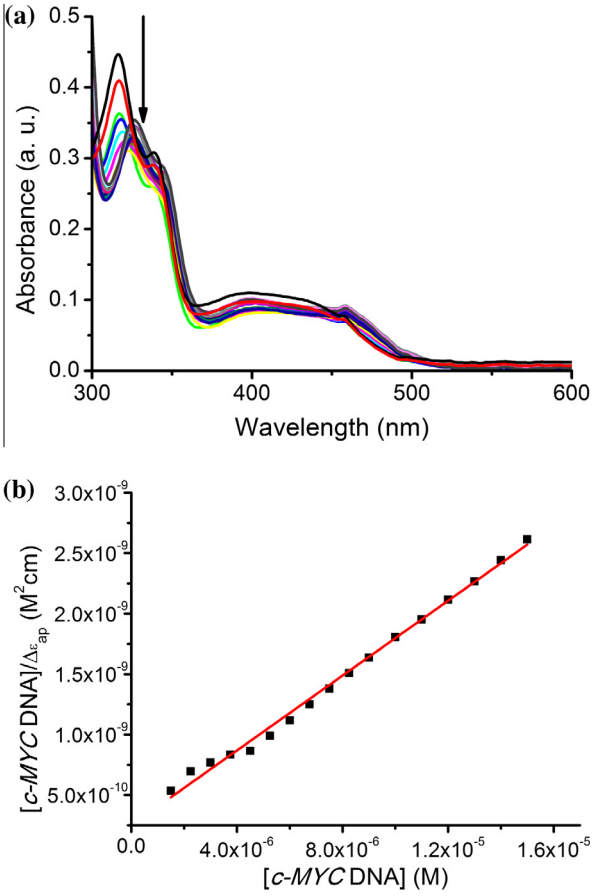

Figure 4. UV–Visible titration spectra and linear plots for **DHCHL** and *c-MYC* quadruplex DNA. Pre-annealed DNA (100 mM KCl and 10 mM lithium cacodylate buffer, pH 7.2) was titrated with **DHCHL** (30 μM in similar salt and buffer conditions) and the data was fitted using half reciprocal equation. (a) UV absorption spectrum; (b) linear fit. Binding constant values are reported as an average from 3 independent experiments.

ligand absorbance can be used to derive the binding constant for the ligand–quadruplex interaction.[22] Titration of pre-annealed *c-MYC* quadruplex DNA with ligands under identical salt and buffer conditions resulted in a decrease in the absorption intensity of the ligands (Figs. 4 and S3, Supporting information). Hypochromicity together with a red shift of 10 nm during titration is an indicative of strong interaction of both the ligands with *c-MYC* quadruplex DNA. Linear fit of the plot shown in Fig. 4b yielded binding constant values, $K = (5.5 \pm 0.7) \times 10^5\ M^{-1}$ for **DHCHL** and $K = (7.35 \pm 0) \times 10^5\ M^{-1}$ for **CHL** (Fig. 4). Binding constant values for the ligands with *c-MYC* quadruplex DNA were similar to those reported for the interaction between **CHL** with telomeric and *c-MYC* quadruplex DNAs.[6]

Table 1
Thermal stabilization of ligands with promoter quadruplex and duplex DNAs measured by CD melting experiments

Ligands	ΔT_m^a (°C)		
	c-MYC DNA	*c-KIT1* DNA	Duplex DNA
DHCHL	24.0 ± 0.2	17.6 ± 0.6	−1 ± 0.2
CHL	19.6 ± 0.9	24.3 ± 0.5	0.1 ± 0.1

ΔT_m^a denotes the difference in melting temperature [$\Delta T_m = T_m$ (DNA+5 molar equivalent ligand) − T_m (DNA)]. Melting experiments were carried out with a DNA concentration of 10 μM in 10 mM lithium cacodylate buffer, pH 7.2. T_m values in the absence of ligands are 57.1 ± 0.4 °C (*c-MYC* DNA in 1 mM KCl and 99 mM LiCl); 46 ± 0.1 °C (*c-KIT1* DNA in 10 mM KCl and LiCl 90 mM) and 63.5 ± 0.4 °C (Duplex DNA in 10 mM KCl and LiCl 90 mM). ΔT_m values are reported as the average values with standard deviations from 3 independent experiments.

2.2.4. *Taq* DNA polymerase stop assay

Efficiency of the ligands for the stabilization of promoter quadruplex DNAs were further assessed with the aid of *Taq* DNA polymerase stop assay by using *c-MYC* DNA as an example. Concentration of the ligands needed for the formation of 50% stop product is the IC_{50} value for the ligand. Extension reaction was performed at 55 °C with increasing concentration of the ligands up to 80 μM (Figs. 5a and S4, Supporting information).[23] Formation of stop products was increased in a concentration dependant manner with the ligands yielding an IC_{50} value ~5.8 μM for **DHCHL** and ~6.6 μM for **CHL**, respectively (Figs. 5b and S4, Supporting information).

Comparable IC_{50} values observed for both the ligands are in good agreement with the results obtained from the biophysical studies revealing their identical binding affinities. Control experiments were performed under identical reaction conditions and ligand concentrations using template containing mutated *c-MYC* DNA that cannot form quadruplex structure. As expected, there was no stop product with the mutated *c-MYC* DNA even after incubating with 80 μM ligand concentrations (Figs. 5a and S4, Supporting information). Absence of stop products with mutated *c-MYC* DNA confirms that the formation of stop products in the polymerase extension reaction is due to ligand induced quadruplex stabilization.

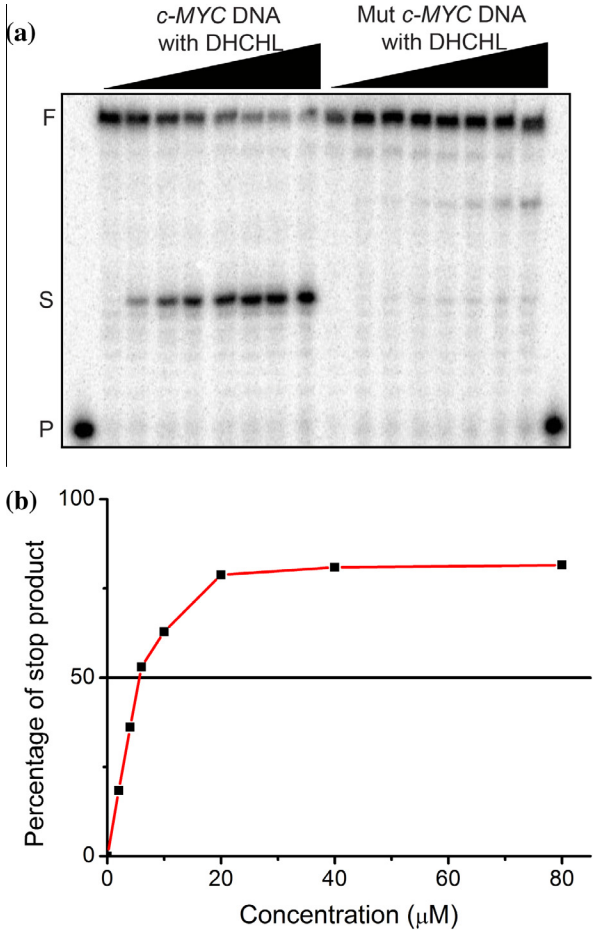

Figure 5. Denaturing PAGE (15%, 7 M urea) and plots of stop products versus ligand concentration for the *Taq* DNA polymerase stop assay in the presence of the *c-MYC* and mutated *c-MYC* DNAs. (a) Denaturing PAGE for the ligand **DHCHL** (0–80 μM) with the *c-MYC* and the mutated *c-MYC* DNA templates; (b) Plot of *Taq* DNA polymerase stop products versus **DHCHL** concentration (0–80 μM). Primer extension reaction was carried out at 55 °C. Conditions: 100 nM template, 50 nM primer, 0.2 mM dNTPs and 0.5 U of *Taq* polymerase in the enzyme buffer (50 mM Tris, 0.5 mM DTT, 0.1 mM EDTA, 5 mM $MgCl_2$, 5 mM KCl). P denotes primer, S denotes stop product and F denotes full length product. Normalized percentage of stop products in each lane was plotted against concentration of ligand. Each data points represent the average from 2 independent experiments with maximum error ⩽4%.

2.2.5. Molecular modeling and dynamics studies

To understand the binding modes and interactions of **DHCHL** with the *c-MYC* G-quadruplex DNA, molecular docking and dynamics (MD) simulations were carried out. The energy optimized structure of ligand (B3LYP/6-311+G(d,p) (Fig. S5, Supporting information) was docked with the energy-minimized structure of *c-MYC* (PDB entry: 2L7V) using AutoDock 4.2. The results showed that **DHCHL** docked on the G-quartet in the 5′ as well as the 3′-end of the DNA (2:1, **DHCHL**:G-quadruplex), which is in agreement with the binding mode of **CHL** (Fig. S6, Supporting information).[5]

MD simulations (1 μs) were carried out based on the docking results. The binding free energies were estimated over the last 100 ns of the trajectory using the MMPBSA.py module in AmberTools12 (Table S1, Supporting information). The free energy of binding (ΔG) for the 5′-ligand was −20.43 ± 4.62 kcal mol^{-1} and for the bottom ligand was −16.81 ± 5.67 kcal mol^{-1}, indicating the binding was energetically more favorable for the top ligand than the bottom one. The binding free energy for both the ligands was found to be −44.87 ± 7.63 kcal mol^{-1}. The RMSD values and Hoogsteen H-bond occupancies for the G-quartet remained stable throughout the simulation, indicating a stabilizing effect upon ligand binding (Figs. S7–S9, Supporting information). The per-residue RMSF values (Fig. S10, Supporting information) show peaks for loops and flanking nucleotides and troughs for guanines in the G-quartet, indicating that the loops and flanking residues were not as stable as the G-quartet over the course of the simulations.

Since the backbone RMSD of loops and flanking nucleotides in the G-quadruplex DNA fluctuated throughout the MD simulations (Fig. S7, Supporting information), clustering was carried out to probe the major conformations involved. The largest cluster contained 36.4% of the frames (Fig. 6), the second largest contained 26.5% (Fig. S11, Supporting information), implying that the complex fluctuated mainly between these two conformations during the course of the MD simulation. Cluster representatives 1 and 2 differ mainly in the nucleotides with which the ligands interact (Figs. 6 and S11, Supporting information). Both showed π-stacking interactions of the ligands with the top and bottom faces of the quadruplex.

The best representative structure of cluster-1 had the top ligand showing π-stacking interactions with nucleotide dG4 and dG8, and the bottom ligand's naphthalene-type ring stacking with dG10 (Fig. 6). Similarly, the best representative structure of cluster-2 had the top ligand stacking with both dG8 and dG13, while the bottom ligand stacked with dG10 via the benzene ring, and with dG15 through its naphthalene ring (Fig. S11, Supporting information). All evidence suggests that both ligands moved over the top and bottom surface of the quadruplex during the timescale of the MD simulation (Figs. S12 and S13, Supporting information).

2.3. Biological activity

2.3.1. Anti-cancer activity

Human cancer cell lines from different tissue origin namely, A431 (human epidermoid cancer), HCT116 (human colorectal cancer), MDA-MB-231 (human breast cancer), HeLa (human cervical cancer), A549 (human lung cancer) and PC-3 (human prostate cancer) [no inhibition in HeLa, A549 and PC-3; data not shown] were used to assess the anticancer potential of the compounds **DHCHL**, (±)-**ADC** and its enantiomers. Among the cancer cells, HCT116 showed significant sensitivity against the test compounds (±)-**ADC** and its enantiomers. This is in line with the earlier report[10] where the compounds showed significant inhibition against the human colorectal cell lines HCT116 and SW620. However, the observed extent of inhibition (Table 2) was less when compared to the earlier report[10] and it might be due to the different source of the compound; synthetic (in our case) *vis-a-vis* plant extract. Interestingly, **ADC** also showed 20% inhibition in the MTT assay with human breast cancer cell line MDA-MB-231 at 15 μM, while it did not show any inhibitory effect against the proliferation of the other cancer cell lines. Moreover, the compound exhibited low level of enantiospecificity in the observed inhibition against the proliferation of the cancer cells. (+)-**ADC** inhibited the proliferation of HCT116 by 47.84% at 15 μM whereas, the other enantiomer (−)-**ADC** and the racemic compound produced 36.88% and 28.73% inhibition, respectively, at the same tested concentrations. Similar pattern was observed in case of MDA-MB-231 cell line although the extent of inhibition was less. Surprisingly, compound **DHCHL** did not show any inhibition against HCT116 & MDA-MB-231 cell lines, though there was moderate inhibitory activity against A431 at 20 μM, suggesting this compound is specific to epidermoid cancer tissues. The anticancer drug doxorubicin, used as positive control, and **CHL** (commercial source, as this compound could not be isolated in pure form in our hand due to significant chemical instability as observed during synthesis) both showed consistent inhibition of more than 90% in all cell lines at a concentration of 20 μM.

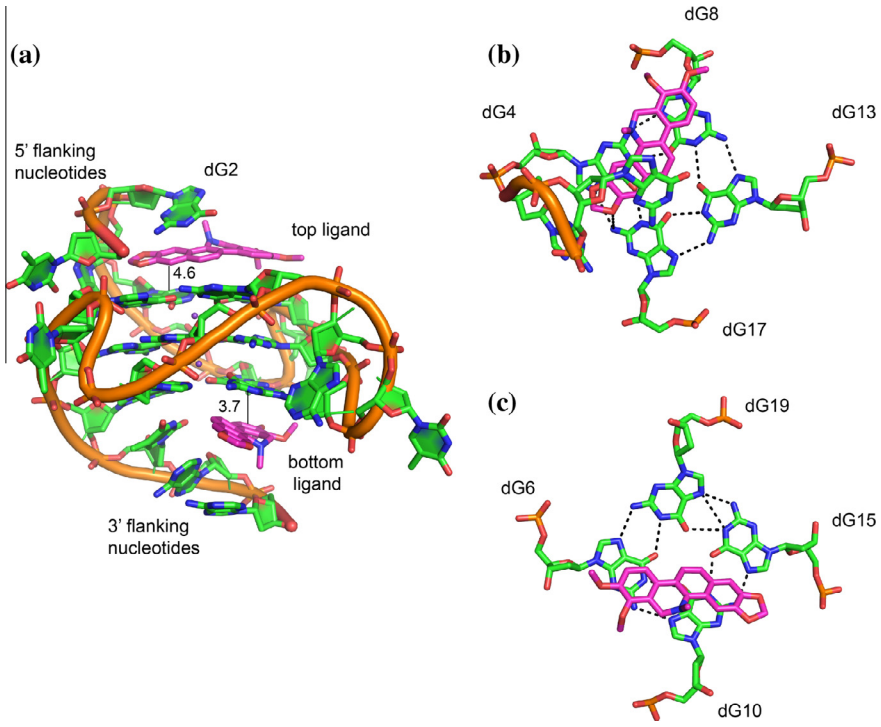

Figure 6. The best representative structure of the cluster-1 of **DHCHL** with the *c-MYC* G-quadruplex over a 1 μs MD simulations. (a) Representative figure showing π-stacking distances; (b) Top view of **DHCHL** stacking with the 5′ quartet, stacking with residues dG4 and dG8; and (c) Top view of **DHCHL** stacking with the 3′ quartet, stacking with residues dG6 and dG10. Ligands are shown in pink. DNA is shown in green. Distances are in Å. Figures are rendered using PyMOL.

Table 2
Effect of **DHCHL** and (±)-**ADC** and its enantiomers (+)-**ADC**, (−)-**ADC** against the proliferation of different cancer cell lines

Compound	Test conc. (μM)	% inhibition in HCT116	% inhibition in MDA-MB-231	% inhibition in A431
(±)-**ADC**	15.0	28.73 ± 0.43***	16.13 ± 1.51*	NA
(+)-**ADC**	15.0	47.84 ± 0.40***	24.30 ± 0.42**	NA
(−)-**ADC**	15.0	36.88 ± 0.19***	20.81 ± 1.49**	NA
DHCHL	20.0	NA	8.65 ± 0.48**	30.39 ± 6.42*
CHL[a]	20.0	100.0 ± 0.90***	100.0 ± 0.03***	100.0 ± 0.08***
Doxorubicin[b]	20.0	97.98 ± 0.29***	92.68 ± 0.44***	98.07 ± 0.08***

The results are averages ± SEM of three independent experiments; NA: not active.
[a] Commercial, purchased from Sigma–Aldrich.
[b] Positive control.
* p <0.05.
** p <0.01.
*** p <0.001 (vs vehicle control).

3. Conclusions

This study has shown that dibromo amine **5** undergo intramolecular Suzuki coupling via in situ generated aryl borane to provide **DHCHL** followed by oxidation gave **CHL**, which on acetonylation afforded the **ADC**. Biophysical and biochemical studies of **DHCHL** with promoter quadruplex DNAs (*c-MYC* and *c-KIT1*) showed the similar stabilization effect as compared to the parent alkaloid **CHL**. Moreover, the binding mode of interaction for the **DHCHL** and *c-MYC* quadruplex DNA was thoroughly investigated by using molecular dynamics and modeling studies. It was found to be well stacked using dual stacking mode by exploiting both the top and bottom quartets of the *c-MYC* quadruplex DNA. **DHCHL**, (±)-**ADC** and its enantiomers were tested across cancer cell lines from different tissue origins for their inhibitory activities on cell proliferation. (±)-**ADC** and its enantiomers showed significant inhibition of the proliferation of HCT 116 cells in the MTT assay which is in line with the earlier observation of the compound's (extracted from natural sources) effect on the colon cancer cells; whereas **DHCHL** showed moderate inhibition against A431 cell line. Importantly, no sensitivity towards the compound by other cell lines raises the possibility of any colon and skin cell specific effect of (±)-**ADC** (& its enantiomers] and **DHCHL**, respectively. Additionally, lack of inhibitory effect on the bacterial cells also rules out detergent or poison-like non-specific cell killing by the compounds [data not shown]. Overall, our results show that **DHCHL** and its derivatives can be harnessed to develop quadruplex mediated anticancer agents.

4. Experimental section

4.1. Chemistry

All reactions were conducted using oven-dried glassware under an atmosphere of argon (Ar) or nitrogen (N_2). Commercial grade reagents were used without further purification. Solvents were dried and distilled following usual protocols. Column chromatography was carried out using silica gel (100–200 mesh). TLC was performed on aluminum-backed plates coated with Silica gel 60 with F_{254} indicator. The ^{1}H NMR spectra were recorded with a 400 MHz spectrometer and ^{13}C NMR spectra were recorded with a 100 MHz using $CDCl_3$ and DMSO-d_6. ^{1}H NMR chemical shifts are expressed in parts per million (δ) relative to $CDCl_3$ (δ = 7.26) and DMSO-d_6 (δ = 2.49); ^{13}C NMR chemical shifts are expressed in parts per million (δ) relative to the $CDCl_3$ resonance (δ = 77.0) and DMSO-d_6 (δ = 39.7). High resolution mass spectra (HRMS) were measured with a QTOF I (quadrupole–hexapole TOF) mass spectrometer with an orthogonal Z-spray–electro-spray interface.

4.1.1. 1,2-Dimethoxy-3-methyl-benzene 9

To a solution of 1,2-dimethoxy-benzene **8** (15 g, 108.6 mmol) in dry ether (340 ml) was added *n*-BuLi (68 ml, 2.4 M, 163 mmol) at 0 °C. Reaction mixture was heated at reflux for 6 h; cool to room temperature, dimethyl sulfate (63 ml, 652 mmol) was added slowly to the reaction mixture and heated at reflux for 16 h. Reaction mixture was diluted with ethyl acetate and washed with saturated aq NH_4Cl, water, brine, dried over Na_2SO_4 and evaporated to get the crude which was purified by silica gel column chromatography and gave the pure compound **8** as a pale yellow liquid (13.7 g, 83%). ^{1}H NMR (DMSO-d_6, 400 MHz) δ 6.93 (t, J = 7.8 Hz, 1H), 6.84 (d, J = 7.9 Hz, 1H), 6.74 (d, J = 7.4 Hz, 1H), 3.77 (s, 3H), 3.68 (s, 3H), 2.18 (s, 3H); ^{13}C NMR (DMSO-d_6, 100 MHz): δ 152.2, 146.7, 130.9, 123.5, 122.3, 110.4, 59.2, 55.3, 15.3; GC-MS (EI): 152 m/z [M+].

4.1.2. 1-Bromo-3,4-dimethoxy-2-methyl-benzene 10

To a solution of 1,2-dimethoxy-3-methyl-benzene **9** (55 g, 361.8 mmol) in ACN (1.8 L) was added NBS (65.3 g, 369 mmol) portion wise and the mixture was stirred at rt for 24 h under nitrogen atmosphere. Reaction mixture was diluted with ethyl acetate and washed with sat. aq $NaHCO_3$, water and dried over Na_2SO_4. Concentration of the solvent and recrystallization from MeOH gave the pure product as white solid (67 g, 80%). ^{1}H NMR ($CDCl_3$, 400 MHz) δ 7.22 (d, J = 8.8 Hz, 1H), 6.64 (d, J = 8.8 Hz, 1H), 3.82 (s, 3H), 3.76 (s, 3H), 2.32 (s, 3H). ^{13}C NMR ($CDCl_3$, 100 MHz): δ 152.1, 148.0, 132.2, 127.2, 116.0, 110.9, 60.3, 55.8, 16.0; GC-MS: 230, 230 m/z [M+].

4.1.3. 1-Bromo-2-bromomethyl-3,4-dimethoxy-benzene 7

A solution of 1-bromo-3,4-dimethoxy-2-methyl-benzene **10** (4.8 g, 20.86 mmol), NBS (3.7 g, 20.89 mmol) and AIBN (680 mg) in ethyl acetate (265 ml) was heated overnight at reflux. After filtration and evaporation of the solvent, the residue was dissolved in CH_2Cl_2, washed with sat. aq $NaHCO_3$, water, dried over Na_2SO_4, and evaporated in vacuum to afford white solid (4.7 g, 73.4%) which was pure enough for further use. ^{1}H NMR ($CDCl_3$, 400 MHz) δ 7.26 (d, J = 9.4 Hz, 1H), 6.76 (d, J = 8.8 Hz, 1H), 4.69 (s, 2H), 3.96 (s, 3H), 3.84 (s, 3H); ^{13}C NMR ($CDCl_3$, 100 MHz): δ 152.2, 148.6, 131.5, 127.9, 115.2, 113.8, 61.0, 55.9, 28.0; GC-MS (EI) 310 m/z [M+].

4.1.4. 6,6-Dibromo-7,8-dihydro-6*H*-naphtho[2,3-*d*][1,3]dioxol-5-one 12

A solution of bromine (2.1 ml, 43.1 mmol) in $CHCl_3$ (10 ml) was added drop wise to a stirred solution of 7,8-dihydro-6*H*-naphtho [2,3-*d*][1,3]dioxol-5-one **11** (3.9 g, 20.5 mmol) in $CHCl_3$ (25 ml). The resulting mixture was stirred at ambient temperature overnight. Reaction mixture was quenched with water and extracted with ethyl acetate, dried over Na_2SO_4 and concentrated in vacuum to afford crude compound 6,6-dibromo-7,8-dihydro-6*H* naphtho [2,3-*d*][1,3]dioxol-5-one **12** as a yellow liquid (5 g, 70%), which was used in the following step without further purification. ^{1}H NMR ($CDCl_3$, 400 MHz) δ 7.52 (s, 1H), 6.63 (s, 1H), 6.02 (s, 2H), 3.00 (s, 4H); ^{13}C NMR ($CDCl_3$, 100 MHz): δ 182.9, 153.2, 147.7, 139.4, 121.6, 108.2, 107.6, 102.0, 67.0, 46.0, 29.5; LC–MS (ESI): 348.8 $[M+H]^+$, 366 $[M+NH_4]^+$.

4.1.5. Bromo-naphtho[2,3-*d*][1,3]dioxol-5-ol 13

6,6-Dibromo-7,8-dihydro-6*H*-naphtho[2,3-*d*][1,3]dioxol-5-one **12** (5 g, 14.36 mmol) was stirred in acetonitrile (90 ml) at 40 °C for 15 min. DBU (3.2 ml, 21.55 mmol) was added and the resulting solution was stirred at 40–45 °C for 20 min. After cooling to room temperature, 1 M HCl was added. The reaction mass was extracted with DCM and combined organic phase was washed with water, dried over Na_2SO_4 and evaporated in vacuum to give the crude product which was purified by silica gel column chromatography to get pure compound 6-bromo-naphtho[2,3-*d*][1,3]dioxol-5-ol **13** (2.7 g, 71%). ^{1}H NMR (DMSO-d_6, 400 MHz) δ 9.60 (s, 1H), 7.50 (s, 1H), 7.36 (d, J = 8.7 Hz, 1H), 7.26 (s, 1H), 7.19 (d, J = 8.7 Hz, 1H), 6.13 (s, 2H); ^{13}C NMR (DMSO-d_6, 100 MHz): δ 148.5, 147.6, 147.4, 130.5, 127.8, 122.4, 120.0, 103.9, 103.7, 101.3, 98.4; LC–MS (ESI): 267.0 $[M+H]^+$.

4.1.6. 2-(6-Bromo-naphtho[2,3-*d*][1,3]dioxol-5-yloxy)-2-methyl-propionamide 14

Sodium hydroxide (2.2 g, 56.1 mmol, powder) was added to a solution of the 6-bromo-naphtho[2,3-*d*][1,3]dioxol-5-ol **13** (2.5 g, 9.36 mmol) in DMPU (22 ml) at rt and the resulting mixture was stirred for 15 min. 2-Bromo-2-methylpropanamide (4.6 g, 28.08 mmol) was added and the mixture was stirred vigorously for 5 h at rt. Water was added to the reaction mixture and acidified with 5 M HCl to adjust the pH to neutral. Resulting suspension was added to water and allowed to stand overnight. The solid was filtered, washed with water and dried under vacuum at 60 °C to give pure product as an off-white solid (2.7 g, 81%). ^{1}H NMR ($CDCl_3$, 400 MHz) δ 7.44–7.40 (m, 2H), 7.30 (d, J = 8.6 Hz, 1H), 7.15 (br s, 1H), 7.06 (s, 1H), 6.05 (s, 2H), 1.60 (s, 6H); ^{13}C NMR (DMSO-d_6, 100 MHz): δ 175.8, 148.2, 147.6, 130.7, 128.2, 128.1, 124.7, 113.7, 103.7, 101.6, 99.3, 84.7, 25.2; LC–MS (ESI): 352.2 $[M+H]^+$.

4.1.7. *N*-(6-Bromo-naphtho[2,3-*d*][1,3]dioxol-5-yl)-2-hydroxy-2-methyl-propionamide 15

Sodium hydride (0.422 g, 10.73 mmol) was added to a solution of the 2-(6-bromo-naphtho[2,3-*d*][1,3]dioxol-5-yloxy)-2-methyl-propionamide **14** (3.1 g, 8.80 mmol) in dry DMF (60 ml) and DMPU (15 ml). Resulting mixture was stirred at 100 °C for 2 h. The solution was then poured into water and extracted with ethyl acetate. Organic layer was washed with water, dried over Na_2SO_4, and concentrated. Crude obtained was purified by silica gel column chromatography to get pure compound *N*-(6-bromo-naphtho[2,3-*d*] [1,3]dioxol-5-yl)-2-hydroxy-2-methyl-propionamide **15** as a white solid (2.6 g, 83%). ^{1}H NMR (DMSO-d_6, 400 MHz) δ 9.60 (s, 1H), 7.63 (d, J = 8.7 Hz, 1H), 7.54 (d, J = 8.7 Hz, 1H), 7.37 (s, 1H), 7.17 (s, 1H), 6.15 (s, 2H), 5.71 (s, 1H), 1.43 (s, 6H). ^{13}C NMR (DMSO-d_6, 100 MHz): δ 175.8, 148.4, 147.6, 132.1, 129.8, 129.4, 127.5, 127.3, 118.9, 103.6, 101.5, 100.0, 72.4, 27.6; LC–MS (ESI): 354.0 $[M+H]^+$.

4.1.8. 6-Bromo-naphtho[2,3-*d*][1,3]dioxol-5-ylamine 6

Sodium hydroxide (21.2 g, 530.6 mmol) in H_2O (52 ml) was added to a solution of the *N*-(6-bromo-naphtho[2,3-*d*][1,3]dioxol-5-yl)-2-hydroxy-2-methyl-propionamide **15** (2.6 g, 6.63 mmol) in methanol (26 ml), and the resulting mixture was refluxed for 2 days. After cooling, water and ethyl acetate were added. The phases were separated and the aqueous phase was extracted with ethyl acetate. The combined organic layer was washed with water, dried over Na_2SO_4, and concentrated. Crude obtained was purified by silica gel column chromatography to get pure compound 6-bromo-naphtho[2,3-*d*][1,3]dioxol-5-ylamine **6** as a white solid (0.78 g, 44%). ^{1}H NMR (DMSO-d_6, 400 MHz) δ 7.62 (s, 1H), 7.26 (d, J = 8.6 Hz, 1H), 7.18 (s, 1H), 6.91 (d, J = 8.7 Hz, 1H), 6.10 (s, 2H), 5.61 (s, 2H)′; ^{13}C NMR (DMSO-d_6, 100 MHz): δ 147.1, 146.9, 140.3, 130.1, 127.9, 119.2, 116.5, 103.9, 101.1, 100.9, 99.4; LC–MS (ESI): 265.9 $[M+H]^+$.

4.1.9. 6-bromo-*N*-(6-bromo-2,3-dimethoxybenzyl)naphtho[2,3-*d*][1,3]dioxol-5-amine 16

Sodium hydride (0.164 g, 3.75 mmol) was added to a solution of 6-bromo-naphtho[2,3-*d*][1,3]dioxol-5-ylamine **6** (0.5 g, 1.87 mmol) in dry DMF (6 ml) at 0 °C and stirred at that temp for 30 min. Compound **7** (0.87 g, 2.81 mmol) was added to the reaction mixture at 0 °C and reaction mixture was then allowed to warm to

ambient temperature and stirred for 1 h. The solution was then poured into ice water and extracted with ethyl acetate. Organic layer was washed with water, dried over Na_2SO_4, filtered and concentrated. Crude compound was purified by silica gel column chromatography to get pure compound 6-bromo-*N*-(6-bromo-2,3-dimethoxybenzyl)naphtho[2,3-*d*][1,3]dioxol-5-amine **16** as an off-white solid (0.75 g, 81%). ^{1}H NMR (DMSO-d_6, 400 MHz) δ 7.69 (s, 1H), 7.43–7.29 (m, 4H), 6.97 (d, J = 8.8 Hz, 1H), 6.16 (s, 2H), 4.43–4.33 (m, 3H), 3.79 (s, 3H), 3.49 (s, 3H); ^{13}C NMR (DMSO-d_6, 100 MHz): δ 151.8, 148.2, 147.8, 147.4,141.2, 131.8, 130.6, 127.4, 127.3, 126.0, 123.4, 114.4, 113.9, 112.8, 104.0, 101.4, 100.2, 60.1, 55.8, 47.7; LC–MS (ESI): 495.9 [M+H]$^+$. HRMS (ESI): calcd for $C_{20}H_{17}Br_2NO_4$ 495.9624 m/z [M+H]$^+$, found 495.9624.

4.1.10. 6-bromo-*N*-(6-bromo-2,3-dimethoxybenzyl)-*N*-methylnaphtho[2,3-*d*][1,3]dioxol-5-amine 5

Sodium hydride (0.132 g, 3.03 mmol) was added to a solution of the 6-bromo-*N*-(6-bromo-2,3-dimethoxybenzyl)naphtho[2,3-*d*][1,3]dioxol-5-amine **16** (0.5 g, 1.01 mmol) in dry DMF (26 ml) at 0 °C and stirred at that temp for 30 min. CH_3I (0.26 ml, 4.04 mmol) was added to the reaction mixture at 0 °C and temperature was slowly raised to room temperature, stirred at rt for 5 h. The solution was then poured into ice water and extracted with ethyl acetate. The organic layer was washed with water, dried over Na_2SO_4 and concentrated. Crude compound was purified by silica gel column chromatography to get pure compound 6-bromo-*N*-(6-bromo-2,3-dimethoxybenzyl)-*N*-methylnaphtho[2,3-*d*][1,3]-dioxol-5-amine **5** (0.320 g, 62%). ^{1}H NMR ($CDCl_3$, 400 MHz) δ 7.59 (s, 1H), 7.42 (d, J = 8.7 Hz, 1H), 7.29 (d, J = 8.7 Hz, 1H), 7.22 (d, J = 8.7 Hz, 1H), 6.99 (s, 1H), 6.67 (d, J = 8.7 Hz, 1H), 5.99 (d, J = 8.7 Hz, 2H), 4.57 (q, J = 12.9 Hz, 2H), 3.79 (s, 3H), 3.61 (s, 3H), 2.95 (s, 3H); ^{13}C NMR ($CDCl_3$, 100 MHz): δ 151.9, 149.0, 148.1, 147.6, 145.8, 133.0, 132.3, 130.6, 129.6, 127.6, 125.8, 119.2, 116.9, 112.6, 103.5, 102.2, 100.9, 60.8, 55.9, 52.6, 40.9; LC–MS (ESI): 509.9 [M+H]$^+$. HRMS (ESI): calcd for $C_{21}H_{19}Br_2NO_4$ 531.9602 m/z [M+Na]$^+$, found 531.9602.

4.1.11. 1,2-Dimethoxy-12-methyl-12,13-dihydro-[1,3]dioxolo-[4′,5′:4,5]benzo[1,2-*c*]phenanthridine 4

To a degassed solution of DMSO (degassed by argon, 3.5 ml/mmol) were added 6-bromo-2,3-dimethoxy-benzyl)-(6-bromo-naphtho[2,3-*d*][1,3]dioxol-5-yl)-methyl-amine **5** (0.10 g, 0.196 mmol), bis(pinacolato)diborane (0.065 g, 0.255 mmol), potassium acetate (32.7 mg, 0.333 mmol) and 1,1-bis (diphenylphosphino)ferrocene palladium(II) dichloride [Pd(dppf)$_2$-Cl_2; 0.015 g, 0.019 mmol). Reaction mixture was stirred at 120 °C for 16 h. Water was added to the reaction mixture and extracted with ethyl acetate. Organic layer was washed with water, dried (Na_2SO_4) and concentrated. Crude compound was purified by silica gel column chromatography to get pure compound 1,2-dimethoxy-12-methyl-12,13-dihydro-[1,3]dioxolo[4′,5′:4,5]benzo-[1,2-*c*] phenanthridine **4** as a dark yellow liquid (0.054 g, 79%). ^{1}H NMR ($CDCl_3$, 400 MHz) δ 7.70–7.66 (m, 2H), 7.51–7.45 (m, 2H), 7.10 (s, 1H), 6.93 (d, J = 8.4 Hz, 1H), 6.03 (s, 2H), 4.28 (s, 2H), 3.92 (s, 3H), 3.83 (s, 3H), 2.58 (s, 3H); ^{13}C NMR ($CDCl_3$, 100 MHz): δ 152.2, 148.0, 147.4, 146.1, 142.7, 130.8, 126.3, 126.2, 124.2, 123.7, 120.1, 118.6, 111.0, 104.3, 100.9, 100.7, 61.0, 55.8, 48.7, 41.2; LC–MS (ESI): 350.2 [M+H]$^+$.

4.1.12. 1,2-Dimethoxy-12-methyl-[1,3]dioxolo[4′,5′:4,5]benzo [1,2-*c*]phenanthridin-12-ium 1

To a boiling solution of 1,2-dimethoxy-12-methyl-12,13-dihydro-[1,3]dioxolo[4′,5′:4,5]benzo[1,2-*c*]phenan-thridine **4** (1.1 g, 3.15 mmol) in ethanol was added sodium acetate (5.2 g, 64.1 mmol) and iodine (1.65 g, 6.52 mmol), and refluxed for 2 h. Ethanol was distilled out; the mixture was diluted with water (20 ml) and aqueous 1 N sodium bisulfite solution (20 ml) and extracted with 10% MeOH-DCM mixture. Organic layer was dried over Na_2SO_4 and concentrated to get crude compound 1,2-dimethoxy-12-methyl-[1,3]dioxolo[4′,5′:4,5]benzo[1,2-*c*]phenanthridin-12-ium (0.82 g, crude) as a yellow liquid which was taken forward to the next step without any purification on the basis of LCMS monitoring.

4.1.13. 1-(1,2-Dimethoxy-12-methyl-12,13-dihydro-[1,3]dioxolo-[4′,5′:4,5]benzo[1,2-*c*]phenanthridin-13-yl)-propan-2-one[(±)-6-acetonyldihydro chelerythrine] (±)-3

To a stirred solution of 1,2-dimethoxy-12-methyl-[1,3]dioxolo [4′,5′:4,5]benzo [1,2-*c*]phenanthri-din-12-ium **1** (0.80 g, 2.29 mmol) in dry acetone (40 ml) was added aqueous Na_2CO_3 (1.58 g, 14.94 mmol in 20 ml H_2O) solution. Resulting mixture was refluxed for 6 h. Excess acetone was evaporated and the residue was diluted with ethyl acetate, washed successively with water and brine, dried over Na_2SO_4 and concentrated. Crude compound was purified by silica gel column chromatography eluting with 2–5% DCM in hexane to get pure racemic compound (±)-**3** as a brown solid (0.30 g, 60%). 1H NMR ($CDCl_3$, 400 MHz) δ 7.70 (d, J = 8.5 Hz, 1H), 7.53 (d, J = 8.5 Hz, 1H), 7.50 (s, 1H), 7.47 (d, J = 8.6 Hz, 1H), 7.09 (s, 1H), 6.94 (d, J = 8.4 Hz, 1H), 6.03 (s, 2H), 5.04–5.01 (m, 1H), 3.94 (s, 3H), 3.91 (s, 3H), 2.63 (s, 3H), 2.56–2.53 (m, 1H), 2.26–2.22 (m, 1H), 2.05 (s, 3H). ^{13}C NMR ($CDCl_3$, 100 MHz): δ 207.6, 152.1, 148.1, 147.5, 145.5, 139.2, 131.0, 128.1, 127.3, 124.8, 123.8, 123.2, 119.7, 118.7, 111.5, 104.3, 101.0, 100.6, 60.9, 55.8, 54.8, 46.8, 42.8, 31.1; LC–MS (ESI): 406.0 [M+H]$^+$.

HPLC analysis: Two enantiomers are separated by chiral preparative purification using Chiralpak AD-H column (20 × 250 mm) 5 μ, mobile phase: EtOH/DEA: 100/0.1(v/v), flow rate: 10 ml/min, at 285 nm. Run time: 30 min. Enantiomer (+)-**ADC**: $[\alpha]_D^{25}$ = +279 (c 0.20, $CHCl_3$), HPLC analysis—Chiralpak AD-H, EtOH/DEA: 100/0.1(v/v), 0.5 ml/min, 285 nm, t_R 9.05 min. Enantiomer (−)-**ADC**: $[\alpha]_D^{25}$ = −255 (c 0.20, $CHCl_3$), HPLC analysis—Chiralpak AD-H, EtOH/DEA: 100/0.1 (v/v), 0.5 ml/min, 285 nm, t_R 18.73 min.

4.2. Materials and methods

4.2.1. Oligonucleotides

Oligonucleotides used for CD and UV–Visible titrations, CD melting and *Taq* DNA polymerase stop assay were synthesized in a Mermade-4 DNA/RNA synthesizer and were purified by 20% PAGE using standard protocols. Sequences used for the biophysical studies were *c-MYC* (5′-TGAGGGTGGGTAGGGTGGGGAA-3′) and *c-KIT1* (5′GGGAGGGCGCTGGGAGGAGGG-3′) DNAs. For stop assay, primer (5′-ACGACTCACTATAGCAATTGCG-3′), template with *c-MYC* DNA (5′-TGAGGGTGGGGAGGGTGGGGAAGCCA CCGCAATTGC-TATAGTGAGTCGT-3′) and template with mutated *c-MYC* DNA (5′-TGAGGGTGGGTAGAGTGGGTAAGC CACCGCAATTGCTATAGTGAG TCGT-3′) were used. Concentration of all oligonucleotides was measured at 260 nm in UV–Vis spectrophotometer using appropriate molar extinction coefficients (ε).

4.2.2. CD spectroscopy

CD spectra were recorded on a Jasco 815 CD spectrophotometer in the wavelength range of 220–320 nm using a quartz cuvette with 1.0 mm path length. The scanning speed of the instrument was set to 100 nm/min and response time was 2 s. Baseline was measured using 50 mM Tris buffer, pH 7.2. The strand concentration of oligonucleotide used was 12.5 μM and ligand stock solution was 5 mM in DMSO. Each spectrum is an average of 3 measurements at 25 °C. All spectra were analyzed using Origin 8.0 software.

4.2.3. CD melting studies

CD melting studies were recorded on a Jasco 815 CD spectrophotometer using a quartz cuvette with 1.0 mm path length.

For melting studies, 10 μM strand concentration of oligonucleotide in 10 mM lithium cacodylate (pH 7.2), required amount of monovalent salts like LiCl, KCl and 5 molar equivalents of ligands (50 μM) were used. Promoter quadruplex DNAs, *c-MYC* (10 μM in 1 mM KCl and 99 mM LiCl) and *c-KIT1* DNAs (10 μM DNA in 10 mM KCl and 90 mM LiCl) were annealed by heating at 95 °C for 5 min followed by gradual cooling to room temperature. After the annealing 5 equiv of ligands were added and incubated for overnight. Thermal melting was monitored at 263 nm for the promoter quadruplex DNAs at the heating rate of 1 °C/min from 20–95 °C for *c-MYC* and from 15–95 °C for *c-KIT1* DNAs. All spectra were fitted by sigmoidal curve fit and analyzed using Boltzmann function in Origin 8.0 software.

4.2.4. UV–Visible absorption spectroscopy

UV–Visible absorption titration experiments were carried out on a PerkinElmer (Lambda Bio+) instrument. Absorption spectra measured in the range of 225–600 nm using quartz cuvette with 10 mm path length. DNA was pre-annealed in 100 mM KCl and 10 mM lithium cacodylate buffer, pH 7.2 by heating at 95 °C for 5 min followed by slow cooling to room temperature. Initially ligand (30 μM in 100 mM KCl and 10 mM lithium cacodylate buffer, pH 7.2) absorbance was measured. Increasing concentration of pre-annealed DNA was titrated against the ligand till the saturation level and the absorbance spectrum was recorded. Binding constant was derived by using the absorbance values at 316 nm and fitting the data using half reciprocal equation as reported previously.[22] Plot of $[DNA]/\Delta\varepsilon_{ap}$ versus [DNA] provides slope and intercept. Slope was divided by intercept to get binding constant. $[DNA]/\Delta\varepsilon_{ap} = [DNA]/\Delta\varepsilon + 1/Kb$ ($\Delta\varepsilon$). Here, $\Delta\varepsilon_{ap} = |\varepsilon_b - \varepsilon_f|$; ε_b is a molar extinction coefficient of DNA-ligand bound complex and ε_f is molar extinction coefficient of ligand.

4.2.5. 5′-End-radiolabeling of oligonucleotides

Labeling of the primer was performed by following the previously reported procedure.[23] DNA (10 pmol) was 5′ end labeled by T4 polynucleotide kinase (PNK) enzyme (5 U) in 1 × PNK buffer for forward reaction [50 mM Tris–HCl pH 7.6, 10 mM $MgCl_2$, 5 mm DTT, 0.1 mM each spermidine and 0.1 mM EDTA] and [γ-^{32}P]ATP (30 μCi) in a total volume of 10 μL for 1 h at 37 °C followed by deactivation of the enzyme by heating at 70 °C for 3 min. The end labeled DNA was then purified using a QIAquick Nucleotide removal kit protocol provided by the manufacturer.

4.2.6. *Taq* DNA polymerase stop assay

This assay was performed using reported procedures.[23] Appropriate amount of labeled primer oligonucleotide (~20,000 CPM) was mixed with cold primer (50 nM) and template (100 nM) and they were annealed in an annealing buffer [5 mM Tris (pH 8), 10 mM NaCl, 0.1 mM EDTA] by heating at 95 °C for 5 min and then gradual cooling to room temperature over 4 to 5 h. The annealed primer-template was mixed with 1 × polymerase buffer [50 mM Tris, 0.5 mM DTT, 0.1 mM EDTA, 5 mM $MgCl_2$, 5 mM KCl for *c-MYC* template], 1 μg/μl BSA in 5% glycerol (v/v), and 0.2 mM dNTPs. The ligands in appropriate concentration were added to the reaction mixture (10 μl total volumes) and incubated for 30 min at room temperature. Finally the primer extension reaction was initiated by adding *Taq* DNA polymerase (0.5 U) and incubated at 55 °C for 30 min. The extension reaction was stopped by adding 10 μl of 2 × stop buffer (10 mM EDTA, 10 mM NaOH, 0.1% each bromophenol blue (w/v) and xylene cyanole (w/v) in formamide). Samples were analysed in 15% denaturing PAGE in which 1 × TBE (89 mM of each Tris and boric acid and 2 mM of EDTA, pH ~8.3) was used as running buffer and gels were autoradiographed using a phosphorimager. Quantification of gels was performed using ImageQuant 5.2 software.

4.2.7. Molecular modeling and dynamics studies

The 22-mer NMR solution structure of the *c-MYC* G-quadruplex (PDB ID: 2L7V;[24] after removing the ligand quindoline) was used as the receptor starting structure. The sdf file containing the 3D structure of **DHCHL** was obtained from PubChem database (CID: 485077). It was optimized using Gaussian09 at a B3LYP level of theory with a 6-311+G(d,p) basis set.[25] It was then fitted with RESP charges calculated using Gaussian09 at the HF level of theory with a 6-31G(d) basis set, using the Antechamber module of AmberTools14.[26] In accordance with the earlier study on **CHL**,[5] **DHCHL** was docked twice, once with *c-MYC* (1:1) and then with a system containing the most commonly-occurring docked conformation (2:1). The input files used for docking were prepared using AutoDockTools-1.5.6.[27] An MD simulation was run using the ACEMD program for accelerated MD.[28] Input files for *c-MYC* as well as the docked complex were created in xleap module of AmberTools14 with the *ff14SB* force field parameters applied for DNA and the GAFF parameters applied for **DHCHL**. The system was then solvated in a cubic box of explicit TIP3P water with the edges 8.0 Å away from any of the solute atom. For the negatively charged docked complex, K^+ ions were added to neutralize; and 20 Na^+ and 20 Cl^- ions were added to bring the simulation closer to experimental conditions. The system was then subjected to 1000 cycles of conjugate gradient minimization in ACEMD, followed by 0.5 ns of heating with harmonic constraints on the complex. The Berendsen thermostat was used for temperature control and the SHAKE algorithm used to constrain hydrogens. An integration time step of 4 fs was used. Finally, equilibration was performed, with scaling of the constraints at a rate of 0.8/step. The production run for the docked complex was carried out under constant temperature and volume conditions at 300 K for 1 μs. The trajectory was saved in an interval of every 2 ps. The MMPBSA.py module of AmberTools12 was used to calculate the binding free energies for the last 100 ns with an interval of 100 ps. Trajectories were visualized in UCSF Chimera and PyMOL. All figures were rendered using PyMOL. Trajectories were analyzed using the cpptraj module of the AmberTools14 suite. Root mean square deviations (RMSDs) of DNA backbone atoms, G-quartets and of each ligand were calculated with respect to the first frame of equilibration as well as the averaged structure over the entire period of simulation. Clustering was done to a total of 50,000 frames, using a sieve of every 10 frames, to calculate pairwise RMSDs on 5000 frames to the limit of 10 clusters, with an average standard deviation of 0.593, using the hierarchical agglomeration algorithm. Cluster representatives were chosen based on closeness to the centroid. Root mean square fluctuations (RMSFs) were calculated with respect to the averaged structure, on a per residue basis. Intermolecular hydrogen bonds were analyzed with the following cutoffs: >3.5 Å between the acceptor, and donor heavy atoms and >135° D–H–A angle.

4.2.8. Anti-cancer activity

Effects of the compounds on the viability of human cancer cell lines from different tissue origin (in order to assess cell specific effect) were determined by colorimetric assay using MTT.[29] HeLa (human cervical cancer), A549 (human lung cancer), A431 (human epidermoid cancer), HCT116 (human colorectal cancer), PC-3 (human prostate cancer) and MDA-MB-231 (human breast cancer) cell lines, all were procured from ATCC (American Type Culture Collection, Manassas, USA) and cultured following their instructions. Around 5000 cells/well were plated in 96-well plate 24 h prior to the experiment and incubated at 37 °C in a CO_2 incubator. Cells were treated with either vehicle (0.5% DMSO) or with serially diluted test compounds (0.1 to 15 or 20 μM) or doxorubicin (20 μM as positive control) in a final volume of 200 μl/well and incubated at 37 °C in a CO_2 incubator for 72 h. Following incubation, cells were treated with 100 μg of MTT and incubated at 37 °C for 4 h.

Supernatants were carefully removed (without disturbing the formazan crystals formed) and 150 μl DMSO was added to each well. The plate was kept on the plate shaker until the crystals were dissolved and the absorbance was read at 570 nm. The absorbance values from test compound wells were compared to that for the control wells to calculate the percentage of inhibition.

4.3. Statistical analysis

In vitro experiments for the assessment of anticancer activity of the compounds were performed in triplicate and data have been reported as means ± SEM. Statistical significance was determined using two-sided Student's *t*-test.

Acknowledgments

We are thankful to Department of Biotechnology (DBT)-Government of India (sanction no.: 102/IFD/SAN/1191/2009-2010 to TCGLS and Pilot Project Grants for Young Investigators in Cancer Biology, Grant No: 6242-P4/RGCB/PMD/DBT/PKPI/2015, to P.I.P.) and IRCC-IIT Bombay for providing financial support. Computer center, IIT Bombay is gratefully acknowledged for providing high performance computing facilities. We are thankful Dr. Ruchi Anand for providing access to her laboratory facilities and S. Harikrishna for assistance in the molecular modeling studies. D.K.V. thanks Council of Scientific and Industrial Research, India (CSIR) for the fellowship.

Supplementary data

Supplementary data associated with this article can be found, in the online version, at http://dx.doi.org/10.1016/j.bmc.2016.04.059.

References and notes

1. (a) Simanek, V. In *The Alkaloids*; Brossi, A., Ed.; Academic Press: New York, 1985; Vol. 26, p 185; (b) Krane, B. D.; Fagbule, M. O.; Shamma, M.; Gozler, B. *J. Nat. Prod.* **1984**, *47*, 1.
2. (a) Vavreckov, C.; Gawlik, I.; Muller, K. *Planta Med.* **1996**, *62*, 397; (b) Schemeller, T.; Latz-Bruning, B.; Wink, M. *Phytochemistry* **1997**, *44*, 257; (c) Huang, F.-C.; Kutchan, T. M. *Phytochemistry* **2000**, *53*, 555.
3. (a) Taira, Z.; Matsumoto, M.; Ishida, S.; Ichikawa, T.; Sakiya, Y. *Chem. Pharm. Bull.* **1994**, *42*, 1556; (b) Herbert, J. M.; Augereau, J. M.; Gleye, J.; Maffrand, J. P. *Biochem. Biophys. Res. Commun.* **1990**, *172*, 993; (c) Fang, S.-D.; Wang, L.-K.; Hecht, S. M. *J. Org. Chem.* **1993**, *58*, 5025; (d) Nakanishi, T.; Suzuki, M. *J. Nat. Prod.* **1998**, *61*, 1263.
4. (a) Collie, G. W.; Parkinson, G. N. *Chem. Soc. Rev.* **2011**, *40*, 5867; (b) Monchaud, D.; Teulade-Fichou, M. P. *Org. Biomol. Chem.* **2008**, *6*, 627.
5. (a) Bai, L.-P.; Hagihara, M.; Nakatani, K.; Jiang, Z.-H. *Nat. Sci. Rep.* **2014**, *4*, 2015. http://dx.doi.org/10.1038/srep06767; (b) Ghosh, S.; Jana, J.; Kar, R. K.; Chatterjee, S.; Dasgupta, D. *Biochemistry* **2015**, *54*, 974.
6. (a) Ghosh, S.; Dasgupta, D. *Biochem. Biophys. Res. Commun.* **2015**, *459*, 75; (b) Cui, X.; Lin, S.; Yuan, G. *Int. J. Biol. Macromol.* **2012**, *50*, 996.
7. Hurley, L. H.; Neidle, S. *Nat. Rev. Drug Disc.* **2011**, *10*, 261.
8. Yang, X.-J.; Miao, F.; Yao, Y.; Cao, F.-J.; Yang, R.; Ma, Y.-N.; Qin, B.-F.; Zhou, L. *Molecules* **2012**, *17*, 13026.
9. Chang, Y.-C.; Hsieh, P.-W.; Chang, F.-R.; Wu, R.-R.; Liaw, C.-C.; Lee, K.-H.; Wu, Y.-C. *Planta Med.* **2003**, *69*, 148.
10. Mansoor, T. A.; Borralho, P. M.; Luo, X.; Mulhovo, S.; Rodrigues, C. M. P.; Ferreira, M.-J. U. *J. Nat. Prod.* **2014**, *77*, 1825.
11. (a) MacKay, S. P.; Meth-Cohn, O.; Waigh, R. D. *Adv. Heterocycl. Chem.* **1997**, *67*, 345; (b) Richardson, T.; Robinson, R.; Seijo, E. *J. Chem. Soc.* **1937**, 835; (c) Ishii, H.; Ichikawa, Y.-I.; Kawanabe, E.; Ishikawa, M.; Ishikawa, T.; Kuretani, K.; Inomata, M.; Hoshi, A. *Chern. Pharm. Bull.* **1985**, *33*, 4139; (d) Kessar, S. V.; Gupta, Y. P.; Balakrishnan, P.; Sawal, K. K.; Mohammad, T.; Dutt, M. *J. Org. Chem.* **1988**, *53*, 1708; (e) Clark, R. D.; Jahangir, J. *Org. Chem.* **1988**, *53*, 2378; (f) Beugelmans, R.; Bois-Choussy, M. *Tetrahedron* **1992**, *48*, R285; (g) Sotomayor, N.; Dominguez, E.; Lete, E. *Tetrahedron Lett.* **1994**, *35*, 2973; (h) Hanaoka, M.; Mukai, C. In *Studies in Natural Products Chemistry*; Atta-ur-Rahman, Ed.; Elsevier: Amsterdam, 1994; Vol. 14, p 769; (i) Seraphin, D.; Lynch, M. A.; DuVal, O. *Tetrahedron Lett.* **1995**, *36*, 5731; (j) Harayama, T.; Akiyama, T.; Kawano, K. *Chern. Pharm. Bull.* **1996**, *44*, 1634.
12. Geen, G. R.; Mann, I. S.; Mullane, M. V. *Tetrahedron* **1998**, *54*, 9875.
13. Lv, P.; Huang, K.; Xie, L.; Xu, X. *Org. Biomol. Chem.* **2011**, *9*, 3133.
14. Korivi, R. P.; Cheng, C.-H. *Chem. Eur. J.* **2010**, *16*, 282.
15. Clement, B.; Weide, M.; Wolschendorf, U.; Kock, I. *Angew. Chem., Int. Ed.* **2005**, *44*, 635.
16. De, S.; Mishra, S.; Kakde, B. N.; Dey, D.; Bisai, A. *J. Org. Chem.* **2013**, *78*, 7823.
17. Castillo, J.-C.; Quiroga, J.; Abonia, R.; Rodriguez, J.; Coquerel, Y. *Org. Lett.* **2015**, *17*, 3374.
18. (a) Levy, A. A.; Rains, H. C.; Smiles, S. *J. Chem. Soc.* **1931**, 3264; (b) Matsui, K.; Maeno, N.; Suzuki, S.; Shizuka, H.; Morita, T. *Tetrahedron Lett.* **1970**, *11*, 1467; (c) Wang, Z. In *Comprehensive Organic Name Reactions and Reagents*; Wiley: Hoboken, 2010.
19. (a) Sambiagio, C.; Marsden, S. P.; Blacker, A. J.; McGowan, P. C. *Chem. Soc. Rev.* **2014**, *43*, 3525; (b) Hassan, J.; Sevignon, M.; Gozzi, C.; Schulz, E.; Lemaire, M. *Chem. Rev.* **2002**, *102*, 1359.
20. (a) Paramasivan, S.; Rujan, I.; Bolton, H. P. *Methods* **2007**, *43*, 324; (b) Randazzo, A.; Spada, G.; Silva, M. *Top. Curr. Chem.* **2013**, *330*, 67.
21. Guedin, A.; Lacroix, L.; Mergny, J. L. *Methods Mol. Biol.* **2010**, *613*, 25.
22. Kieltyka, R.; Englebienne, P.; Moitessier, N.; Sleiman, H. In *G-Quadruplex DNA*; Baumann, P., Ed.; Humana Press, 2010; Vol. 608,.
23. (a) Han, H.; Hurley, L. H.; Salazar, M. *Nucleic Acids Res.* **1999**, *27*, 537; (b) Seenisamy, J.; Bashyam, S.; Gokhale, V.; Vankayalpati, H.; Grand, C. L.; Siddiqui-Jain, A.; Streiner, N.; Wilson, W. D.; Hurley, L. H. *J. Am. Chem. Soc.* **2005**, *127*, 2944.
24. Dai, J.; Carver, M.; Hurley, L. H.; Yang, D. *J. Am. Chem. Soc.* **2011**, *133*, 17673.
25. Frisch, M. J.; Trucks, G. W.; Schlegel, H. B.; Scuseria, G. E.; Robb, M. A.; Cheeseman, J. R.; Scalmani, G.; Barone, V.; Mennucci, B.; Petersson, G. A.; Nakatsuji, H.; Caricato, M.; Li, X.; Hratchian, H. P.; Izmaylov, A. F.; Bloino, J.; Zheng, G.; Sonnenberg, J. L.; Hada, M.; Ehara, M.; Toyota, K.; Fukuda, R.; Hasegawa, J.; Ishida, M.; Nakajima, T.; Honda, Y.; Kitao, O.; Nakai, H.; Vreven, T.; Montgomery, J. A., Jr.; Peralta, J. E.; Ogliaro, F.; Bearpark, M.; Heyd, J. J.; Brothers, E.; Kudin, K. N.; Staroverov, V. N.; Kobayashi, R.; Normand, J.; Raghavachari, K.; Rendell, A.; Burant, J. C.; Iyengar, S. S.; Tomasi, J.; Cossi, M.; Rega, N.; Millam, J. M.; Klene, M.; Knox, J. E.; Cross, J. B.; Bakken, V.; Adamo, C.; Jaramillo, J.; Gomperts, R.; Stratmann, R. E.; Yazyev, O.; Austin, A. J.; Cammi, R.; Pomelli, C.; Ochterski, J. W.; Martin, R. L.; Morokuma, K.; Zakrzewski, V. G.; Voth, G. A.; Salvador, P.; Dannenberg, J. J.; Dapprich, S.; Daniels, A. D.; Farkas, Ö; Foresman, J. B.; Ortiz, J. V.; Cioslowski, J.; Fox, D. J. Gaussian 09, Revision D.01, 2014, Gaussian, Wallingford CT.
26. Case, D. A.; Babin, V.; Berryman, J. T.; Betz, R. M.; Cai, Q.; Cerutti, D. S.; Cheatham, T. E., III; Darden, T. A.; Duke, R. E.; Gohlke, H.; Goetz, A.W.; Gusarov, S.; Homeyer, N.; Janowski, P.; Kaus, J.; Kolossvry, I.; Kovalenko, A.; Lee, T. S.; LeGrand, S.; Luchko, T.; Luo, R.; Madej, B.; Merz, K. M.; Paesani, F.; Roe, D. R.; Roitberg, A.; Sagui, C.; Salomon-Ferrer, R.; Seabra, G.; Simmerling, C. L.; Smith, W.; Swails, J.; Walker, R.C.; Wang, J.; Wolf, R.M.; Wu, X.; Kollman, P. A. AMBER 14, 2014, University of California, San Francisco.
27. Harvey, M.; Giupponi, G.; De Fabritis, G. *J. Chem. Theory Comput.* **2009**, *5*, 1632.
28. Morris, G. M.; Huey, R.; Lindstrom, W.; Sanner, M. F.; Belew, R. K.; Goodsell, D. S.; Olson, A. J. *J. Comput. Chem.* **2009**, *16*, 2785.
29. Mosmann, T. *J. Immunol. Methods* **1983**, *65*, 55.

Bioorganic & Medicinal Chemistry
journal homepage: www.elsevier.com

Dihydrochelerythrine and its derivatives: Synthesis and their application as potential G-quadruplex DNA stabilizing agents

Rajesh Malhotra,[a#] Chhanda Rarhi,[a,b#] K. V. Diveshkumar,[c#] Rajib Barik,[b] Ruhee D'cunha,[c] Pranab Dhar,[b] Mrinalkanti Kundu,[b*] Subrata Chattopadhyay,[b] Subho Roy,[b] Sourav Basu,[b] P. I. Pradeepkumar,*[c] and Saumen Hajra*[d]

[a] *Department of Chemistry, Guru Jambheshwar University of Science and Technology, Hisar, Haryana-125001, India*
[b] *TCG Lifesciences Pvt. Ltd., BN-7, Salt Lake, Kolkata-700091, India. E-mail: mrinal.kundu@tcgls.com*
[c] *Department of Chemistry, Indian Institute of Technology Bombay, Mumbai – 400076, India. E-mail: pradeep@chem.iitb.ac.in*
[d] *Centre of Biomedical Research, SGPGIMS Campus, Lucknow 226014, India; E-mail: saumen.hajra@cbmr.res.in*

CD spectra for CHL with *c-MYC* and *c-KIT1* DNAs in the absence of added metal ions

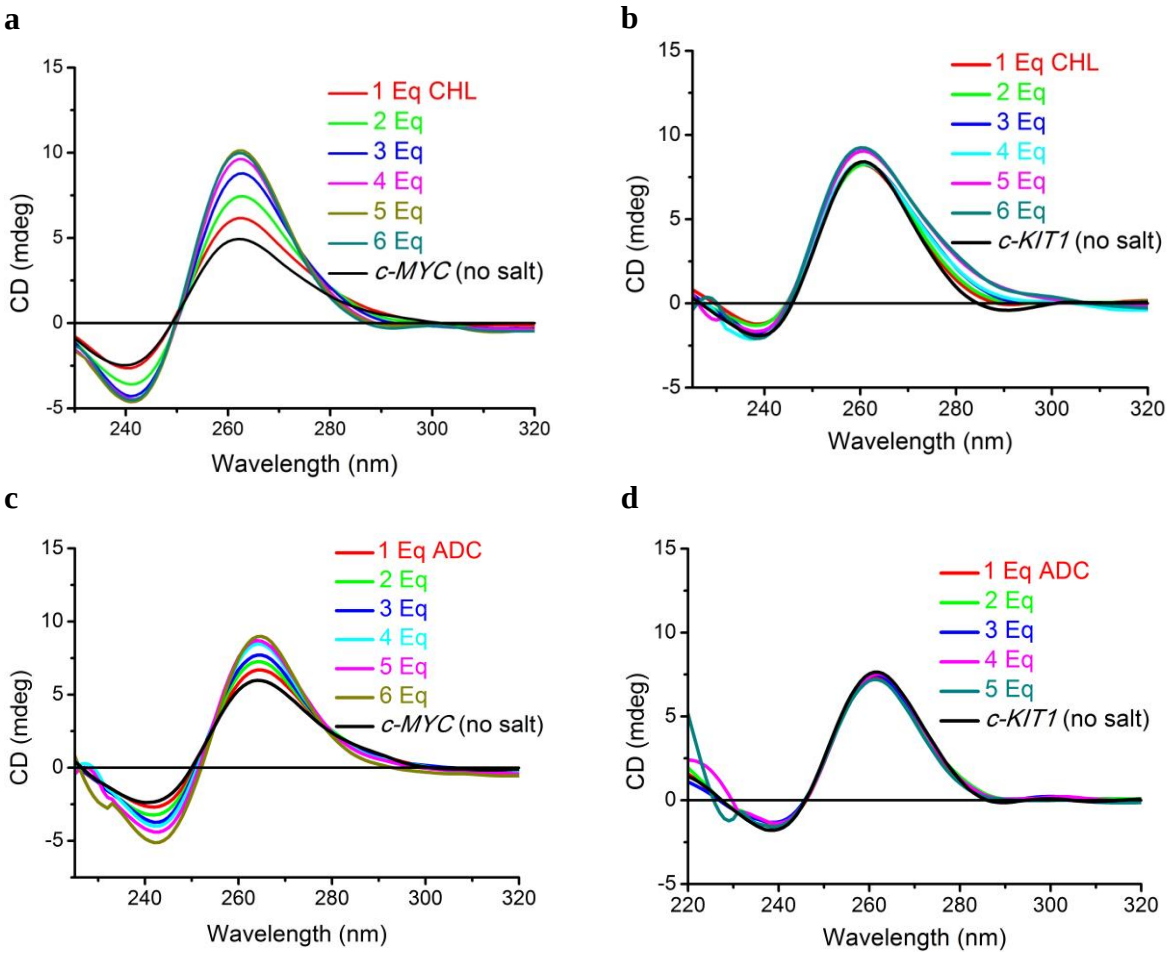

Figure S1: CD titration spectra for **CHL** and **ADC** with promoter quadruplex DNAs (12.5 µM DNA in 50 mM Tris pH 7.2) in the absence of added metal ions. (a) *c-MYC* DNA with **CHL**; (b) *c-KIT1* DNA with **CHL**; (c) *c-MYC* DNA with **ADC**; (d) *c-KIT1* DNA with **ADC**.

CD melting curves for telomeric, *c-MYC* quadruplex and duplex DNAs

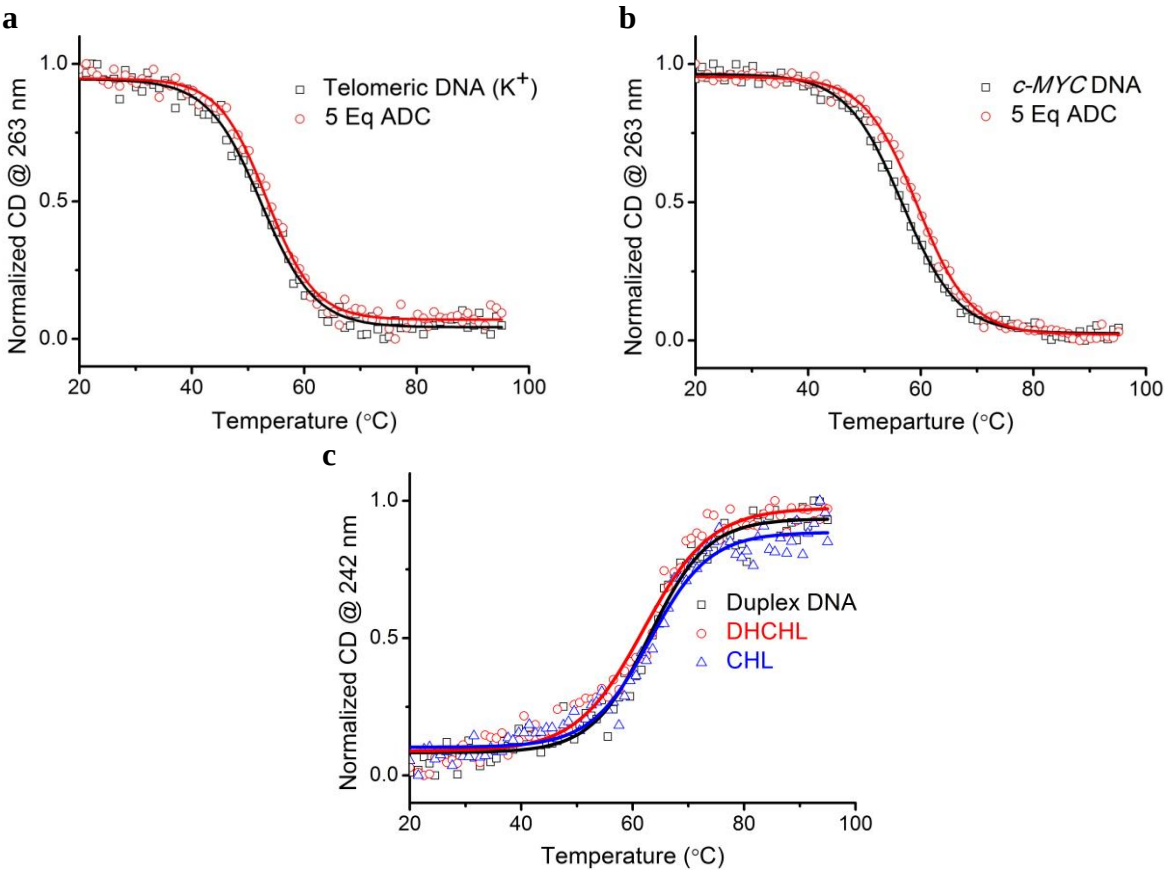

Figure S2: CD melting curves for telomeric, *c-MYC* quadruplex (10 µM in 10 mM Lithium cacodylate buffer, pH 7.2) and duplex DNAs (15 µM). (a) Telomeric DNA with **ADC**, (10 mM KCl, 90 mM LiCl); (b) *c-MYC* DNA with **ADC**, (1 mM KCl and 99 mM LiCl); (c) Duplex DNA (10 mM KCl and 90 mM LiCl) with **DHCHL** and **CHL**.

UV-Visible absorption curve and plot for CHL with *c-MYC* DNA

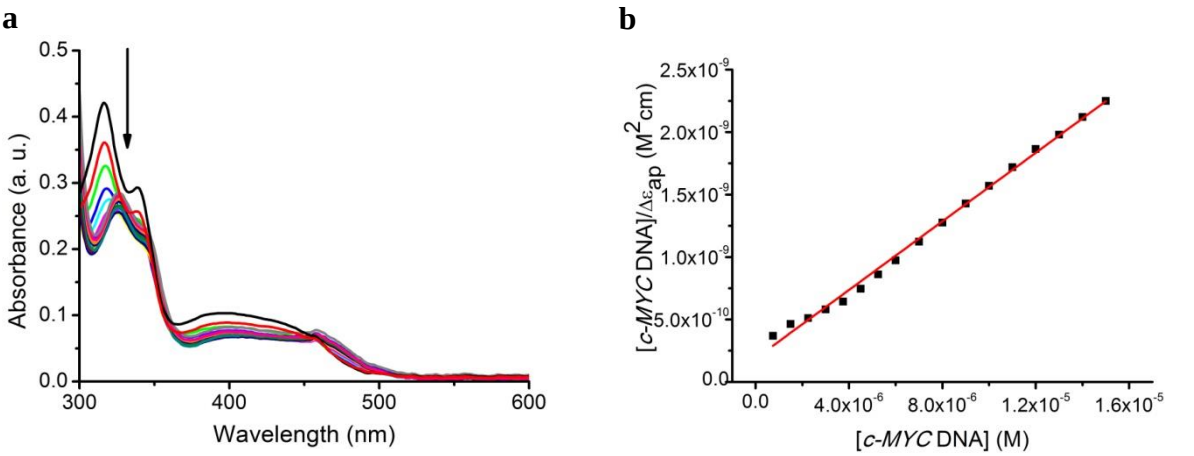

Figure S3: UV-Visible titration spectra and linear plots for **CHL** with *c-MYC* quadruplex DNA. Pre-annealed DNA (100 mM KCl and 10 mM Lithium cacodylate buffer, pH 7.2) was titrated with **CHL** (30 µM in similar salt and buffer conditions) and the data was fitted using half-reciprocal equation. (a) UV absorption spectrum; (b) Linear plot.

PAGE and plot of stop products versus concentration of CHL for stop assay

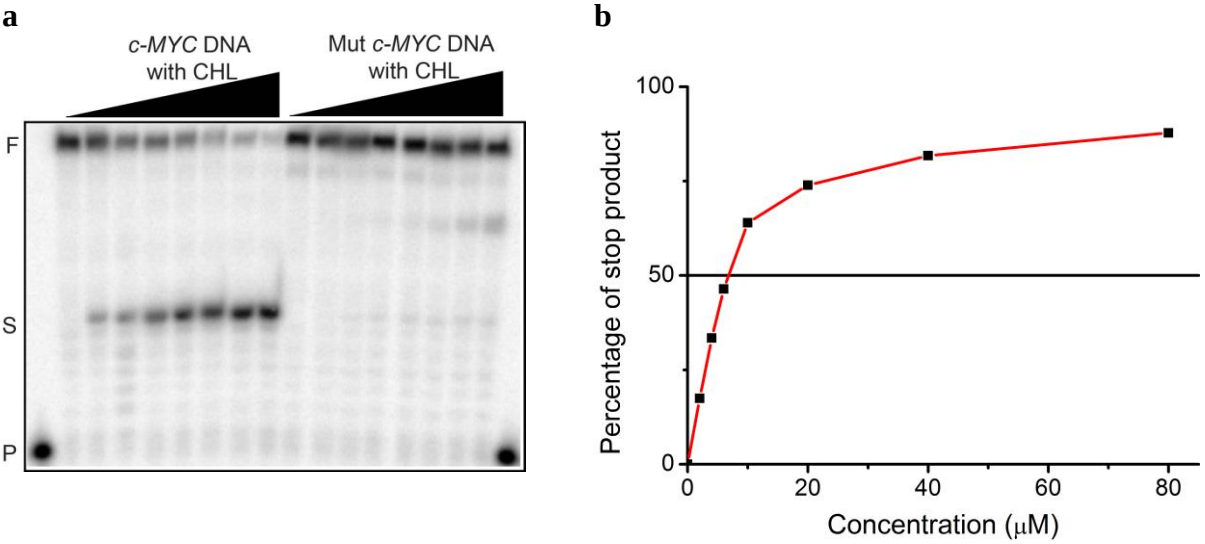

Figure S4: Denaturing PAGE (15%, 7 M urea) and plots of stop products versus ligand concentration for the *Taq* DNA polymerase stop assay in the presence of the *c-MYC* and mutated *c-MYC* DNAs. (a) Denaturing PAGE for **CHL** (0-80 µM) with the *c-MYC* and the mutated *c-MYC* DNA templates; (b) Plot of *Taq* polymerase stop products versus **CHL** concentration (0-80 µM). Primer extension reaction was carried out at 55 °C. Conditions: 100 nM template, 50 nM primer, 0.2 mM dNTPs and 0.5 U of *Taq* polymerase in the enzyme buffer (50 mM Tris, 0.5 mM DTT, 0.1 mM EDTA, 5 mM $MgCl_2$, 5mM KCl). P denotes primer, S denotes stop product andF denotes full length product. Normalized percentage of stop products in each lane was plotted against concentration of ligand. Each data points represent the average from 2 independent experiments with maximum error ≤ 4.5%.

Energy optimized structure of DHCHL (B3LYP/6-311+G(d,p)):

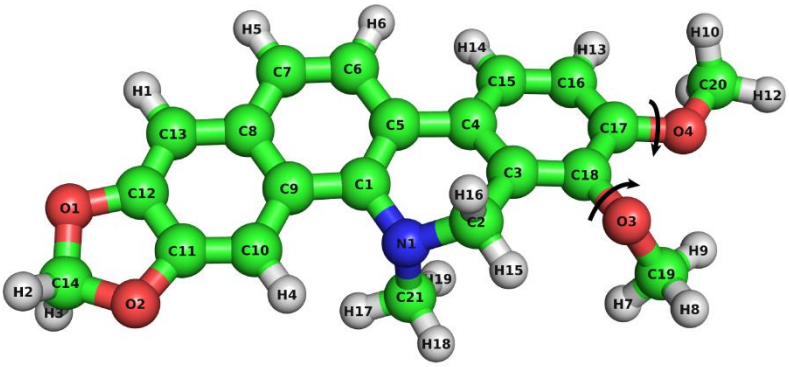

Figure S5. The energy optimized **DHCHL**, showing rotatable bonds. Structure calculated using B3LYP level of theory with a 6-311+G(d,p) basis set using Gaussian 09. RESP charges were calculated at the HF level of theory with a 6-31G(d) basis set in Gaussian 09. A library file was created for the ligand using Antechamber, with parameters from the General Amber Force Field(GAFF).

Docked structure (2:1 stoichiometry)

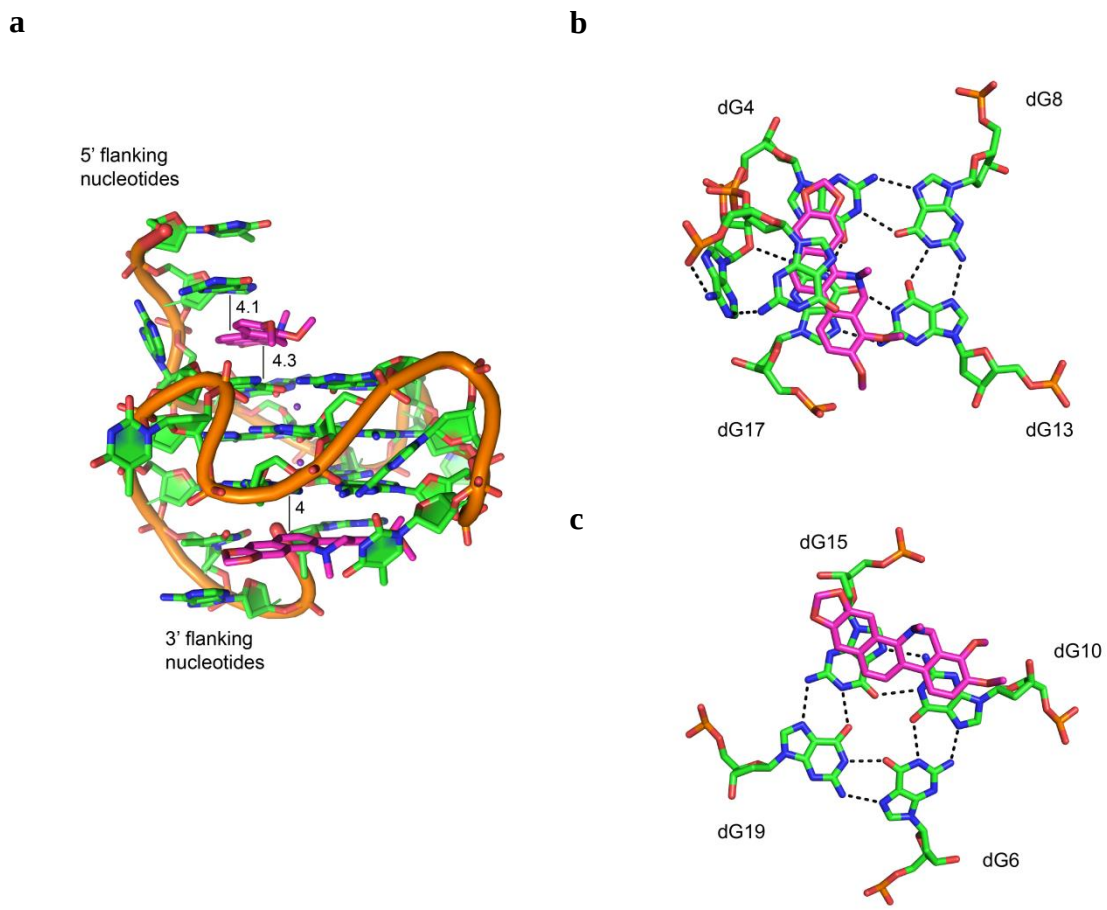

Figure S6. The structure of **DHCHL-***c-MYC* complex after docking using AutoDock 4.2. (a) The docked structure showing π-stacking distances; (b) Top view of the top ligand; and (c) Top view of the bottom ligand, showing the closest interacting residues. There were 2 rotatable bonds in the ligand. Grid maps were created using AutoGrid 4.2.5. The docking was done using the Genetic Algorithm with number of energy evaluations as 25000000 and generations as 270000 in AutoDock 4.2. 34 clusters of the 250 docked conformations were generated using an RMSD-tolerance of 2 Å for the 1:1 system, and 37 clusters for the 2:1 system.

Time-dependent RMSD graphs from the MD simulation

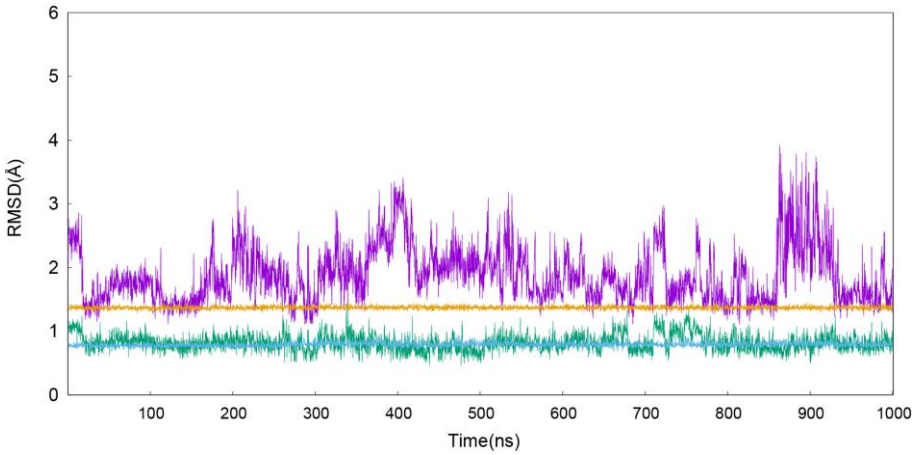

Figure S7. Time-dependent RMSD values with respect to the averaged structure for 1 μs of production of **DHCHL** in complex with the *c-MYC* G-quadruplex. RMSDs of the DNA backbone (purple), *c-MYC* G-quartets (green), 5'-**DHCHL** (orange) and 3'-**DHCHL** (blue) were plotted against time. RMSDs were calculated every 20 ps (every 10th frame) using the cpptraj module in AmberTools14. Backbone atoms are defined as: P, O3',O5',C3',C4',C5'. G-quartets are defined as residues: dG4-dG6, dG8-dG10, dG13-dG15, dG17-dG19.

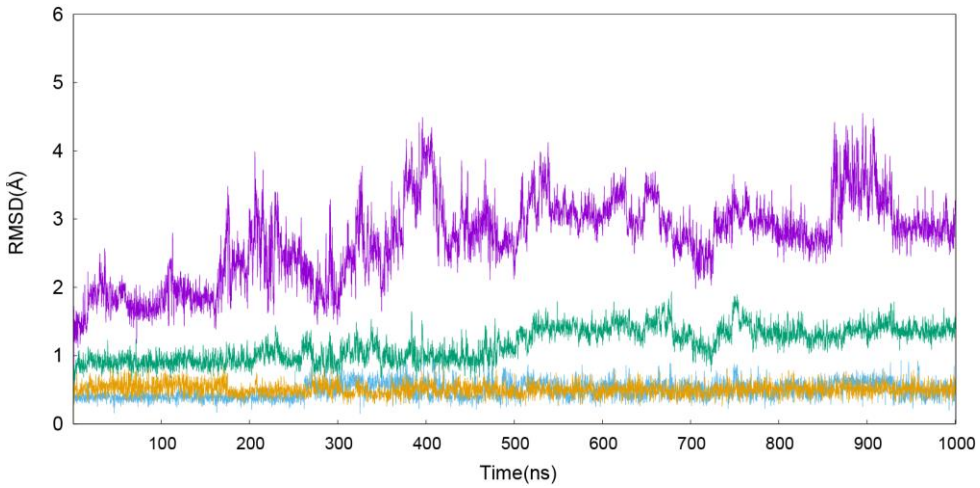

Figure S8. Time-dependent root mean square deviation (RMSD) values with respect to the first frame for 1 μs of production of the docked complex of **DHCHL** with the *c-MYC* G-quadruplex. RMSDs of the system (purple), *c-MYC* G-quartets (green), 3'-**DHCHL** (blue) and 5'-**DHCHL** (orange) were plotted against time. RMSDs were calculated every 20 ps (every 10th frame) using the cpptraj module in AmberTools14.

Hydrogen-bond occupancies for *c-MYC* G-quartets

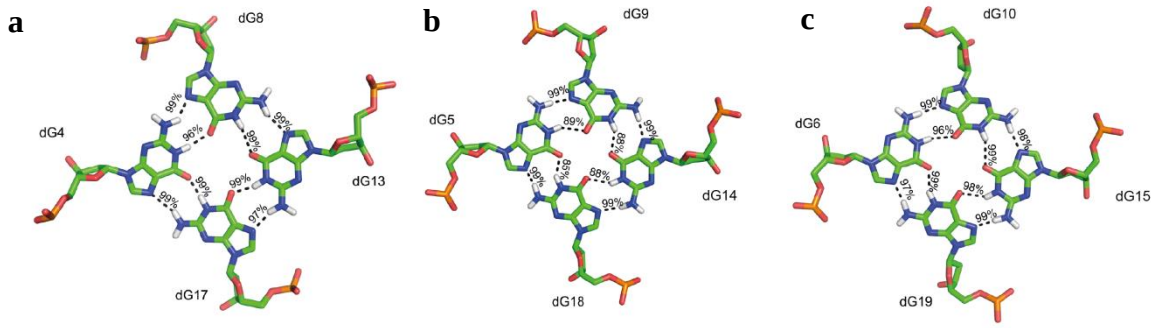

Figure S9. Percentage occupancies of the Hoogsteen hydrogen bonds for each G-quartet. (a) Top Quartet; (b) Middle Quartet; (c) Bottom Quartet for the bound *c-MYC* G-quadruplex. H-bond occupancies of the top and bottom quartets were > 96% and of the middle quartet were > 85% of the total simulation time. Values were calculated every 20 ps(every 10th frame) using the cpptraj module in AmberTools14.

Per-residue RMSF values for the *c-MYC* G-quadruplex

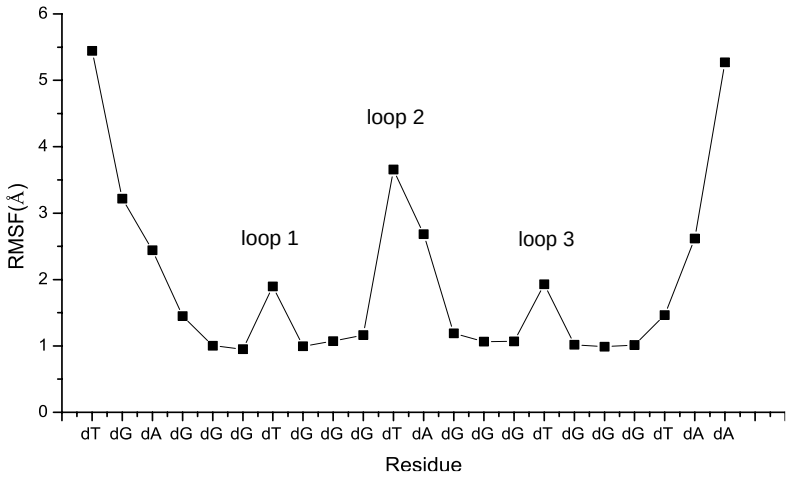

Figure S10. Root mean square fluctuation (RMSF) values, calculated on a per-residue basis, for the *c-MYC* G-quadruplex over the course of the 1 μs MD simulation. Loops are numbered from 5' to 3'. RMS-fitting was performed to the average structure and values were calculated every 20 ps (every 10th frame) using the cpptraj module in AmberTools14.

Minor representative structure of DHCHL-*c-MYC* Complex

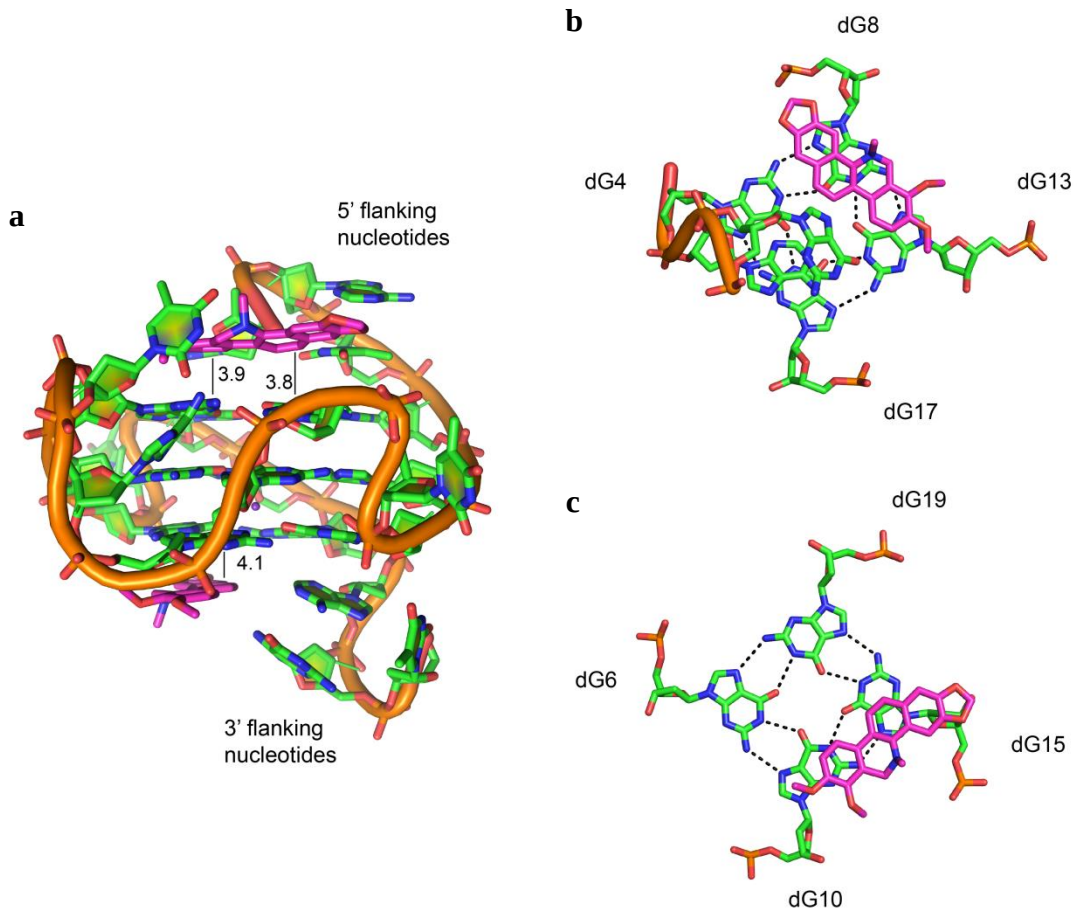

Figure S11. The best representative structure of cluster-2 (26.5% frames) of **DHCHL** with the *c-MYC* G-quadruplex over a 1 μs MD simulation; (a) Representative 2 showing π-stacking distances; (b) Top view of the 5'-ligand; and (c) Top view of the 3'-ligand, showing the closest interacting residues. Ligands are in pink. Distances are mentioned in Å.

Motion of the ligand over the top face of the G-quadruplex

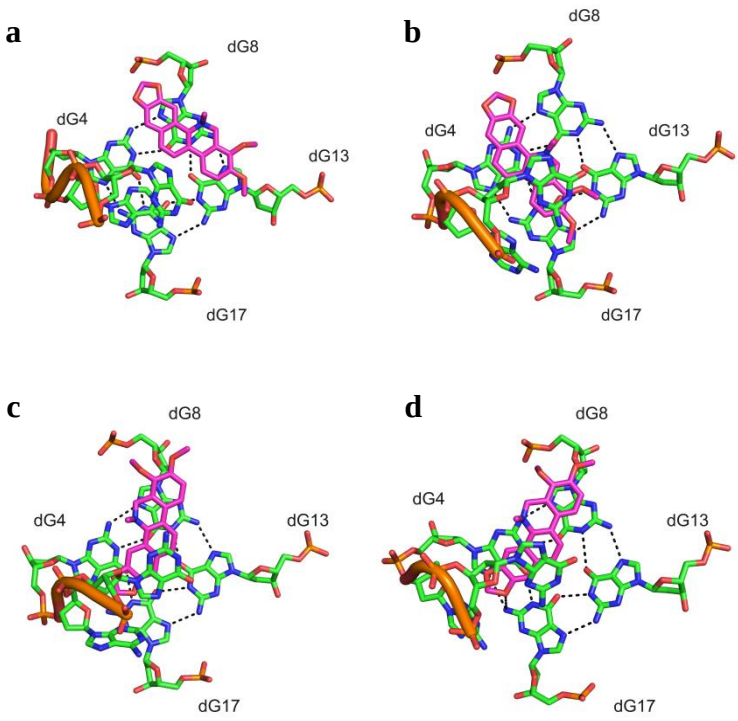

Figure S12. Top views of the 5'-ligand and closest residues, showing motion of the ligand over 1 μs of MD simulation. (a) At 48 ns; (b) At 352 ns; (c) At 450 ns; and (d) At 645 ns. Ligand is shown in pink.

Motion of the ligand over the bottom face of the G-quadruplex

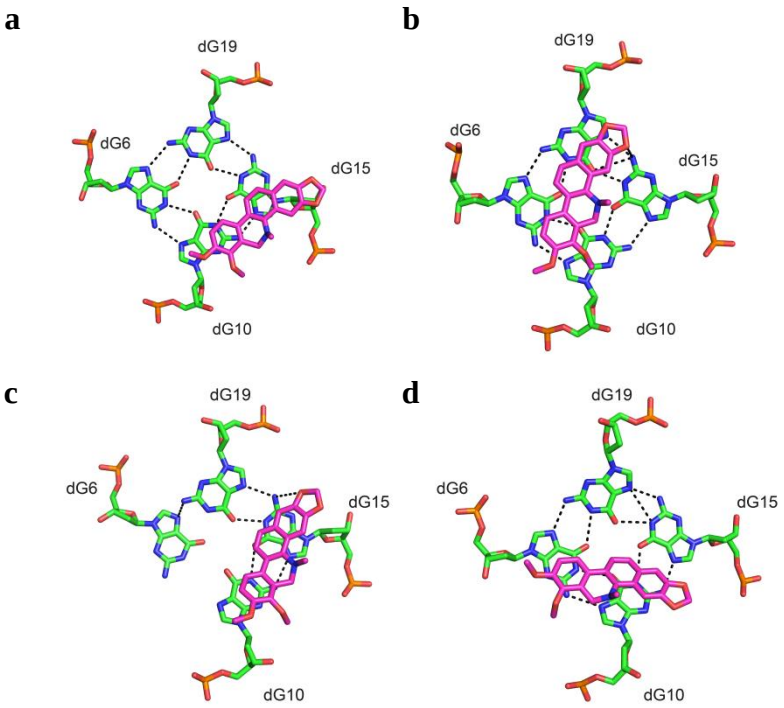

Figure S13. Top views of the 3'-ligand and closest residues, showing motion of the ligand over 1 μs of MD simulation. (a) At 48 ns; (b) At 352 ns; (c) At 450 ns; and (d) At 645 ns. Ligand is shown in pink.

Binding free energies for the DHCHL-*c-MYC* complex

Energy Components	**5'-ligand**	**3'-ligand**	**Both**
ΔE_{ELEC}	–3.30 ± 2.35	–2.71 ± 3.38	–6.01 ± 6.19
ΔE_{VDW}	–50.03 ± 5.25	–48.47 ± 5.86	–98.50 ± 6.22
$\Delta E_{MM}(\Delta E_{Elec}+\Delta E_{VDW})$	–53.33 ± 5.67	–51.19 ± 7.32	–104.52 ± 9.01
ΔPB_{np}	–3.15 ± 0.13	–3.40 ± 0.33	–6.56 ± 0.35
ΔPB_{cal}	21.77 ± 5.31	22.50 ± 5.82	44.19 ± 7.65
ΔPB_{solv} ($\Delta PB_{np}+\Delta PB_{cal}$)	18.61 ± 5.24	19.10 ± 5.55	37.64 ± 7.42
$\Delta H_{PB}(\Delta E_{MM}+\Delta PB_{solv})$	**–34.72 ± 2.28**	**–32.09 ± 3.53**	**–66.88 ± 4.22**
ΔGB_{np}	–2.63 ± 0.17	–2.76 ± 0.32	–5.39 ± 0.35
ΔGB_{cal}	18.51 ± 5.36	19.06 ± 5.35	36.78 ± 7.33
ΔGB_{solv} ($\Delta GB_{np}+\Delta GB_{cal}$)	15.87 ± 5.31	16.30 ± 5.17	31.39 ± 7.17
$\Delta H_{GB}(\Delta E_{MM}+\Delta GB_{solv})$	**–37.46 ± 2.34**	**–34.89 ± 4.65**	**–73.13 ± 5.32**
ΔS_{TRANS}	–12.90 ± 0.00	–12.90 ± 0.00	–13.48 ± 0.00
ΔS_{ROTA}	–10.50 ± 0.03	–10.51 ± 0.03	–12.39 ± 0.04
ΔS_{VIBR}	9.11 ± 4.03	8.13 ± 4.43	3.86 ± 6.34
$T\Delta S$	–14.29 ± 4.04	–15.27 ± 4.45	–22.00 ± 6.35
ΔG ($\Delta H_{PB} - T\Delta S$)	**–20.43 ± 4.62**	**–16.81 ± 5.67**	**–44.87 ± 7.63**

Table S1. Binding free energy values, broken down into components, for the complex of **DHCHL** with the *c-MYC* G-quadruplex DNA. Values were calculated for the last 100 ns, every 100 ps (every 50th frame) using the MMPBSA.py module in AmberTools12. ΔE_{ELEC} is the electrostatic contribution and ΔE_{VDW} is the Vander Waals contribution to the total molecular-mechanical energy ($\Delta E_{MM}= \Delta E_{ELEC} + \Delta E_{VDW} + \Delta E_{ini}$ (zero for all)). ΔGB_{np} is the nonpolar contribution to the solvation energy. ΔH_{PB} and ΔH_{GB} are the electrostatic contribution to the solvation energy using the Poisson-Boltzmann and Generalized Born continuum models; ΔPB_{solv} and ΔGB_{solv} are the total solvation energies. $T\Delta S$ is the solute entropic contribution, where T = 298.15 K and ΔS is the sum of translational, rotational, and vibrational entropies. Entropy was calculated using the normal mode harmonic approximation with a drms value of 0.05 and the maximum number of cycles set at 10000. ΔG is the estimated binding free energy with solute entropic contribution ($\Delta H_{PB} - T\Delta S$). Error is calculated as standard deviation from the mean. All the values are reported in kcal mol^{-1}.

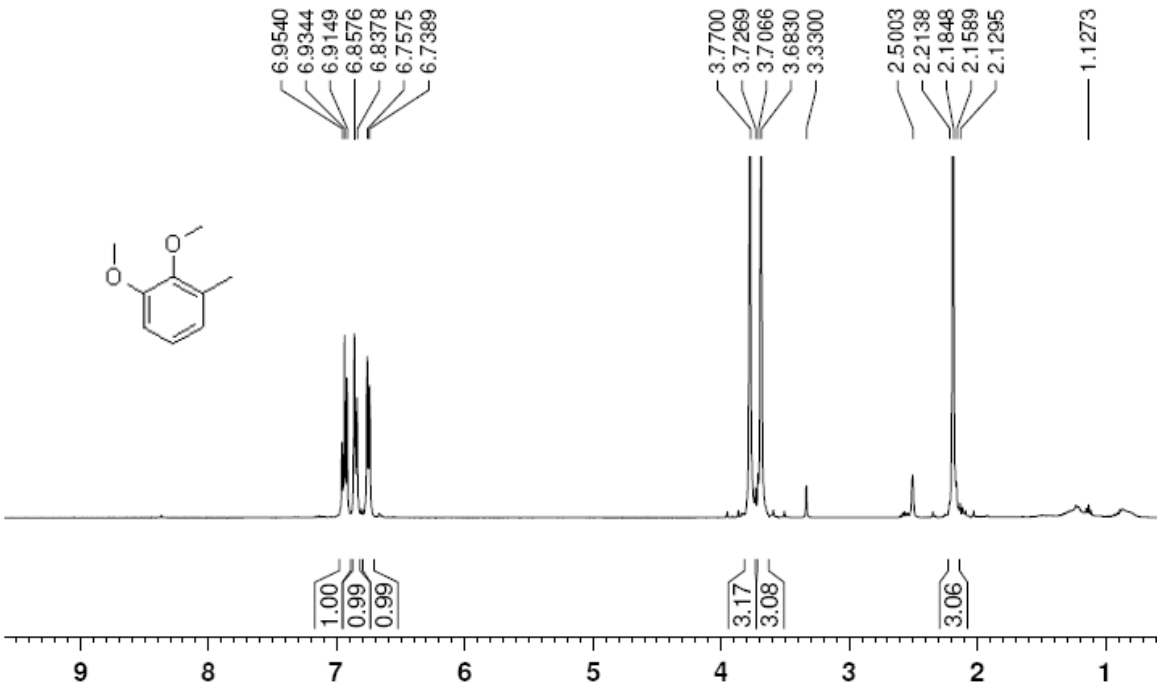

Figure S14. ^{1}H NMR spectrum of compound **9** (DMSO-d6, 400 MHz).

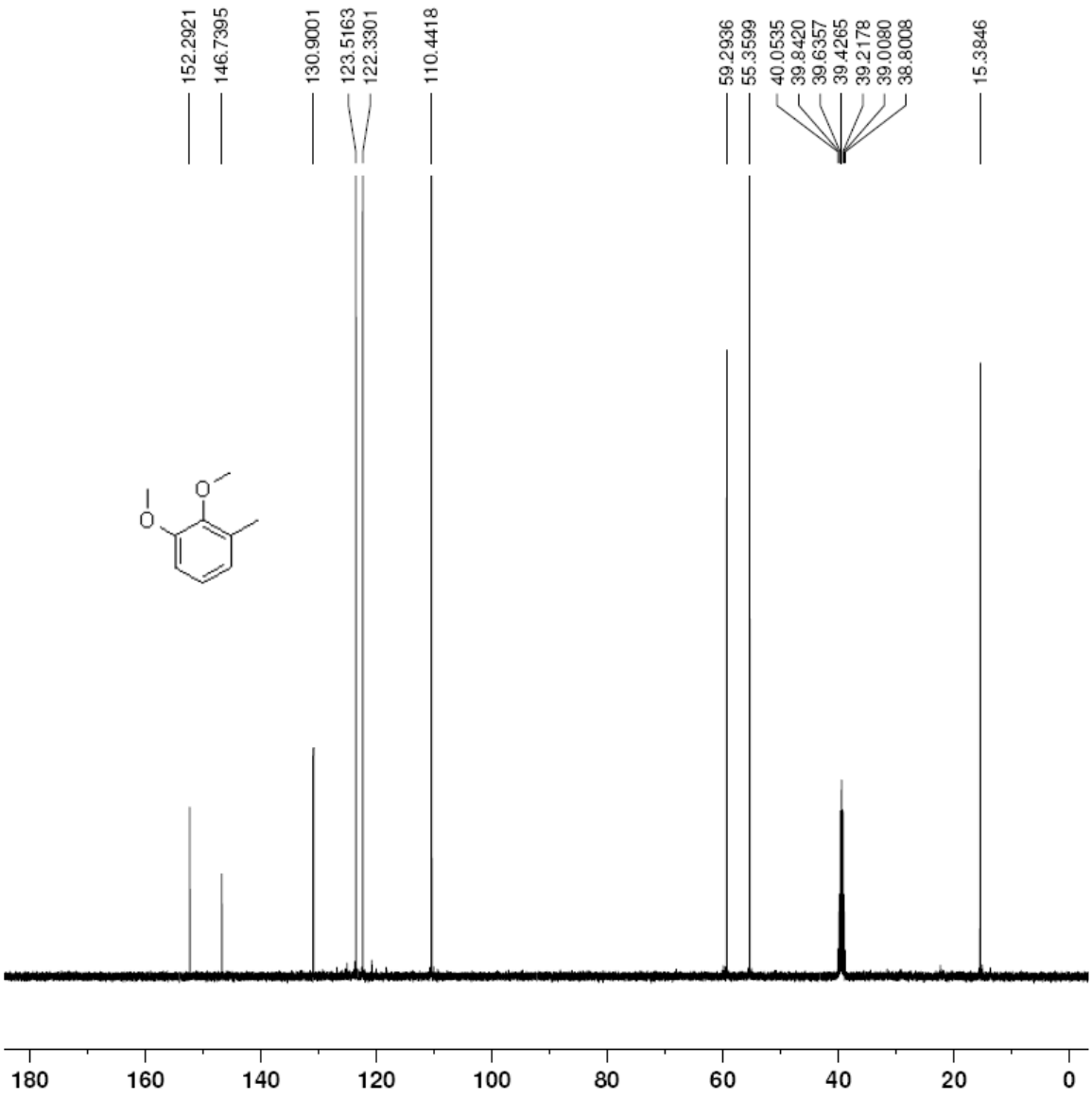

Figure S15. ^{13}C NMR spectrum of compound **9** (DMSO-d6, 100 MHz).

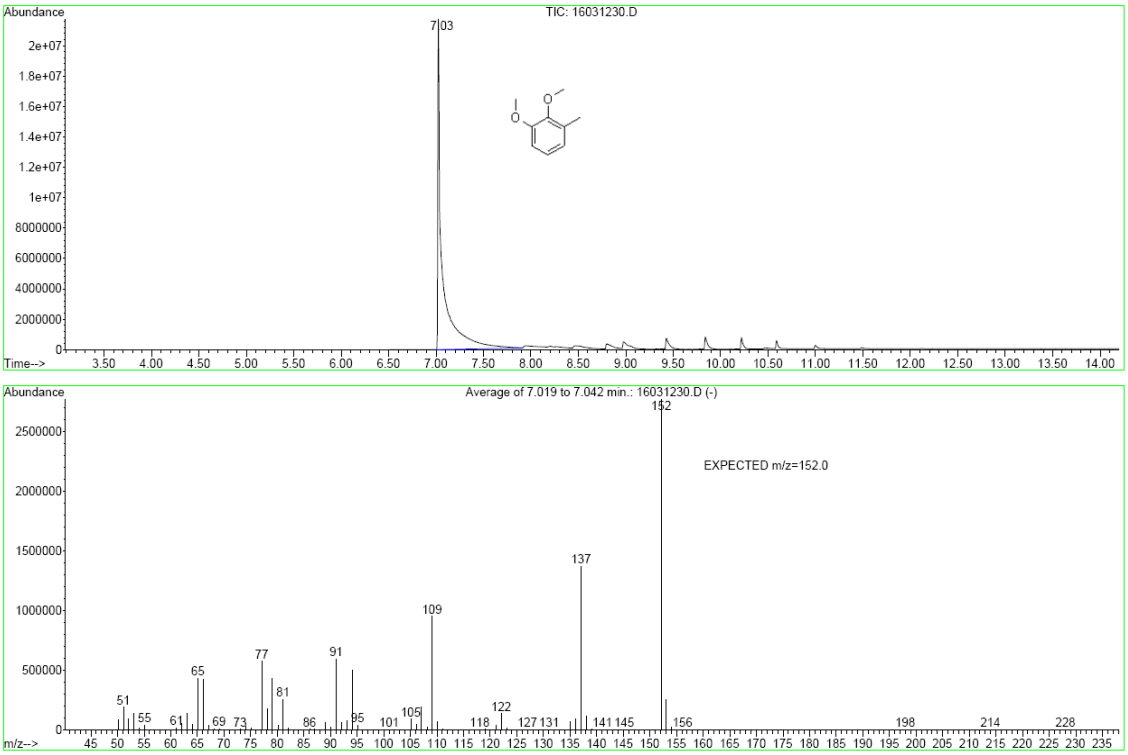

Figure S16. GC-MS spectrum of compound **9**.

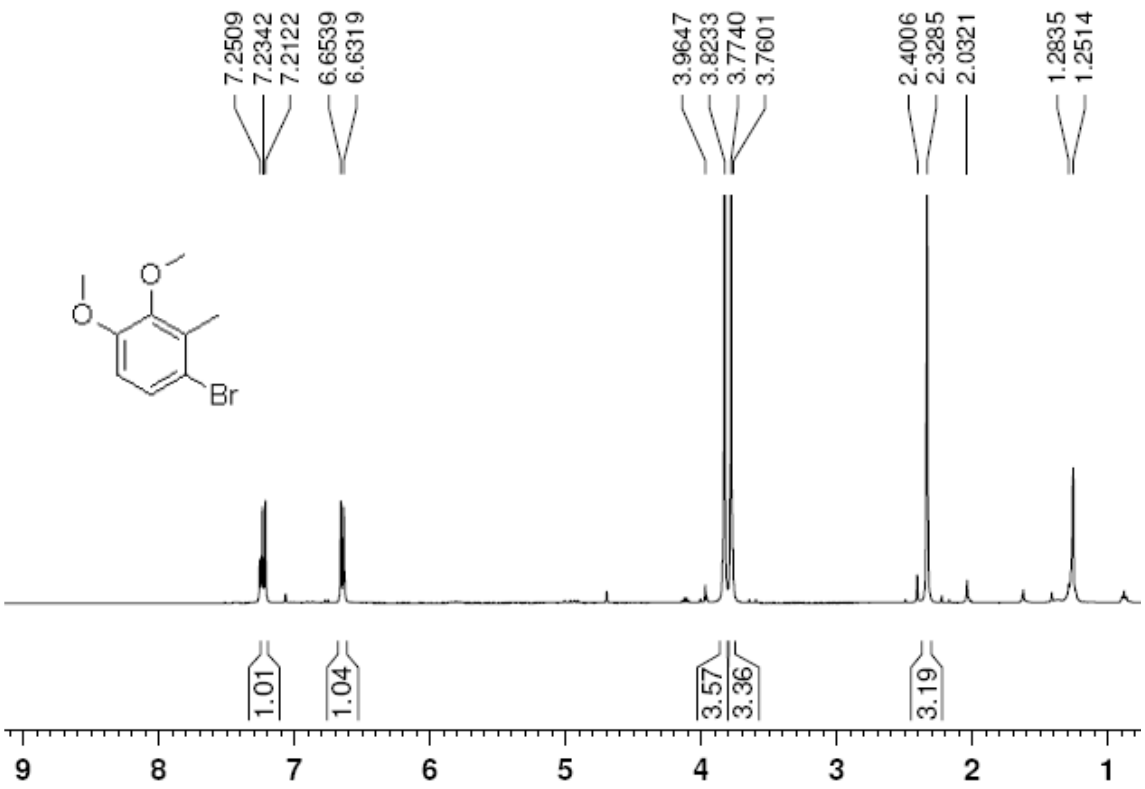

Figure S17. ^{1}H NMR spectrum of compound **10** ($CDCl_3$, 400 MHz).

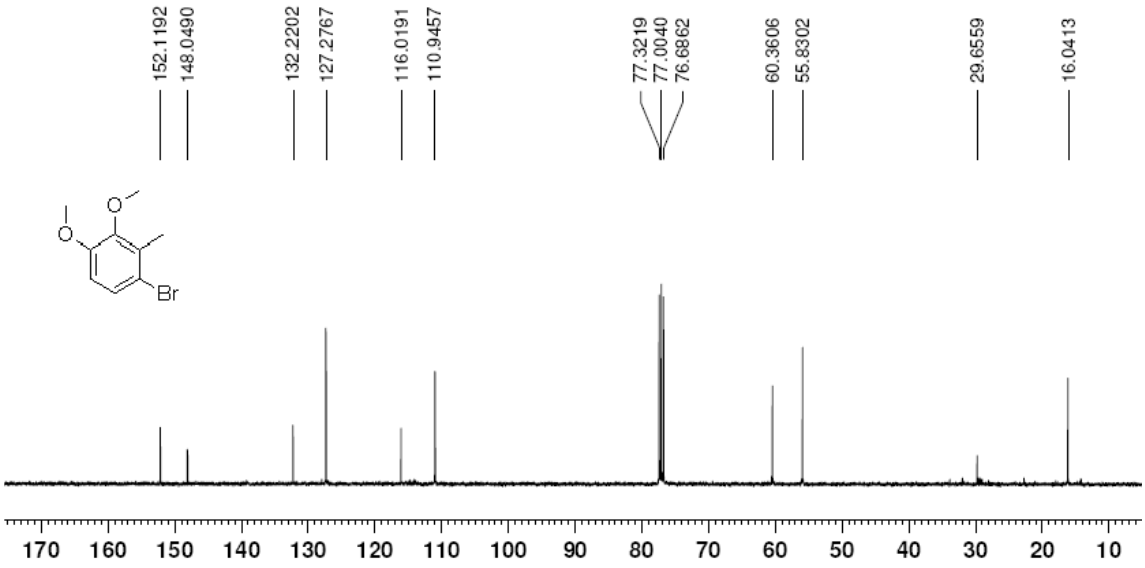

Figure S18. ^{13}C NMR spectrum of compound **10** ($CDCl_3$, 100 MHz).

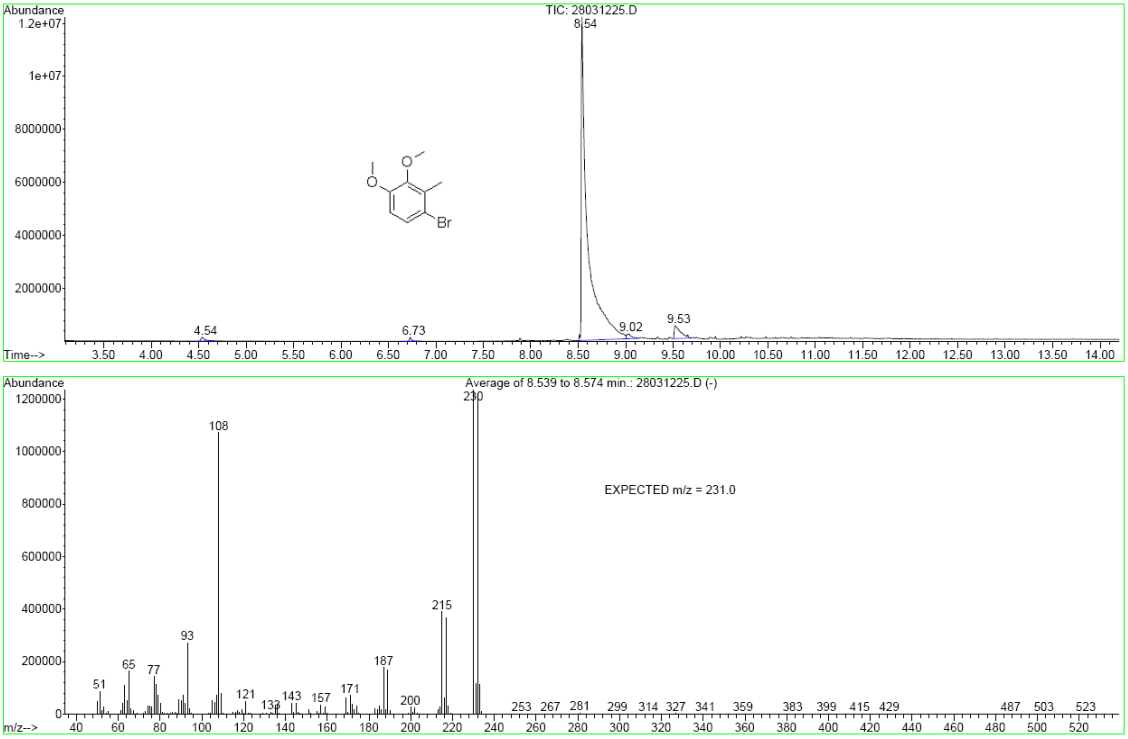

Figure S19. GC-MS spectrum of compound **10**.

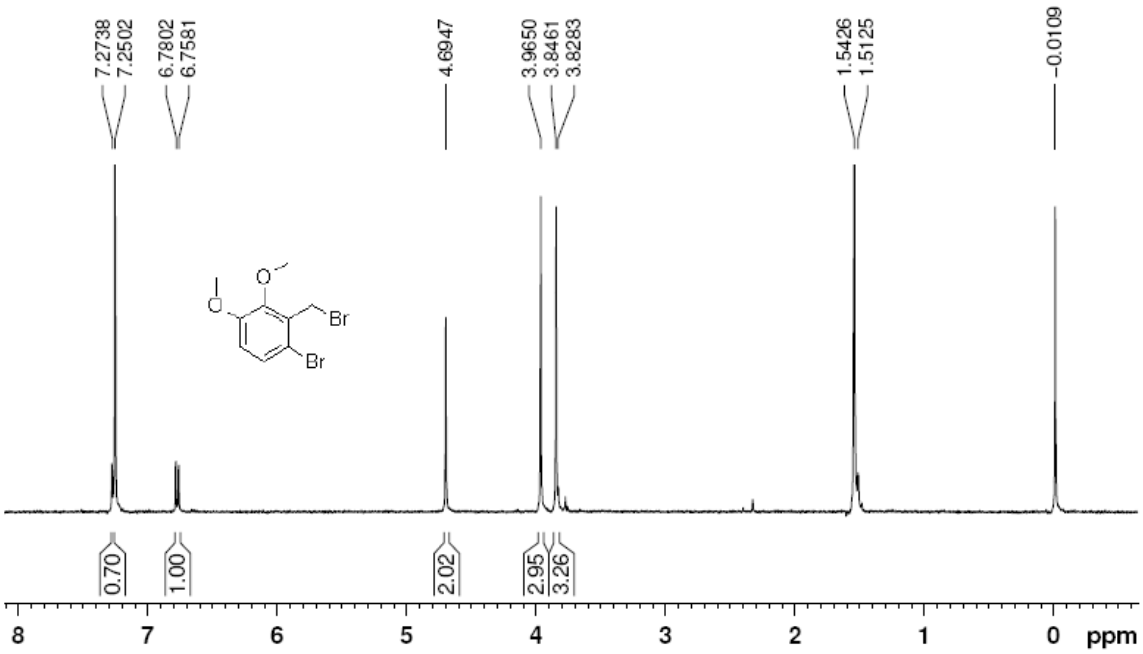

Figure S20. ^{1}H NMR spectrum of compound **7** ($CDCl_3$, 400 MHz).

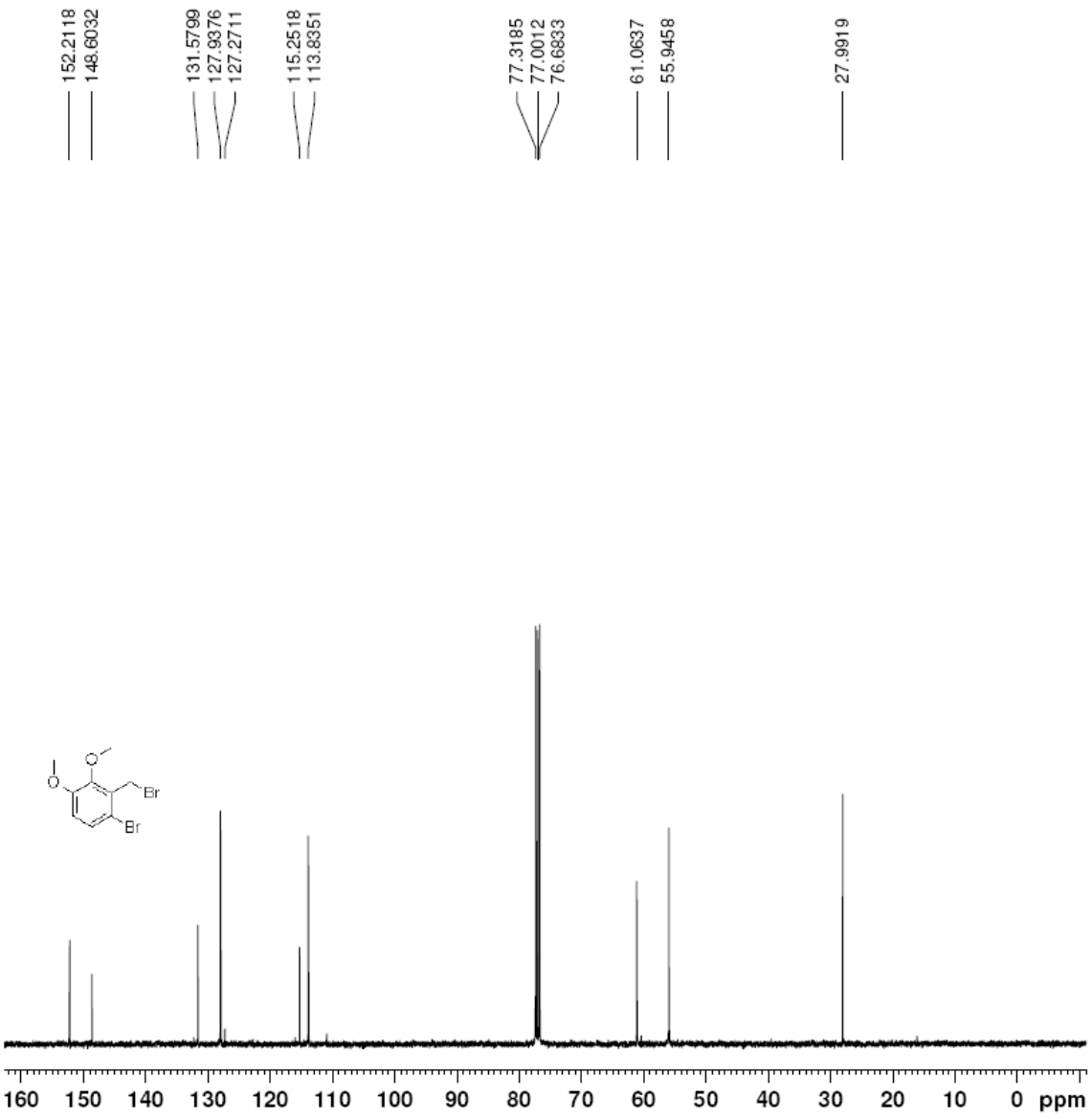

Figure S21. ^{13}C NMR spectrum of compound **7** ($CDCl_3$, 100 MHz).

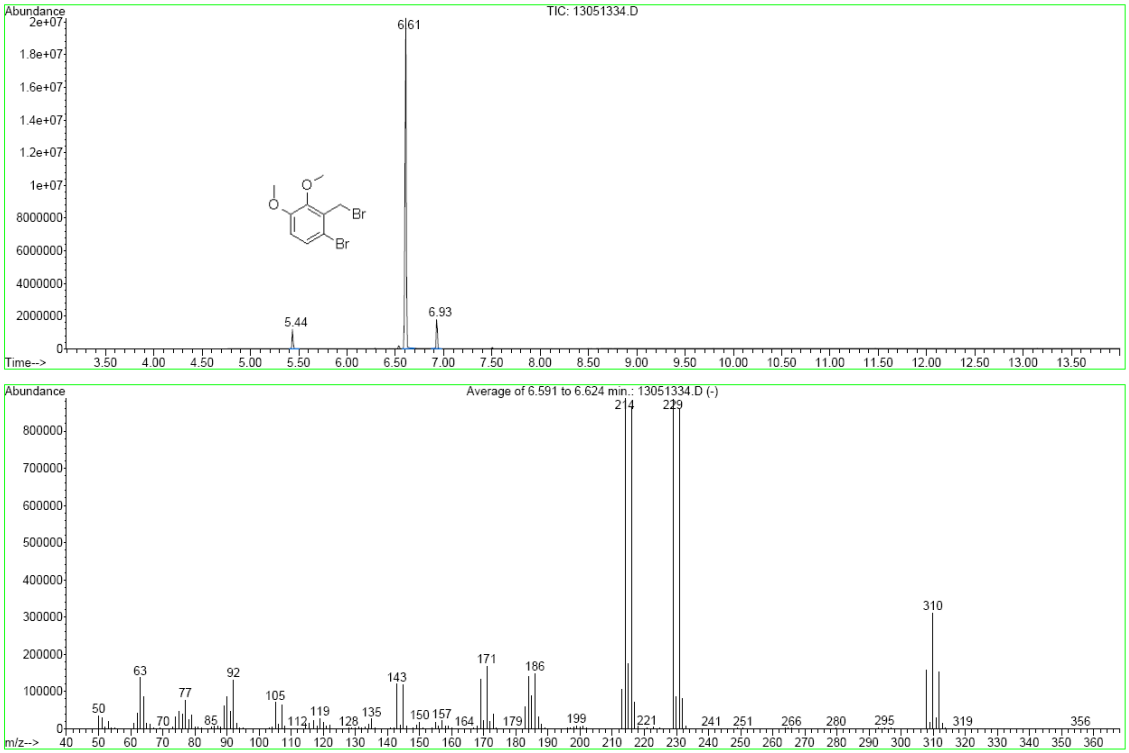

Figure S22. GC-MS spectrum of compound **7**.

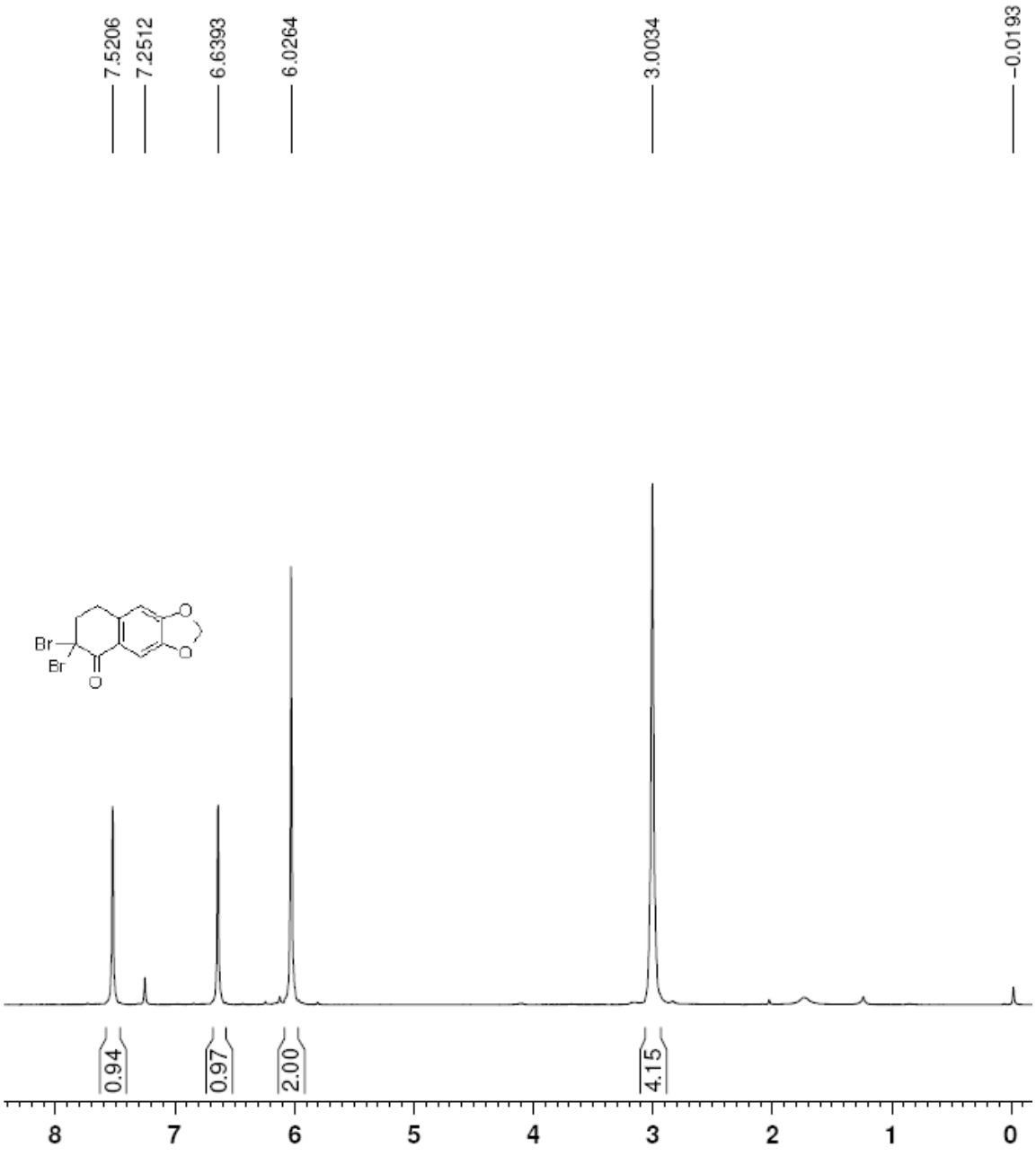

Figure S23. ^{1}H NMR spectrum of compound **12** ($CDCl_3$, 400 MHz).

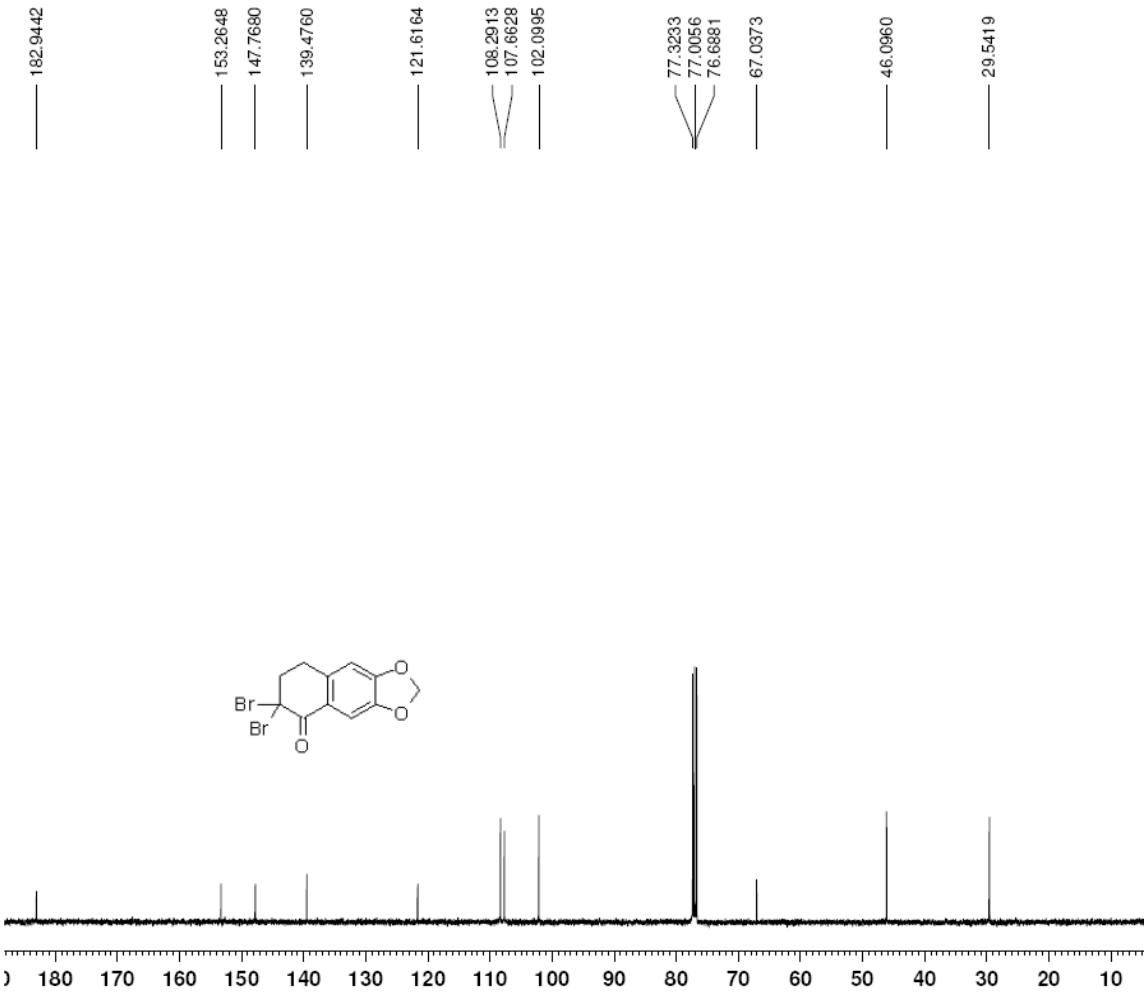

Figure S24. ^{13}C NMR spectrum of compound **12** ($CDCl_3$, 100 MHz).

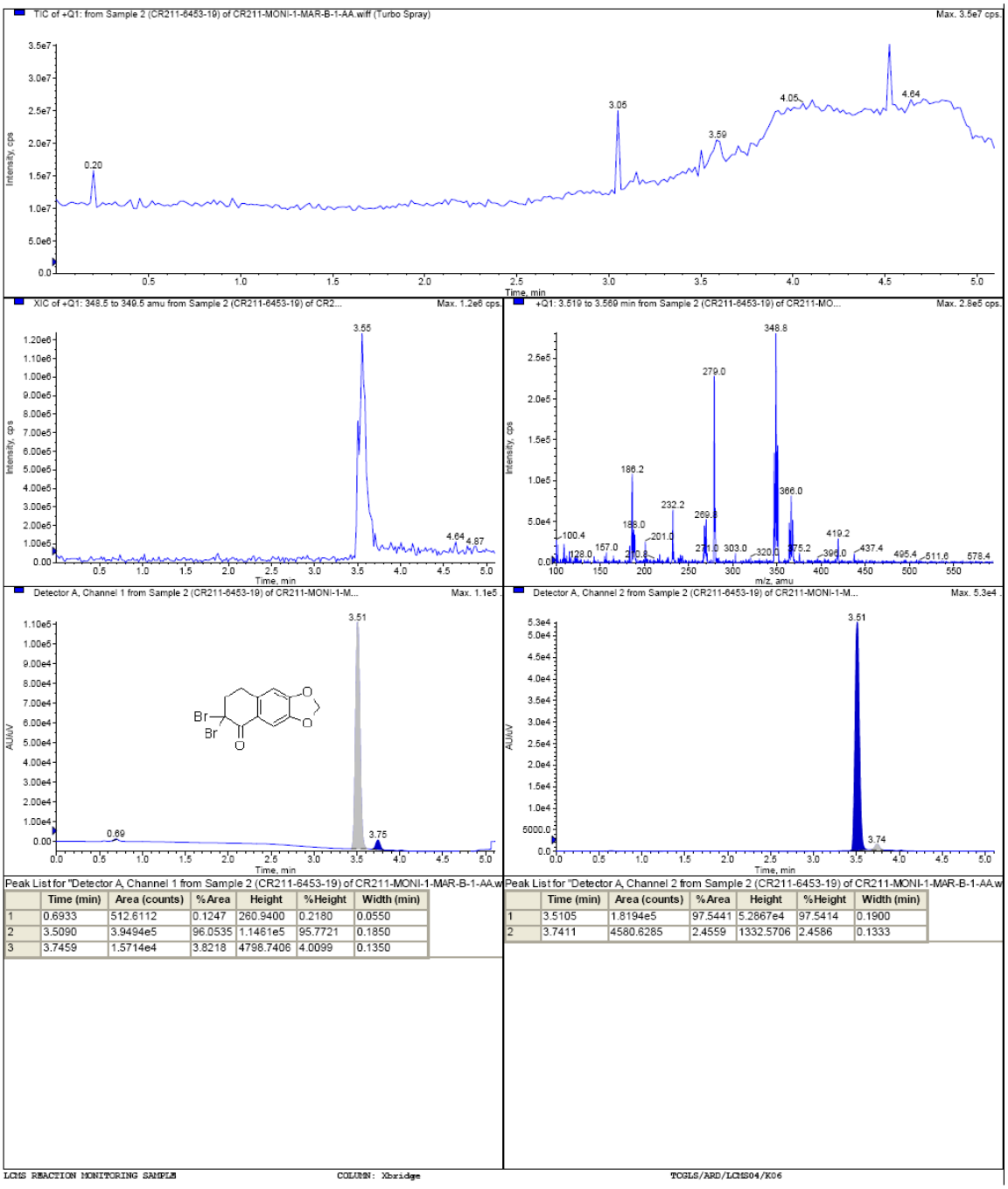

Peak List for "Detector A, Channel 1 from Sample 2 (CR211-6453-19) of CR211-MONI-1-MAR-B-1-AA.w

	Time (min)	Area (counts)	%Area	Height	%Height	Width (min)
1	0.6933	512.6112	0.1247	260.9400	0.2180	0.0550
2	3.5090	3.9494e5	96.0535	1.1461e5	95.7721	0.1850
3	3.7459	1.5714e4	3.8218	4798.7406	4.0099	0.1350

Peak List for "Detector A, Channel 2 from Sample 2 (CR211-6453-19) of CR211-MONI-1-MAR-B-1-AA.w

	Time (min)	Area (counts)	%Area	Height	%Height	Width (min)
1	3.5105	1.8194e5	97.5441	5.2867e4	97.5414	0.1900
2	3.7411	4580.6285	2.4559	1332.5706	2.4586	0.1333

Figure S25. LCMS spectrum of compound **12**

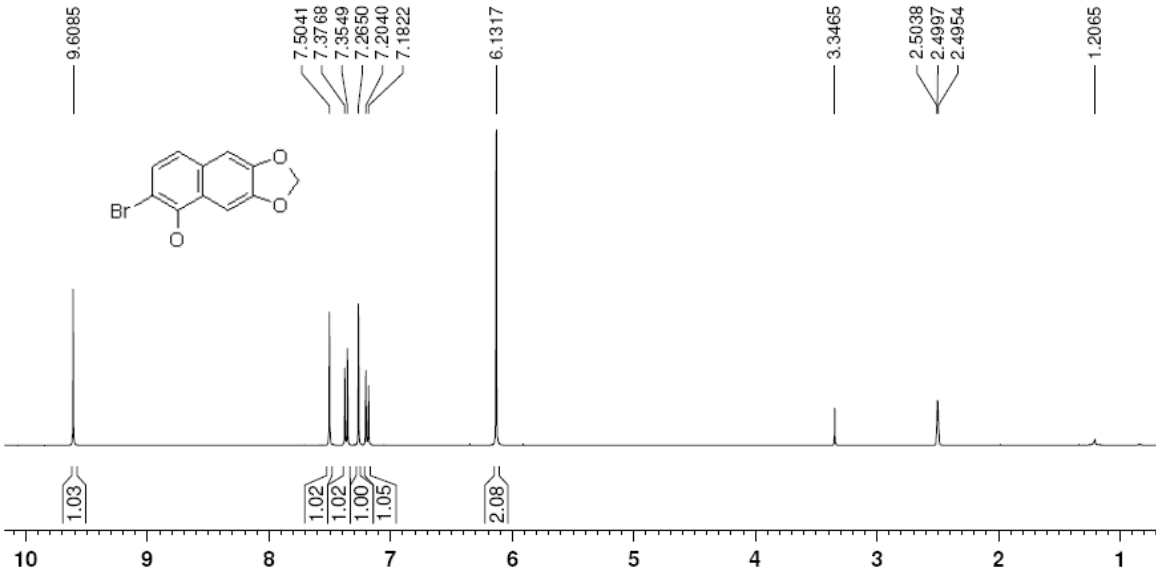

Figure S26. ^{1}H NMR spectrum of compound **13** (DMSO-d6, 400 MHz).

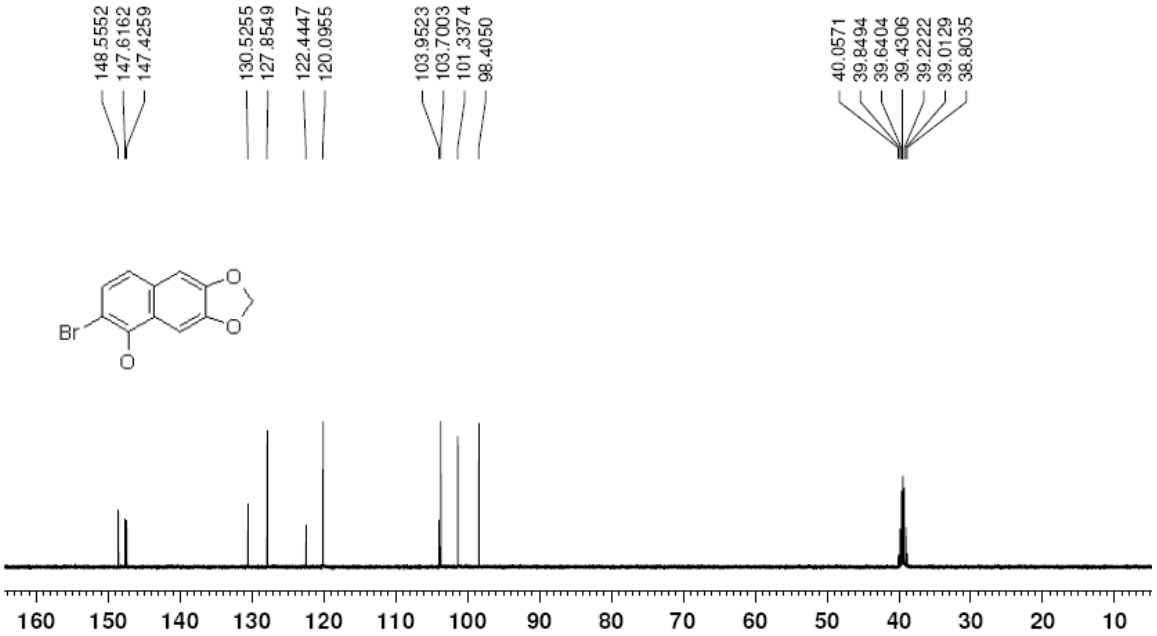

Figure S27. ^{13}C NMR spectrum of compound **13** (DMSO-d6, 100 MHz).

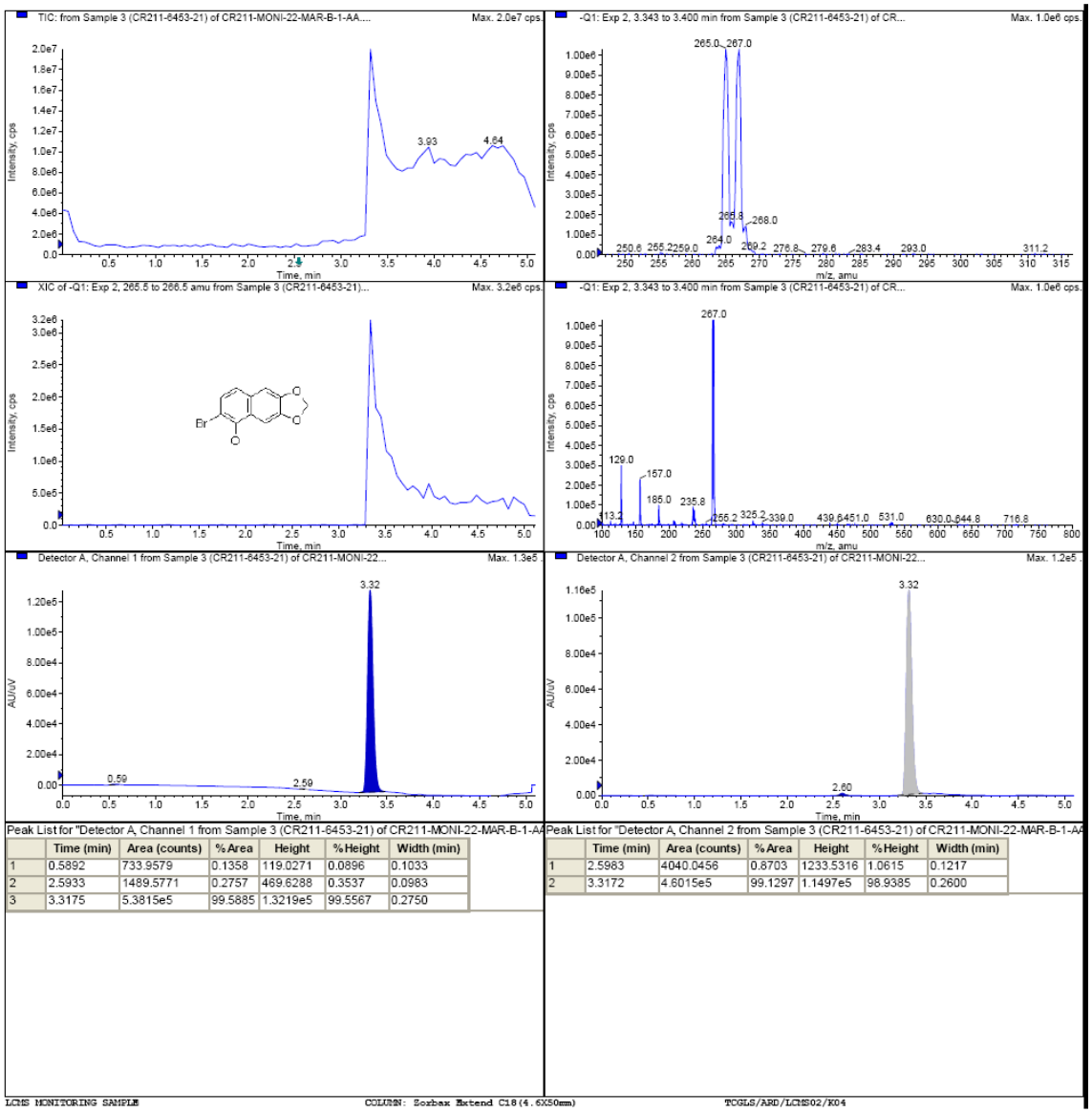

Figure S28. LCMS spectrum of compound **13**

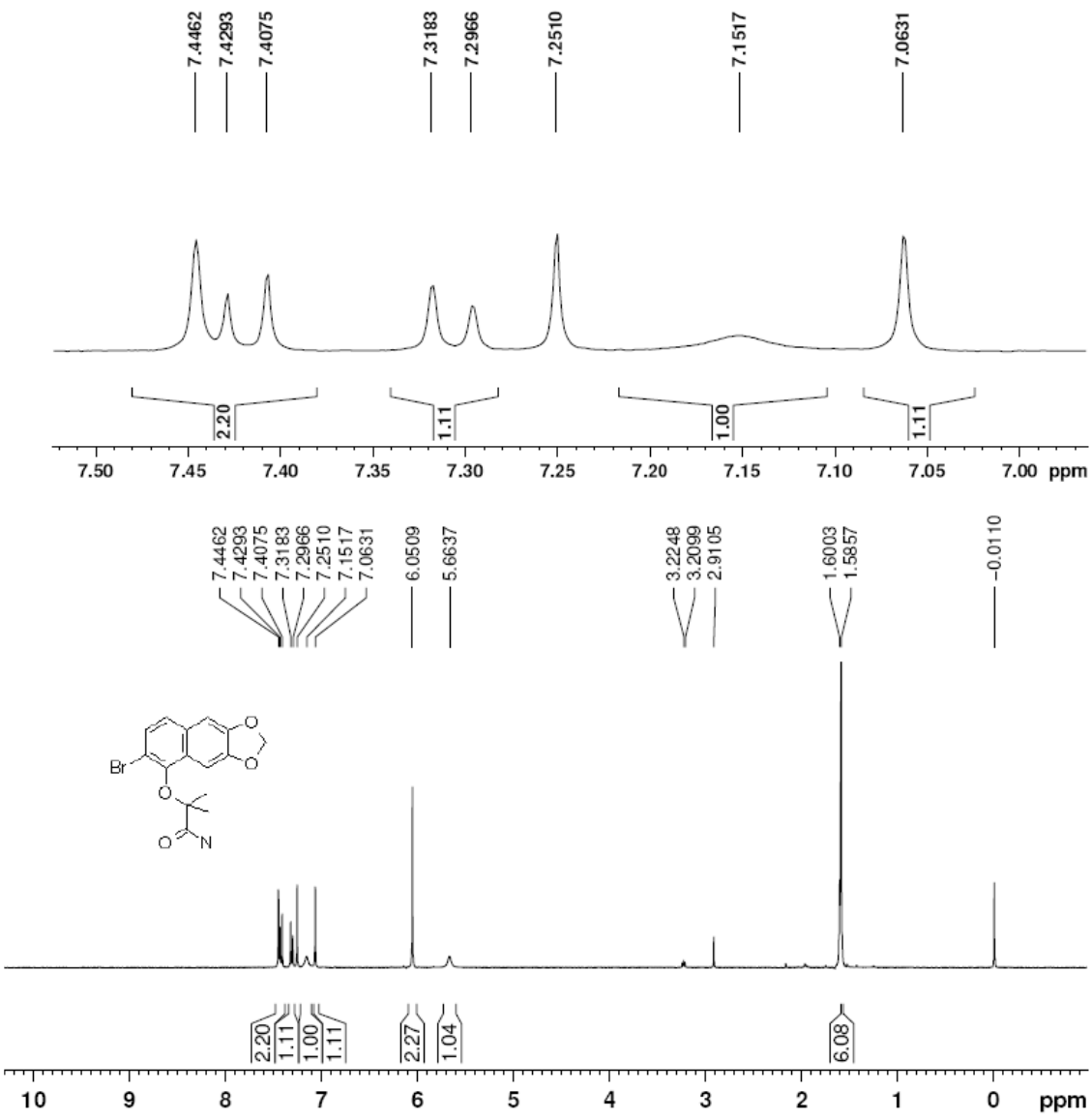

Figure S29. ^{1}H NMR spectrum of compound **14** ($CDCl_3$, 400 MHz).

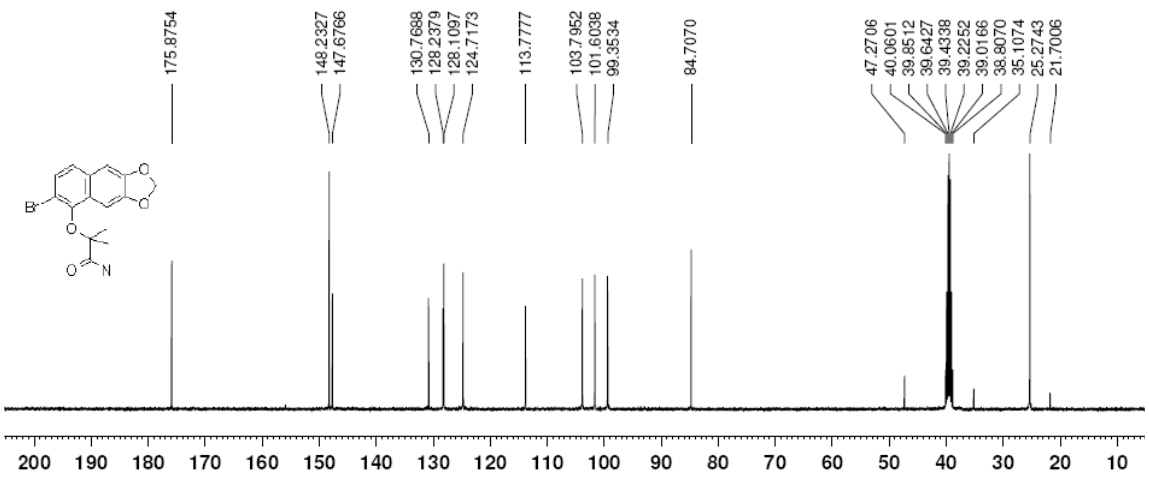

Figure S30. ^{13}C NMR spectrum of compound **14** (DMSO-d6, 100 MHz).

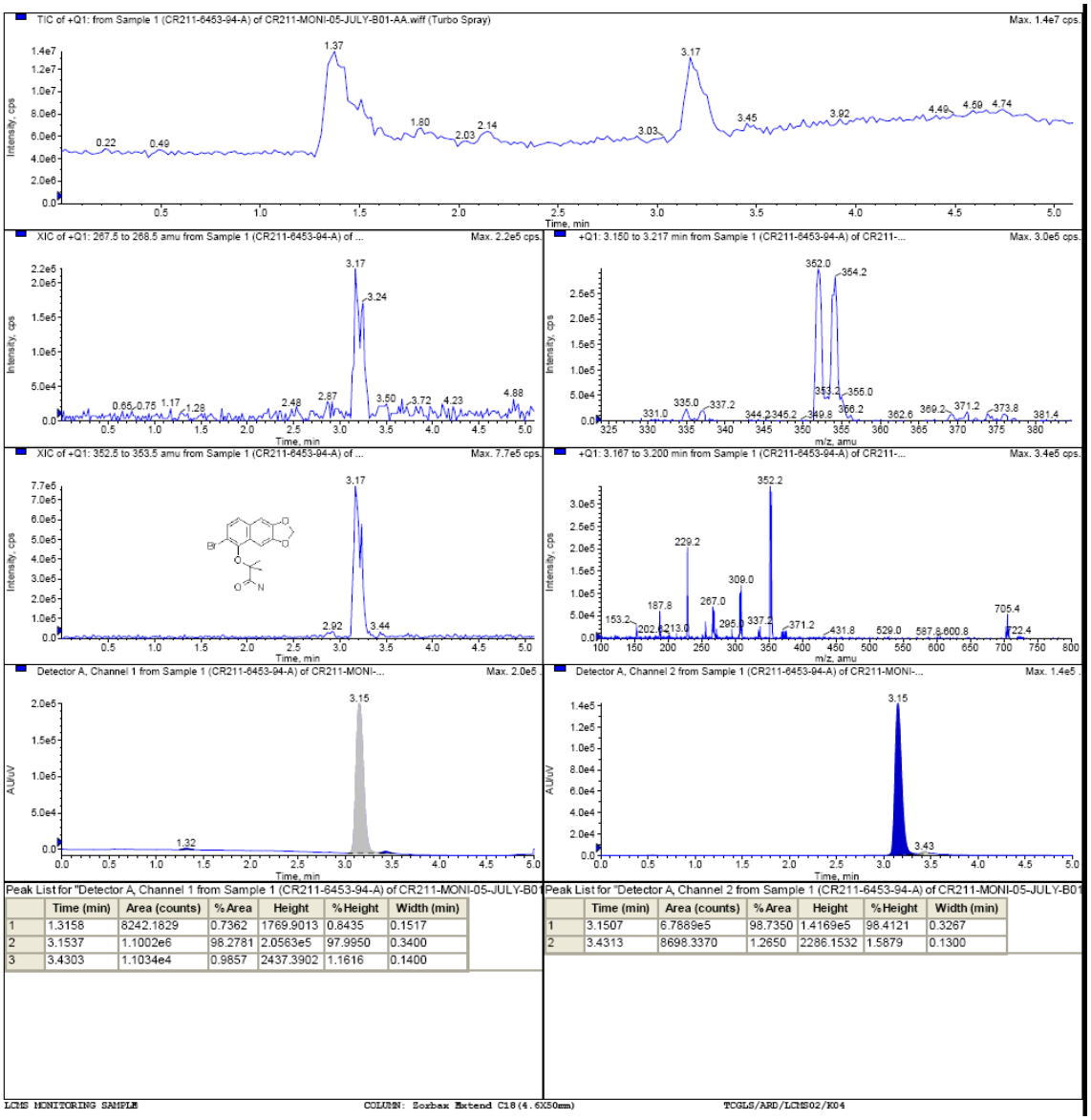

	Time (min)	Area (counts)	%Area	Height	%Height	Width (min)
1	1.3158	8242.1829	0.7362	1769.9013	0.8435	0.1517
2	3.1537	1.1002e6	98.2781	2.0563e5	97.9950	0.3400
3	3.4303	1.1034e4	0.9857	2437.3902	1.1616	0.1400

	Time (min)	Area (counts)	%Area	Height	%Height	Width (min)
1	3.1507	6.7889e5	98.7350	1.4169e5	98.4121	0.3267
2	3.4313	8698.3370	1.2650	2286.1532	1.5879	0.1300

Figure S31. LCMS spectrum of compound **14**

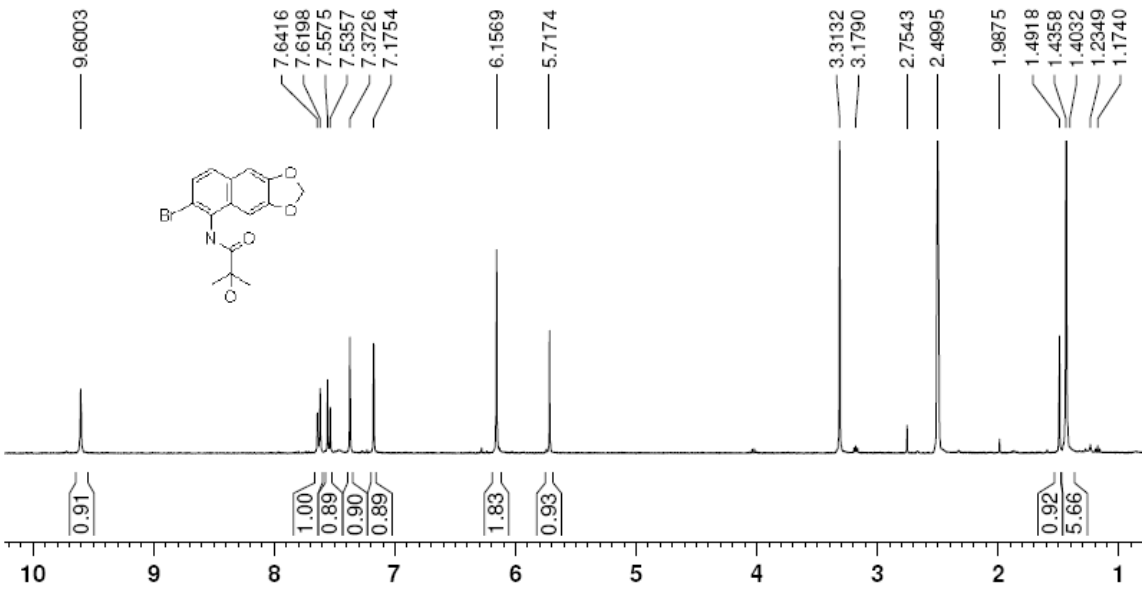

Figure S32. ^{1}H NMR spectrum of compound **15** (DMSO-d6, 400 MHz).

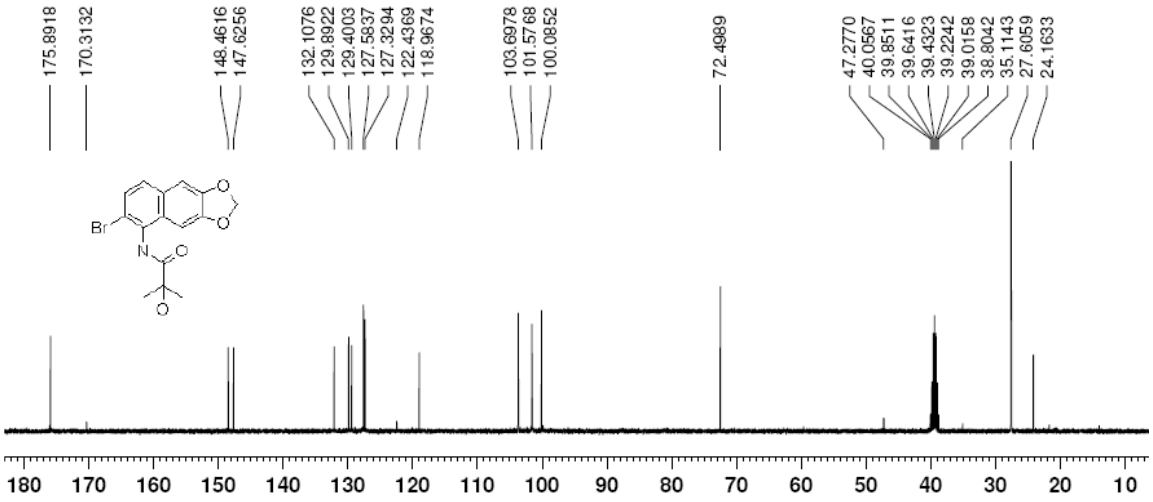

Figure S33. ^{13}C NMR spectrum of compound **15** (DMSO-d6, 100 MHz).

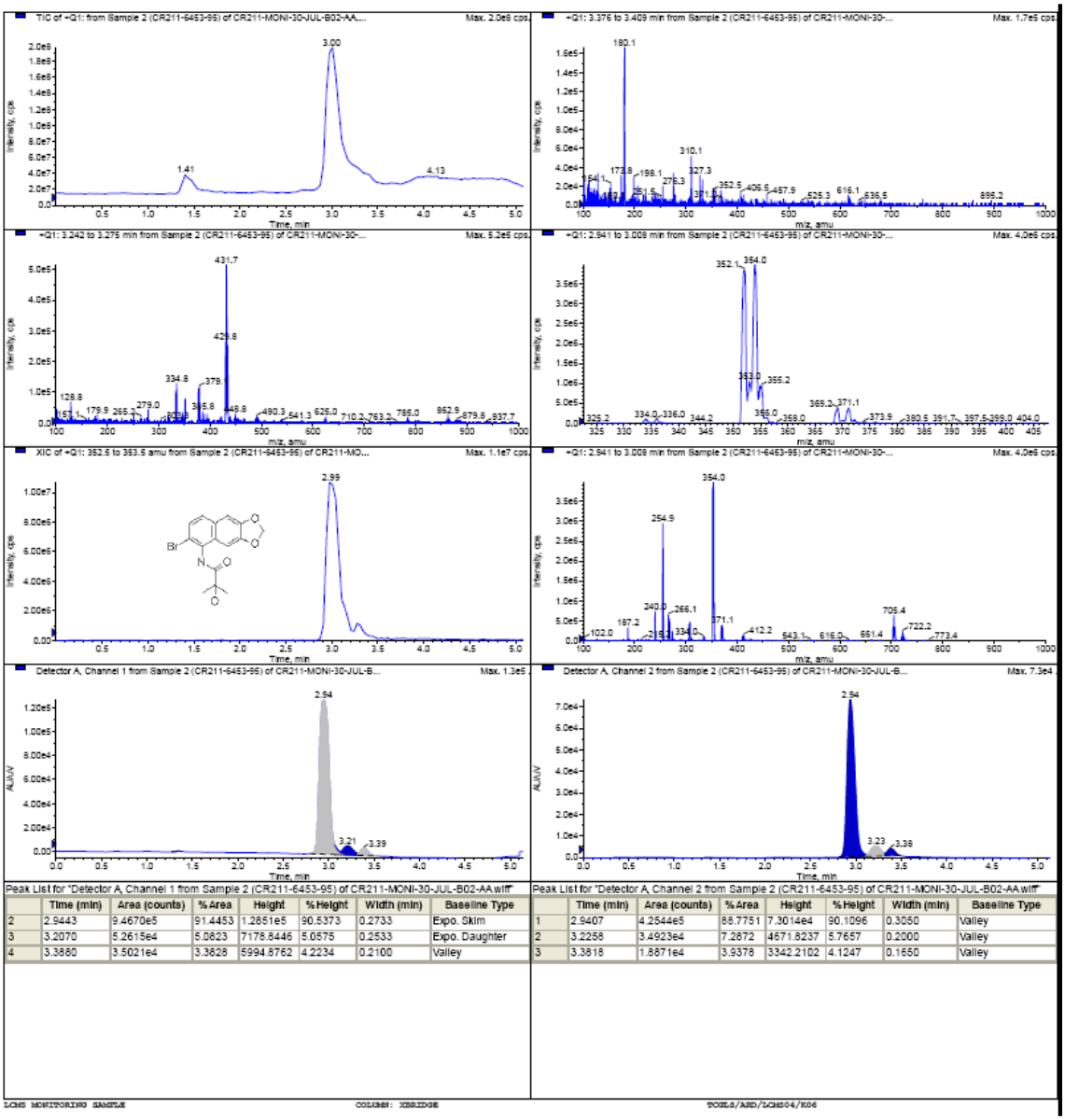

	Time (min)	Area (counts)	% Area	Height	% Height	Width (min)	Baseline Type
2	2.9443	9.4670e5	91.4453	1.2851e5	90.5373	0.2733	Expo. Skim
3	3.2070	5.2615e4	5.0823	7178.8446	5.0575	0.2533	Expo. Daughter
4	3.3880	3.5021e4	3.3828	5994.8762	4.2234	0.2100	Valley

	Time (min)	Area (counts)	% Area	Height	% Height	Width (min)	Baseline Type
1	2.9407	4.2544e5	88.7751	7.3014e4	90.1096	0.3050	Valley
2	3.2258	3.4923e4	7.2872	4671.8237	5.7657	0.2000	Valley
3	3.3818	1.8871e4	3.9378	3342.2102	4.1247	0.1650	Valley

Figure S34. LCMS spectrum of compound **15**

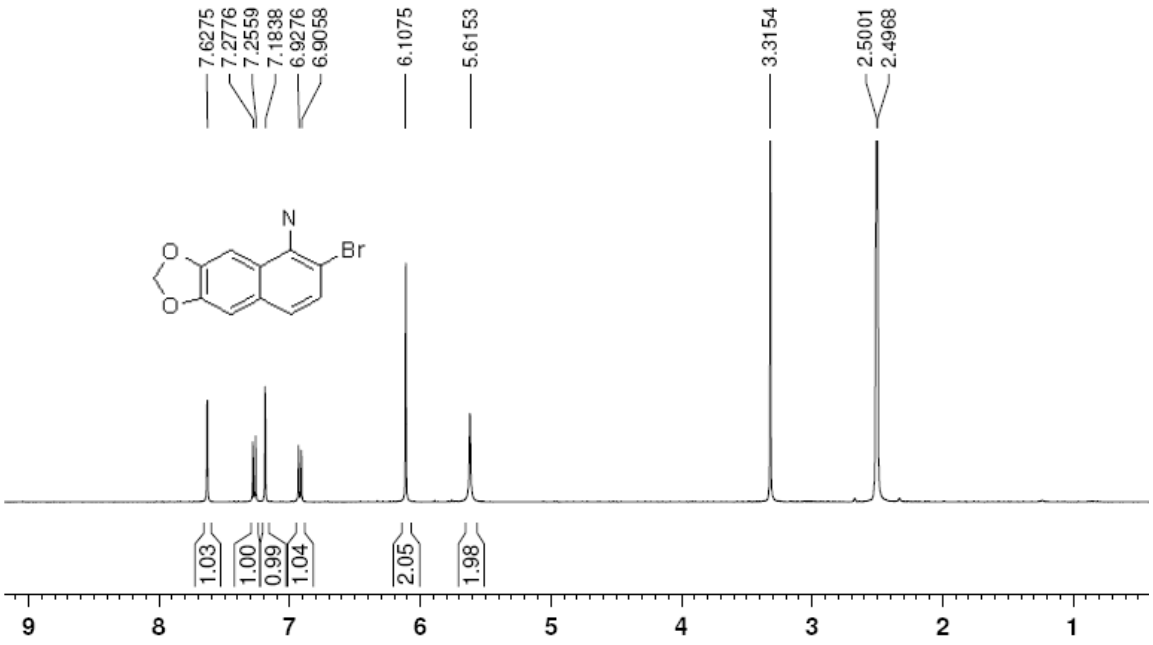

Figure S35. ^{1}H NMR spectrum of compound **6** (DMSO-d6, 400 MHz).

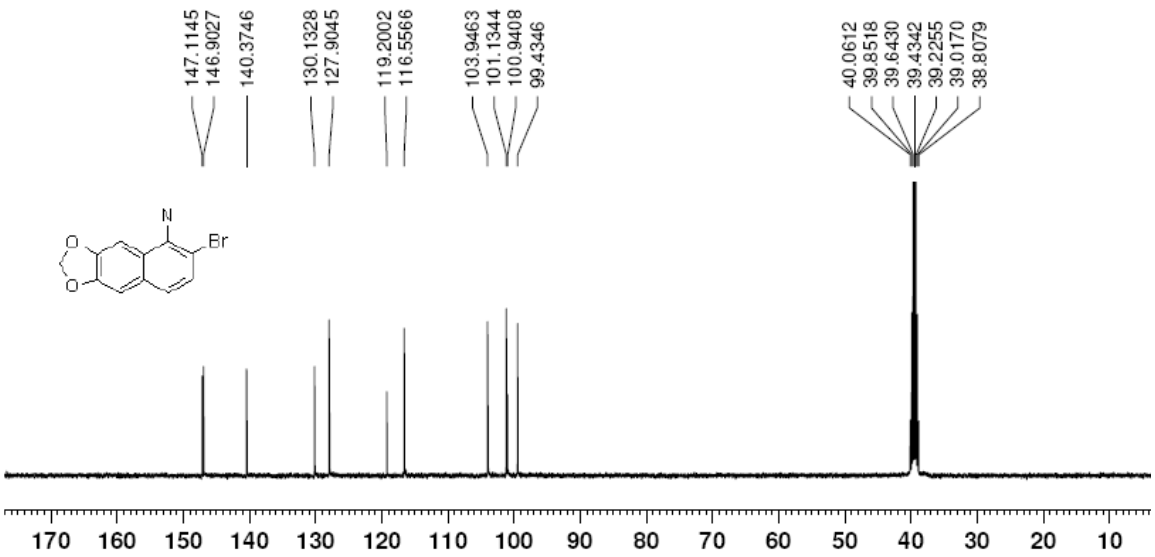

Figure S36. ^{13}C NMR spectrum of compound **6** (DMSO-d6, 100 MHz).

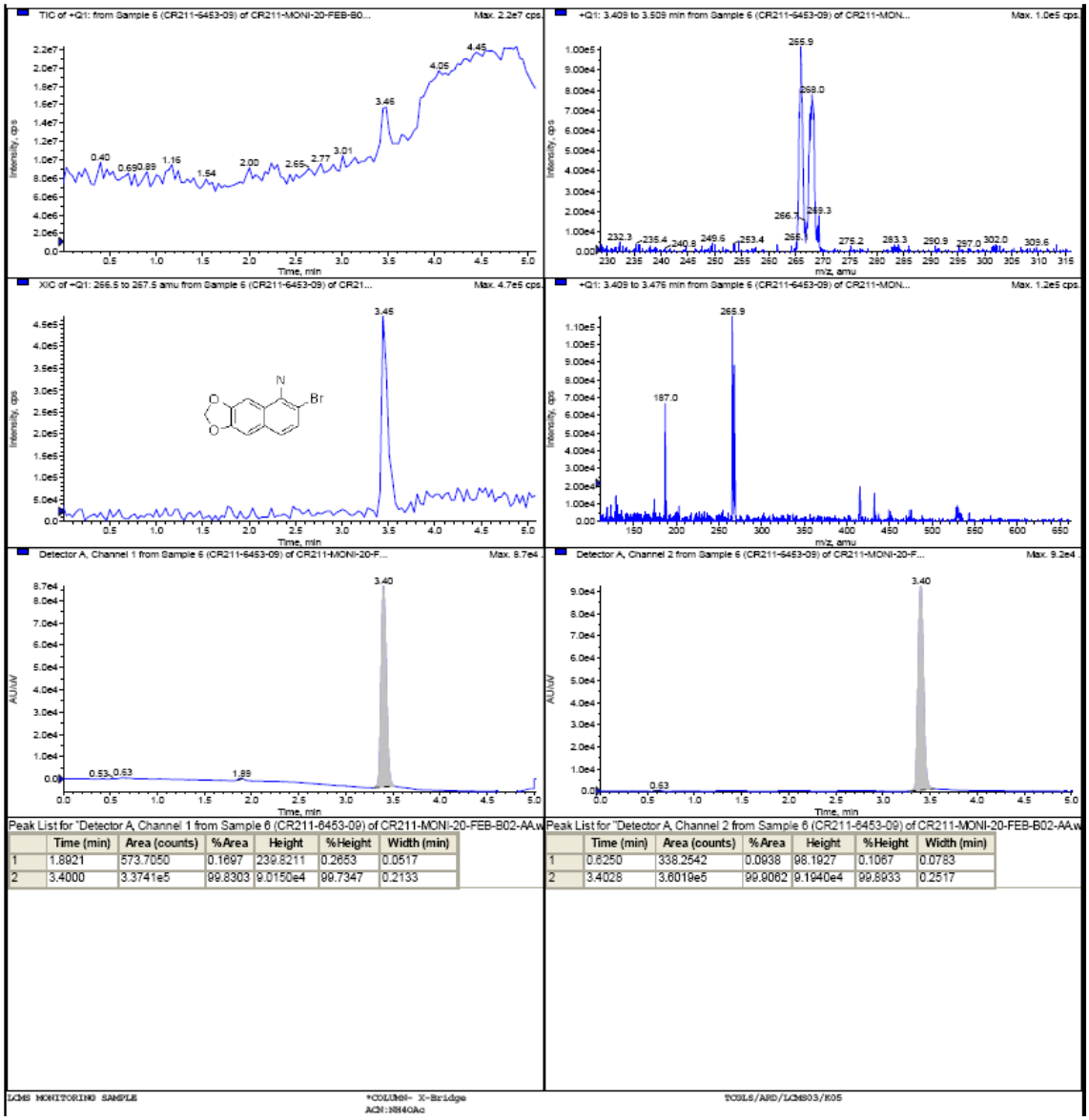

	Time (min)	Area (counts)	%Area	Height	%Height	Width (min)
1	1.8921	573.7050	0.1697	239.8211	0.2653	0.0517
2	3.4000	3.3741e5	99.8303	9.0150e4	99.7347	0.2133

	Time (min)	Area (counts)	%Area	Height	%Height	Width (min)
1	0.6250	338.2542	0.0938	98.1927	0.1067	0.0783
2	3.4028	3.6019e5	99.9062	9.1940e4	99.8933	0.2517

Figure S37. LCMS spectrum of compound **6**

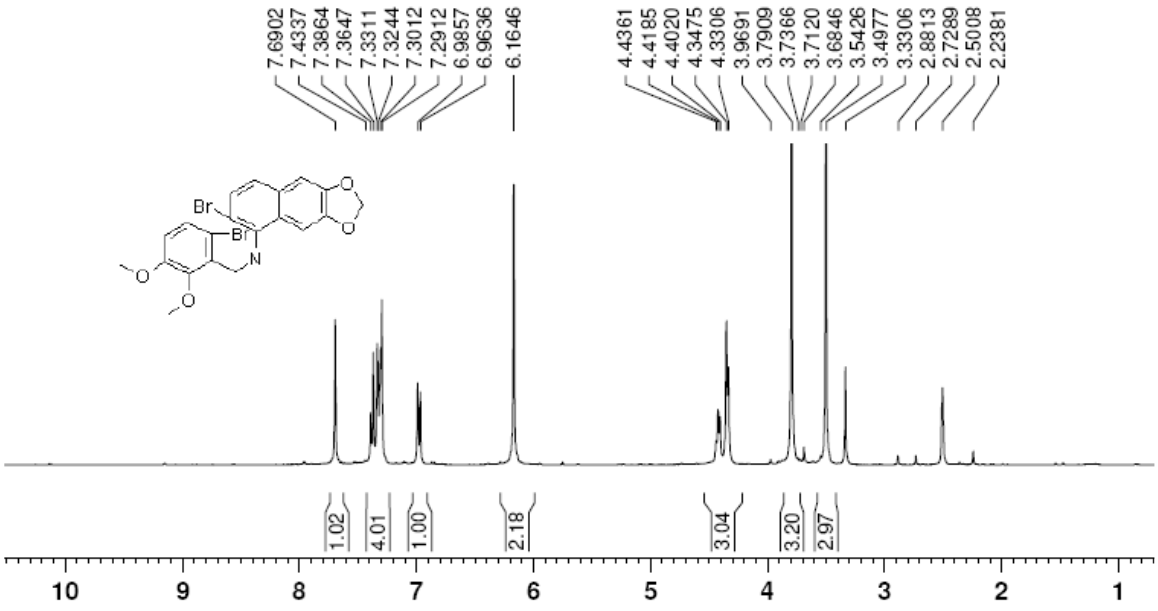

Figure S38. ^{1}H NMR spectrum of compound **16** (DMSO-d6, 400 MHz).

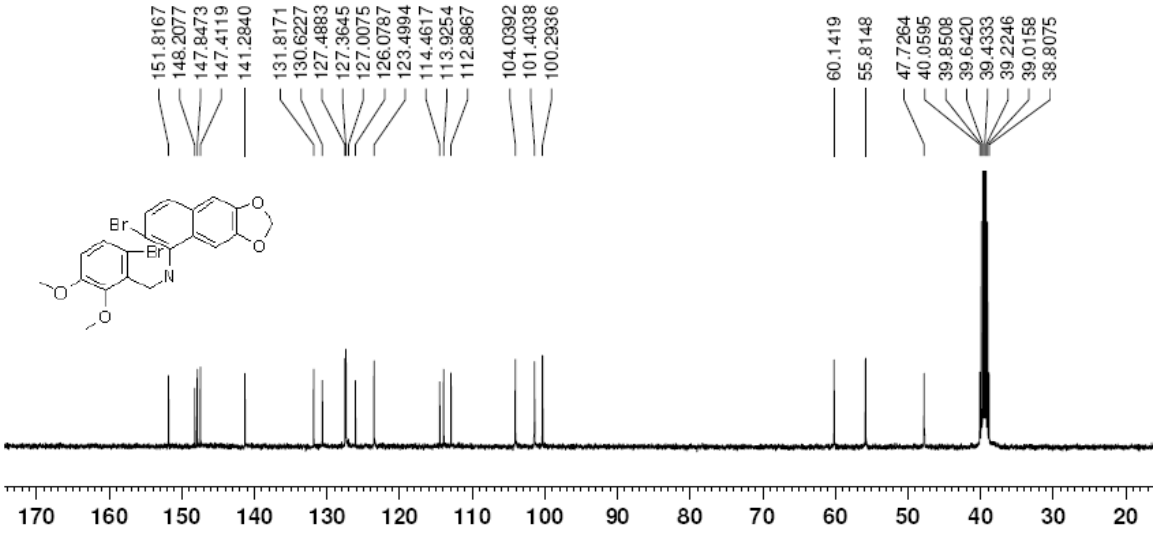

Figure S39. ^{13}C NMR spectrum of compound **16** (DMSO-d6, 100 MHz).

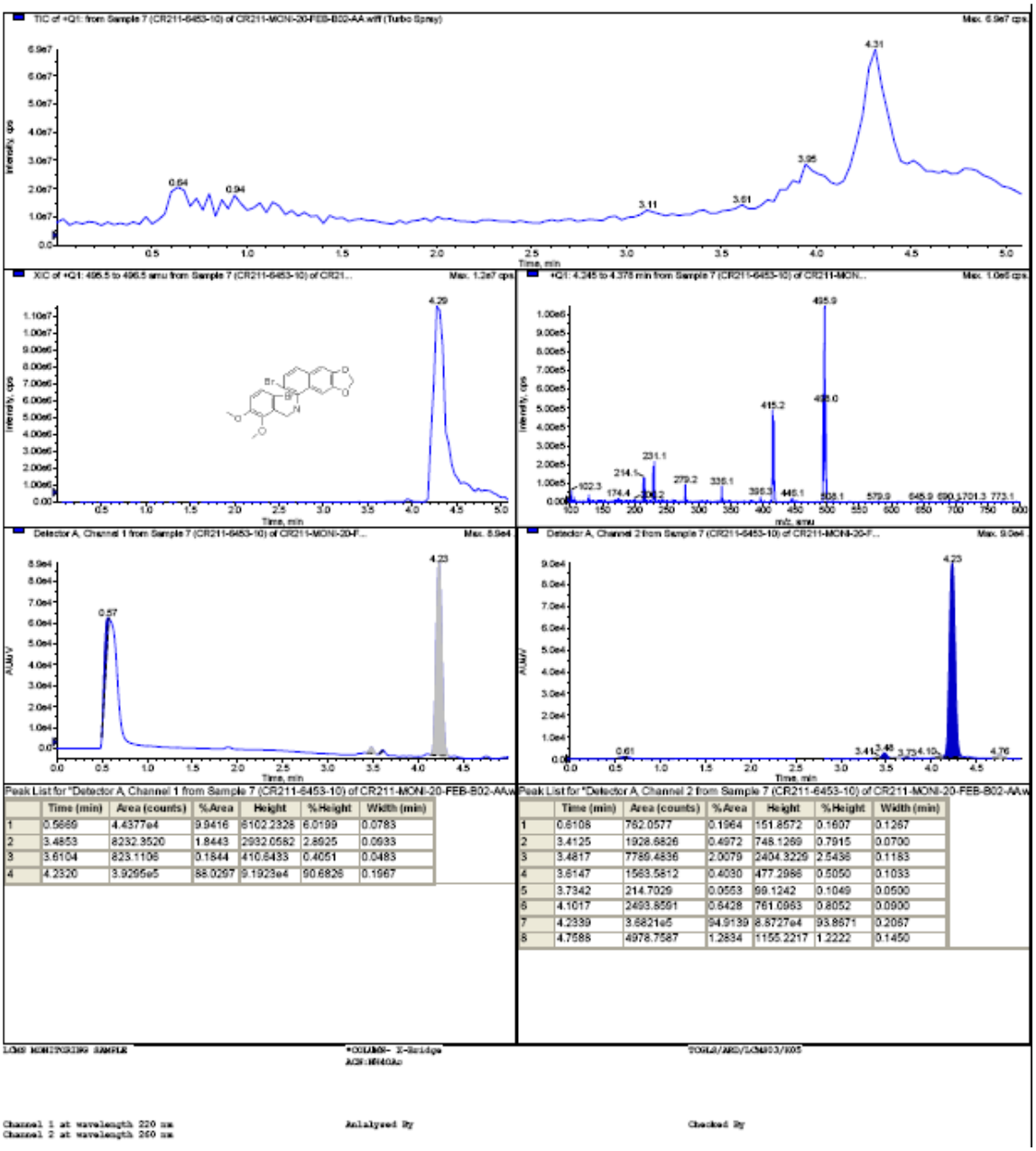

	Time (min)	Area (counts)	%Area	Height	%Height	Width (min)
1	0.5689	4.4377e4	9.9416	6102.2328	6.0199	0.0783
2	3.4853	8232.3520	1.8443	2932.0582	2.8925	0.0933
3	3.6104	823.1106	0.1844	410.8433	0.4051	0.0483
4	4.2320	3.9265e5	88.0297	9.1923e4	90.6826	0.1967

	Time (min)	Area (counts)	%Area	Height	%Height	Width (min)
1	0.6108	762.0577	0.1964	151.8572	0.1607	0.1267
2	3.4125	1928.6826	0.4972	748.1269	0.7915	0.0700
3	3.4817	7789.4836	2.0079	2404.3229	2.5436	0.1183
4	3.6147	1563.5812	0.4030	477.2986	0.5050	0.1033
5	3.7342	214.7029	0.0553	99.1242	0.1049	0.0500
6	4.1017	2493.8591	0.6428	761.0953	0.8052	0.0900
7	4.2339	3.6821e5	94.9139	8.8727e4	93.8871	0.2067
8	4.7588	4978.7587	1.2834	1155.2217	1.2222	0.1450

Figure S40. LCMS spectrum of compound **16**

Data File	SR-21416-14.d	**Sample Name**	SR-21416-14
Sample Type	Sample	**Position**	Vial 22
Instrument Name	Agilent 6530 Accurate-Mass Q-TOF	**User Name**	
Acq Method	Direct Mass.m	**Acquired Time**	21-04-2016 17:34:37
IRM Calibration Status	Success	**DA Method**	Regular.m
Comment			

Sample Group	**Info.**
Acquisition SW Version	6200 series TOF/6500 series Q-TOF B.05.00 (B5042.1)

Compound Table

Compound Label	RT	Mass	Abund	Formula	Tgt Mass	Diff (ppm)	MFG Formula	DB Formula
Cpd 1: C20 H17 Br2 N O4	1.171	492.9571	4720	C20 H17 Br2 N O4	492.9524	9.43	C20 H17 Br2 N O4	C20 H17 Br2 N O4

Compound Label	*m/z*	RT	Algorithm	Mass
Cpd 1: C20 H17 Br2 N O4	495.9624	1.171	Find By Formula	492.9571

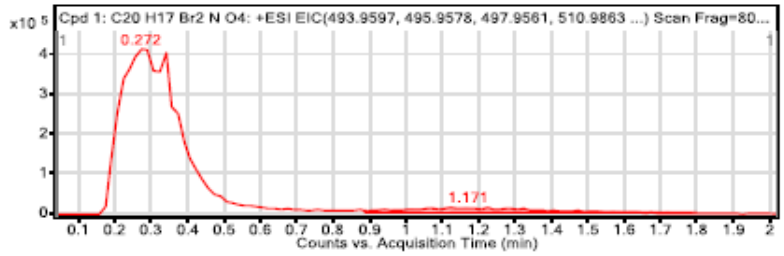

MS Spectrum

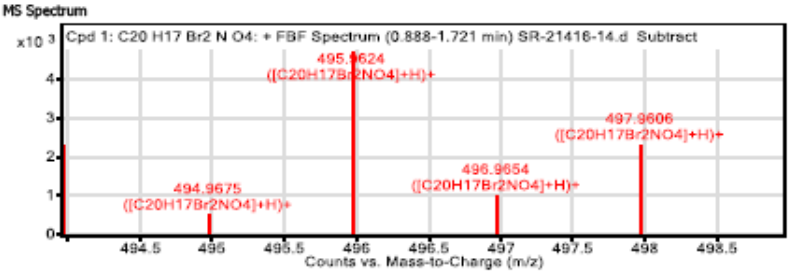

MS Zoomed Spectrum

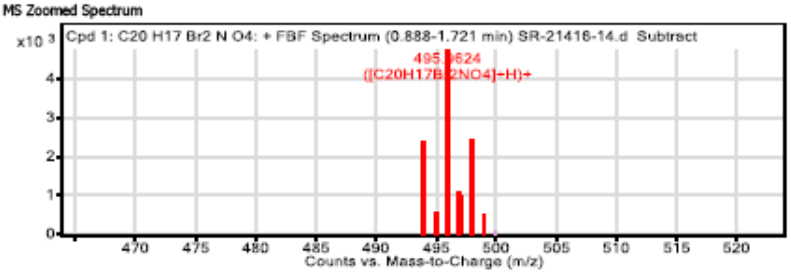

MS Spectrum Peak List

m/z	z	Abund	Formula	Ion
493.9646	1	2334.29	C20H17Br2NO4	(M+H)+
494.9675	1	523.72	C20H17Br2NO4	(M+H)+
495.9624	1	4720.12	C20H17Br2NO4	(M+H)+
496.9654	1	1023.14	C20H17Br2NO4	(M+H)+
497.9606	1	2325.37	C20H17Br2NO4	(M+H)+
498.9642	1	526.38	C20H17Br2NO4	(M+H)+

Figure S41. HRMS spectrum of compound **16**

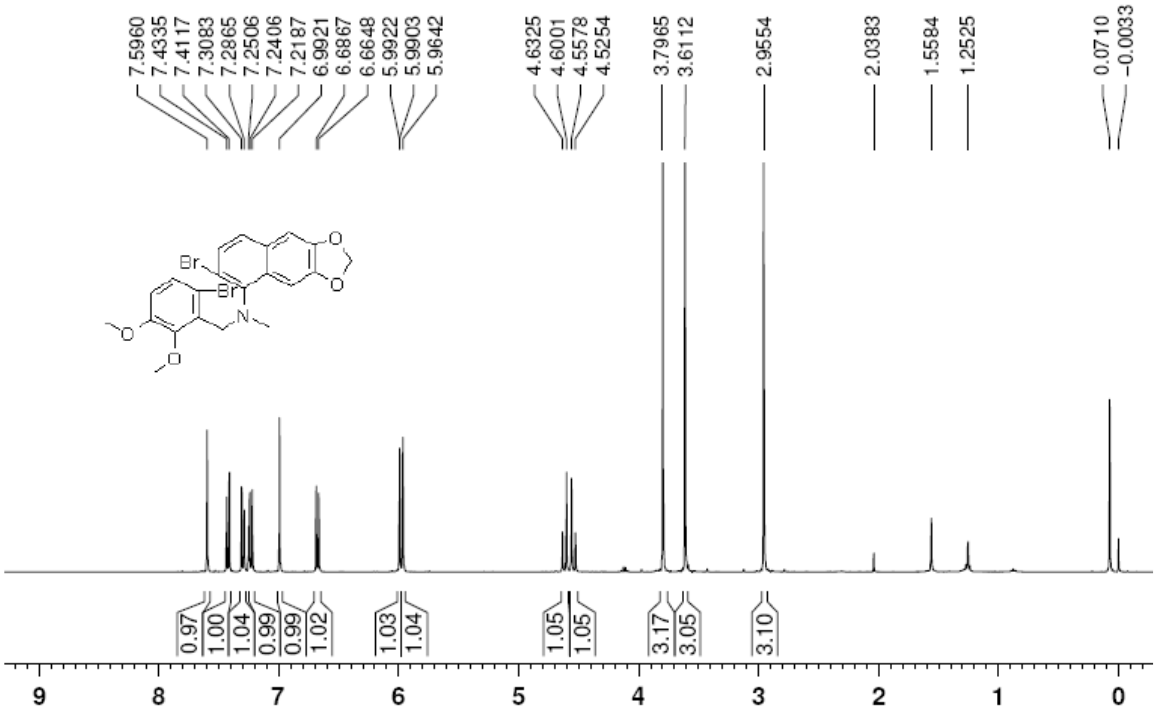

Figure S42. ^{1}H NMR spectrum of compound **5** ($CDCl_3$, 400 MHz).

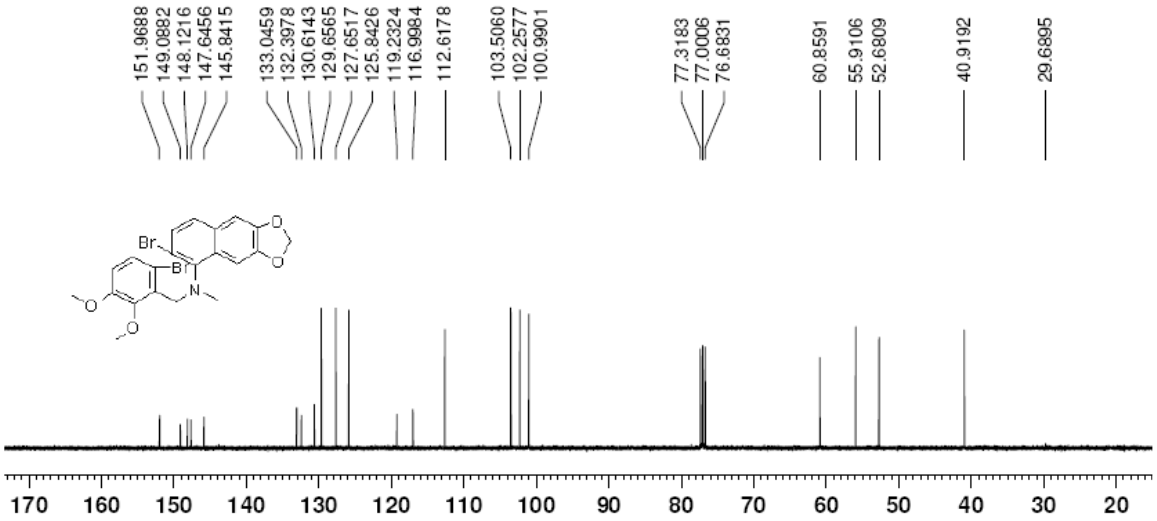

Figure S43. ^{13}C NMR spectrum of compound **5** ($CDCl_3$, 100 MHz).

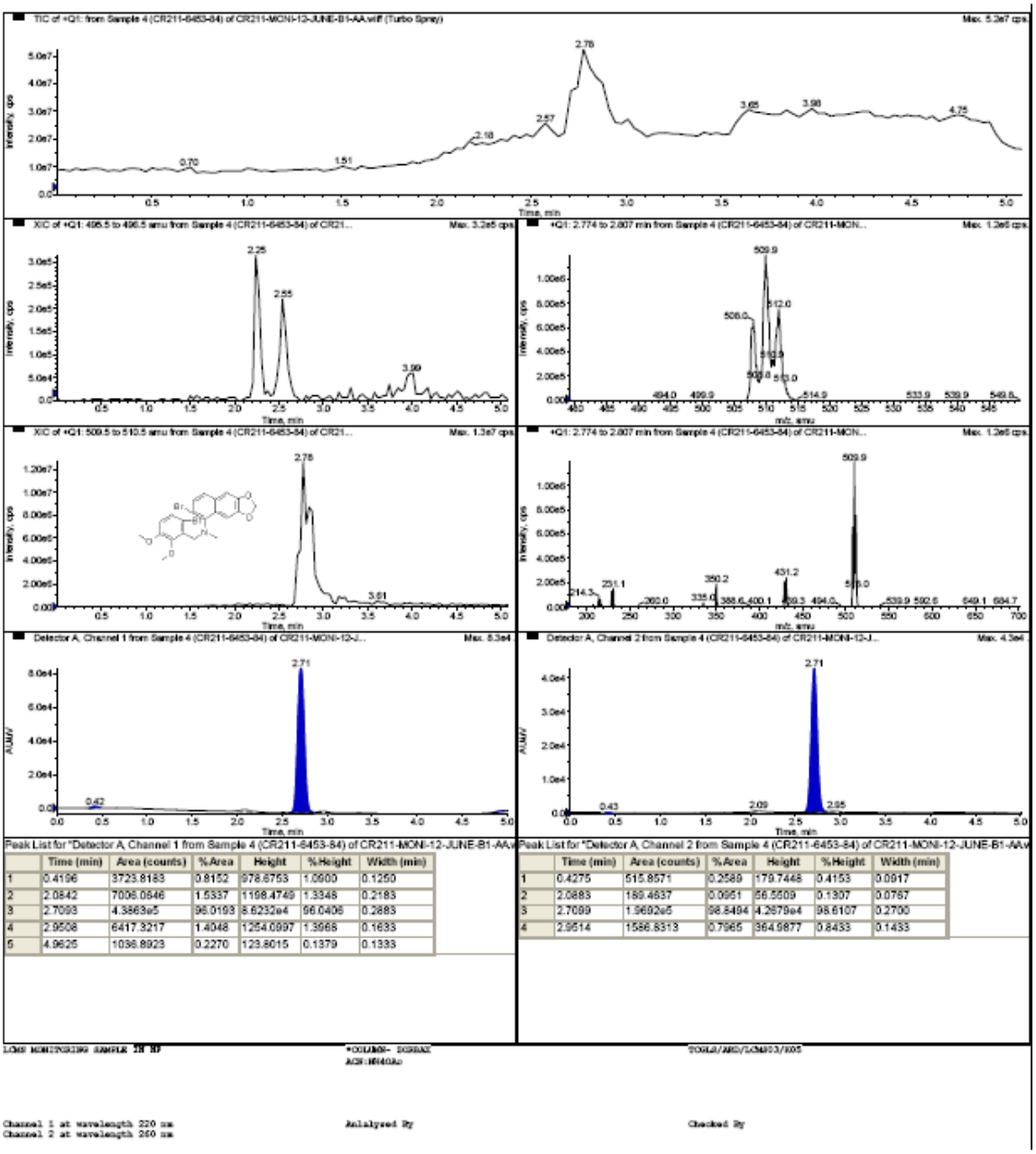

Figure S44. LCMS spectrum of compound **5**

Data File	SR-21416-15.d	**Sample Name**	SR-21416-15
Sample Type	Sample	**Position**	Vial 23
Instrument Name	Agilent 6530 Accurate-Mass Q-TOF	**User Name**	
Acq Method	Direct Mass.m	**Acquired Time**	21-04-2016 17:38:07
IRM Calibration Status	Success	**DA Method**	Regular.m
Comment			

Sample Group	**Info.**
Acquisition SW Version	6200 series TOF/6500 series Q-TOF B.05.00 (B5042.1)

Compound Table

Compound Label	RT	Mass	Abund	Formula	Tgt Mass	Diff (ppm)	MFG Formula	DB Formula
Cpd 1: C21 H19 Br2 N O4	0.2	506.9731	8327	C21 H19 Br2 N O4	506.9681	9.89	C21 H19 Br2 N O4	C21 H19 Br2 N O4

Compound Label	*m/z*	RT	Algorithm	Mass
Cpd 1: C21 H19 Br2 N O4	531.9602	0.2	Find By Formula	506.9731

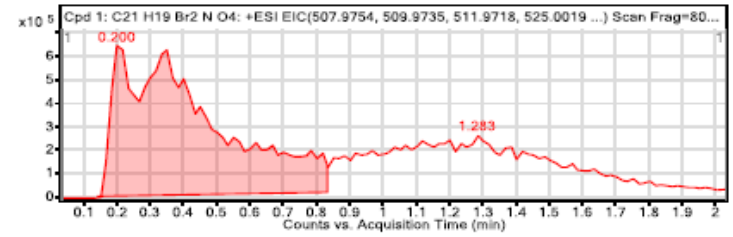

MS Spectrum

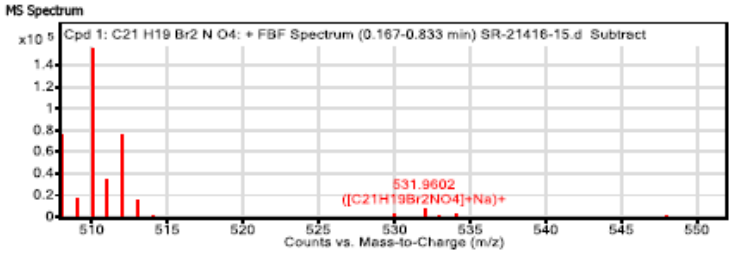

MS Zoomed Spectrum

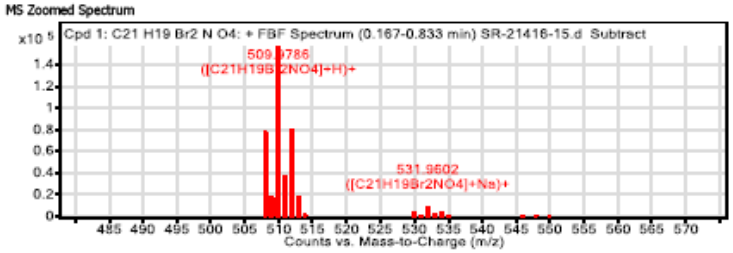

MS Spectrum Peak List

m/z	z	Abund	Formula	Ion
507.9803	1	77448.7	C21H19Br2NO4	(M+H)+
508.9835	1	17529.53	C21H19Br2NO4	(M+H)+
509.9786	1	156207.02	C21H19Br2NO4	(M+H)+
510.9815	1	34533.4	C21H19Br2NO4	(M+H)+
511.9769	1	77642.83	C21H19Br2NO4	(M+H)+
512.9796	1	17041.12	C21H19Br2NO4	(M+H)+
529.9621	1	4197.66	C21H19Br2NO4	(M+Na)+
531.9602	1	8327.36	C21H19Br2NO4	(M+Na)+
533.9584	1	4373.17	C21H19Br2NO4	(M+Na)+
545.9355	1	779.91	C21H19Br2NO4	(M+K)+

--- End Of Report ---

Figure S45. HRMS spectrum of compound **5**

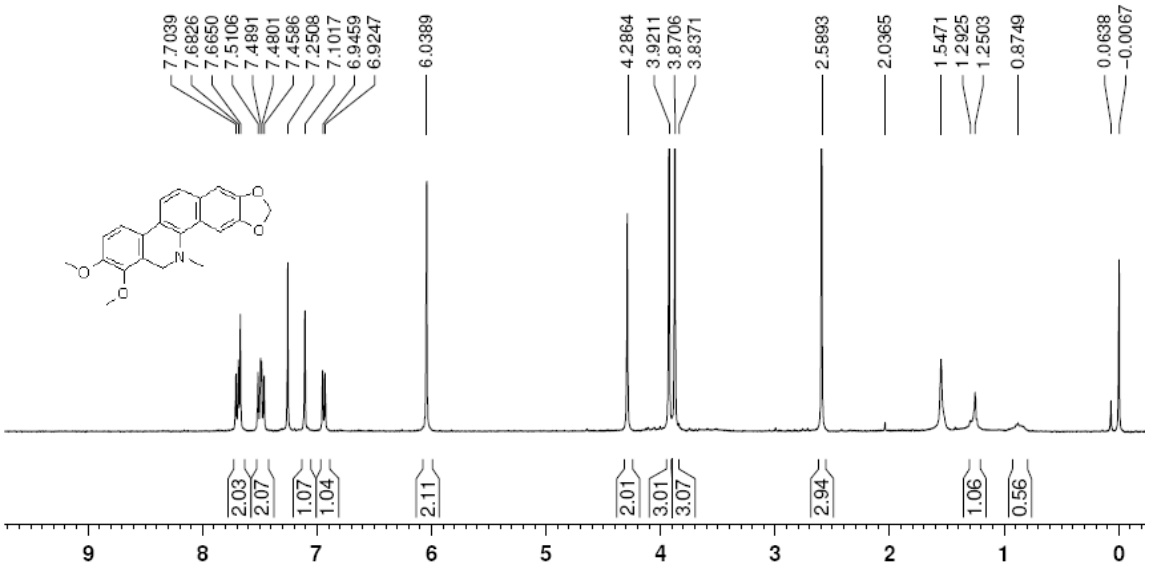

Figure S46. ^{1}H NMR spectrum of compound **4** ($CDCl_3$, 400 MHz).

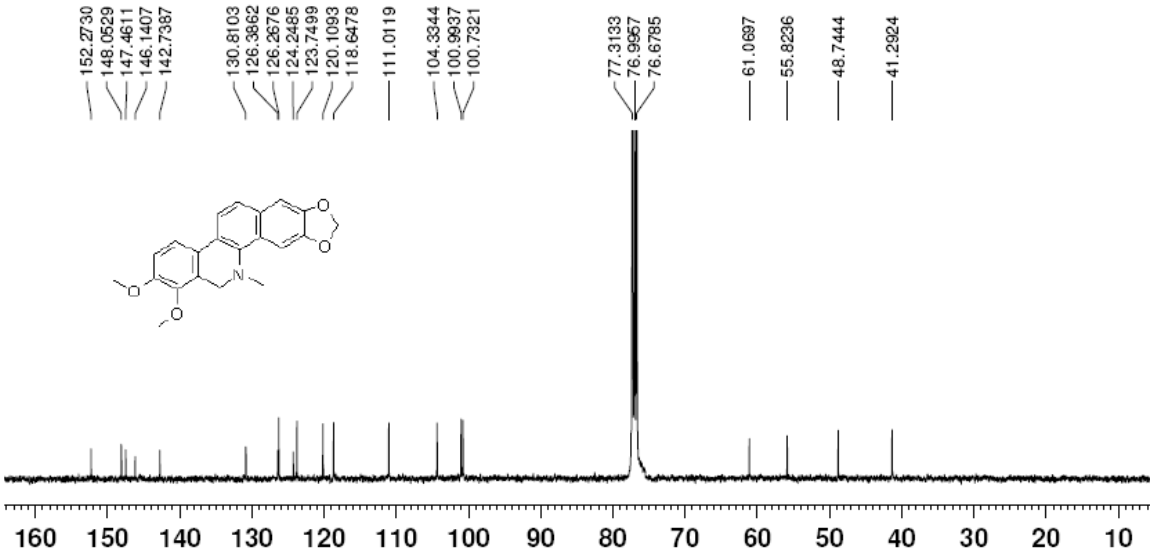

Figure S47. ^{13}C NMR spectrum of compound **4** ($CDCl_3$, 100 MHz).

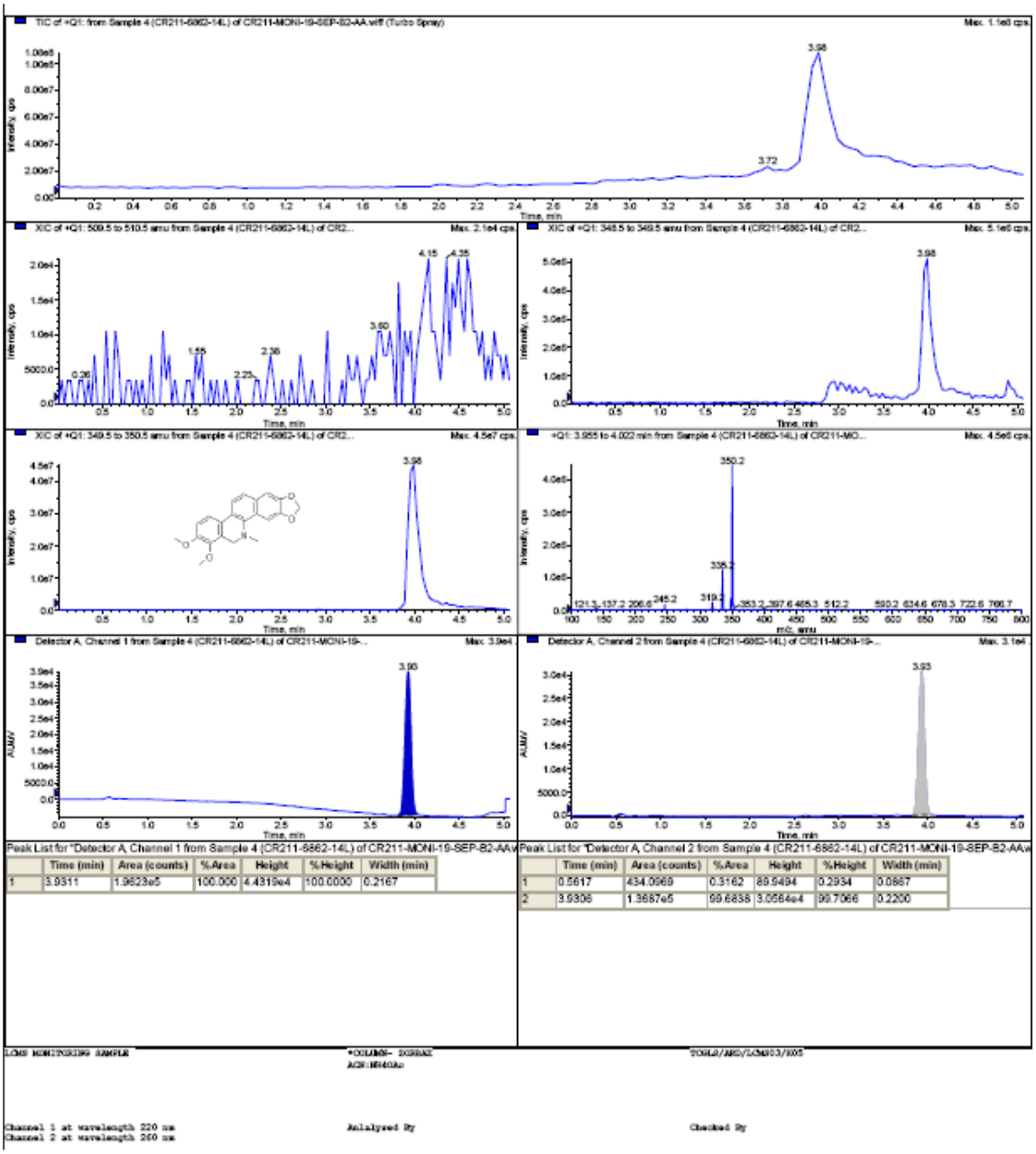

Figure S48. LCMS spectrum of compound **4**

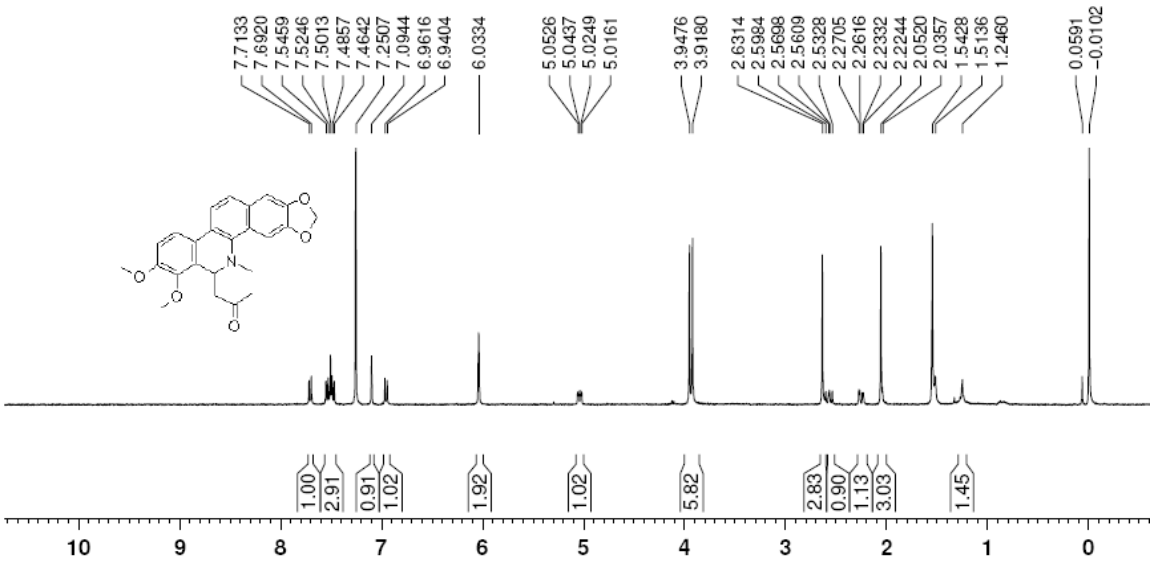

Figure S49. ^{1}H NMR spectrum of compound **3** ($CDCl_3$, 400 MHz).

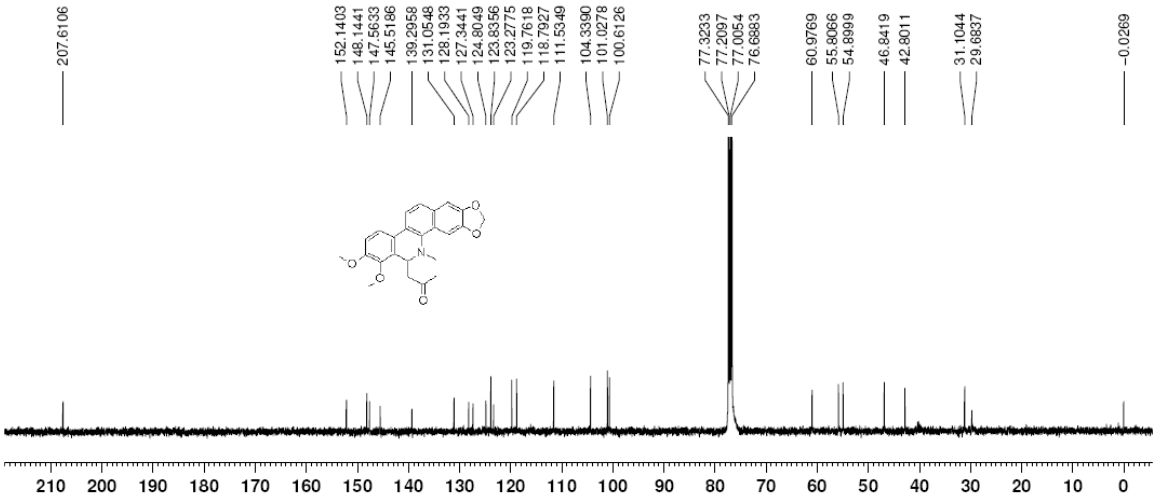

Figure S50. ^{13}C NMR spectrum of compound **3** ($CDCl_3$, 100 MHz).

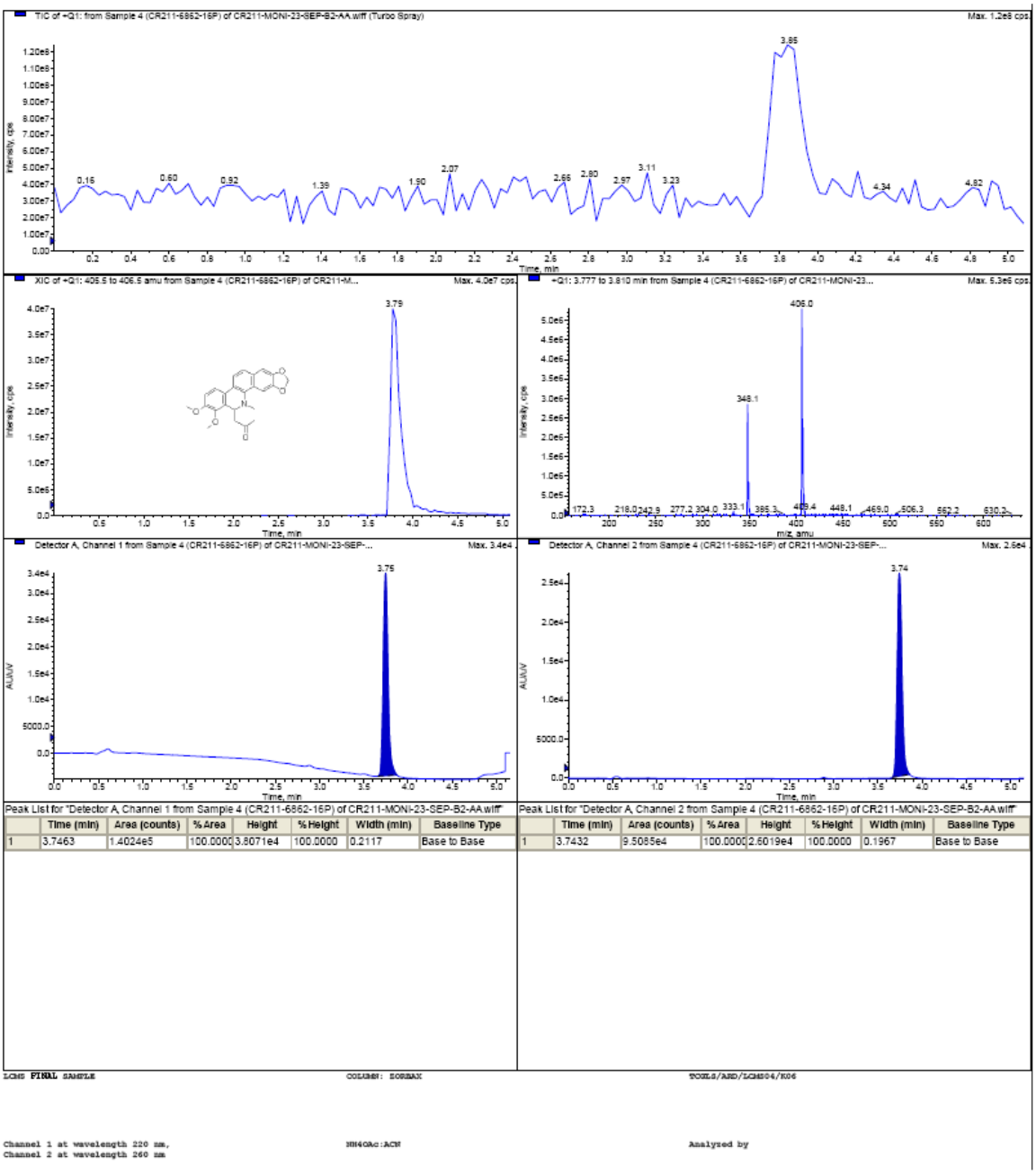

Figure S51. LCMS spectrum of compound **3**

Method File Name	: POLAR50-AA.lcm	Sample Name	: CR211-6862-16P
Data File Name	: 24091313 F.lcd	Tray#	: 2
Acquired by	: Sushovan Ghatak	Vail #	: 64
Data Acquired	: 9/24/2013 1:42:22 PM	Inj Volume	: 2 uL
Data Processed	: 9/24/2013 2:43:34 PM	Column	: GEMINI NX C18 (50x4.6mm)3u
Ref.No	: SG/24.09.13/1181	Mobile phase-A	: ACN
		Mobile phase-C	: 10mM NH4OAC in water
		Diluent	: DMSO

<Chromatogram>

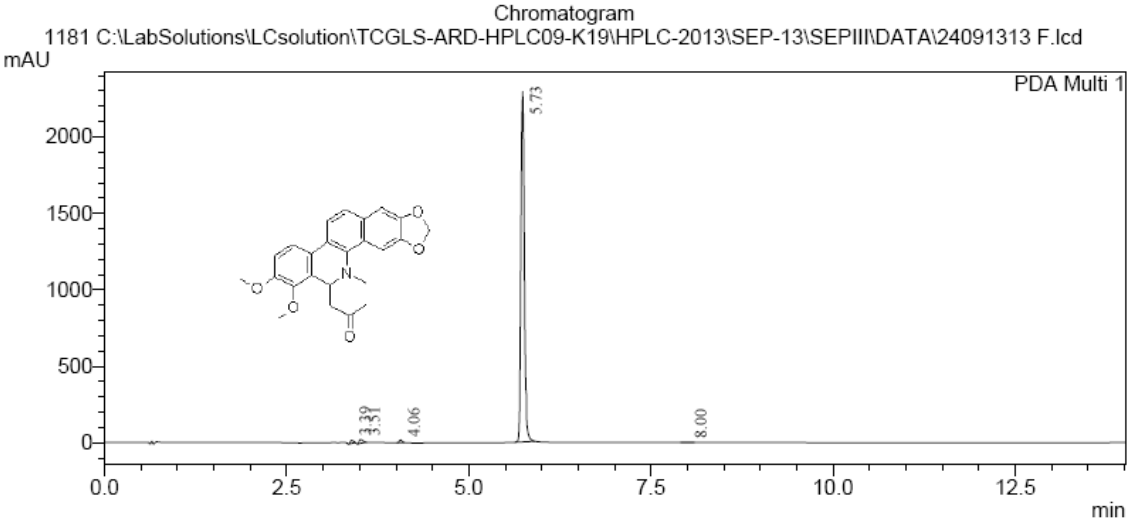

1 PDA Multi 1 / 283nm 4nm

PeakTable

PDA Ch1 283nm 4nm

Peak#	Ret. Time	Area	Area %
1	3.39	63313	0.81
2	3.51	93033	1.19
3	4.06	45756	0.59
4	5.73	7582686	97.30
5	8.00	8379	0.11
Total		7793167	100.00

Figure S52. HPLC purity of compound (±)-**3**.

```
Sample Name     : CR211-6453-88-1                          Seq Line->    8
                                                 Location   :     Vial 74
Acq Operator    : NARESH                         Inj. No.   :        1
  Injection Date: 6/21/2013                      Inj. Vol.  :     10 µl
Acq. Method     : C:\Chem32\1\DATA\JUNE-13\210613 2013-06-21 08-44-35\->
Analysis Method : C:\CHEM32\1\METHODS\A3.M
Last Changed    : Fri, 21. Jun. 2013, 08:34:13 am

Sample ID : CR211-6453-88-1

Column name : CHIRALCEL OJ-H (4.6x250mm) 5µ ,
ARD/K/7731 ,
Mobile Phase : MeOH/DEA : 100/0.1 ,
Flow rate : 1.0  ml/min ,
Slubility : MeOH .                                                    ->
                                                 Ref : KNS/21.06.13/927
```

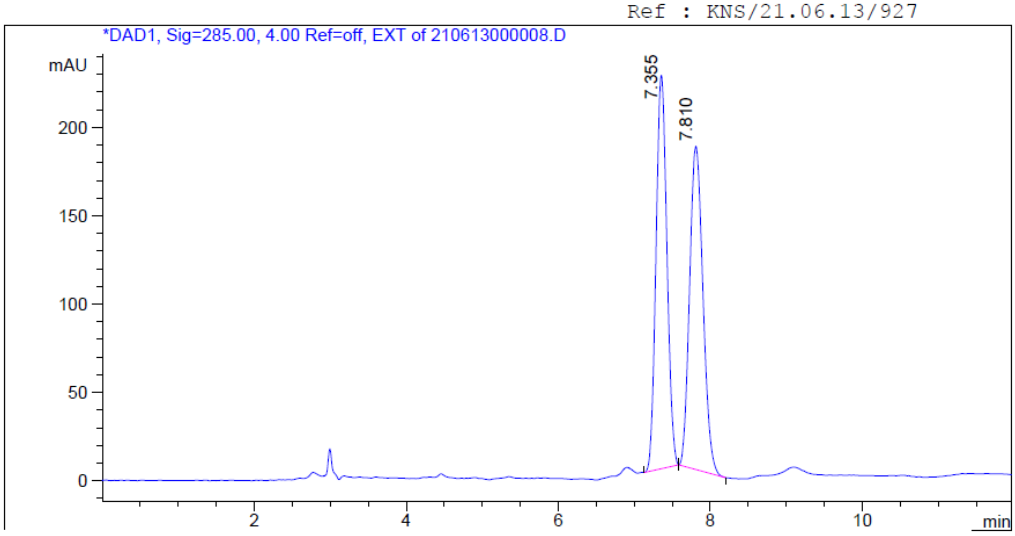


```
==========================================================================


Signal  1: DAD1, Sig=285.00, 4.00 Ref=off, EXT

|Peak|   RT     |   Area    |  Area %  |
| #  |  [min]   |-----------|----------|
|----|----------|           |          |
|   1|      7.36|   2217.59|     49.77|
|   2|      7.81|   2237.86|     50.23|
---------------------------------------
```

Figure S53. Chiral HPLC of compound (±)-**3**.

C:\LabSolutions\LCsolution\TCGLS-ARD-HPLC09-K19\HPLC-2013\OCT-13\OCT-I\DATA\08101318 F.lcd

Method File Name	: POLAR50-AA.lcm	Sample Name	: CR211-6862-16P-2-A-P
Data File Name	: 08101318 F.lcd	Tray#	: 1
Acquired by	: Sushovan Ghatak	Vail #	: 42
Data Acquired	: 10/8/2013 5:10:22 PM	Inj Volume	: 2 uL
Data Processed	: 10/9/2013 8:16:32 AM	Column	: ZORBAX SB-C18 (50x4.6mm)3u
Ref.No	: SG/09.10.13/307	Mobile phase-A	: ACN
		Mobile phase-C	: 10mM NH4OAC in water
		Diluent	: DMSO

<Chromatogram>

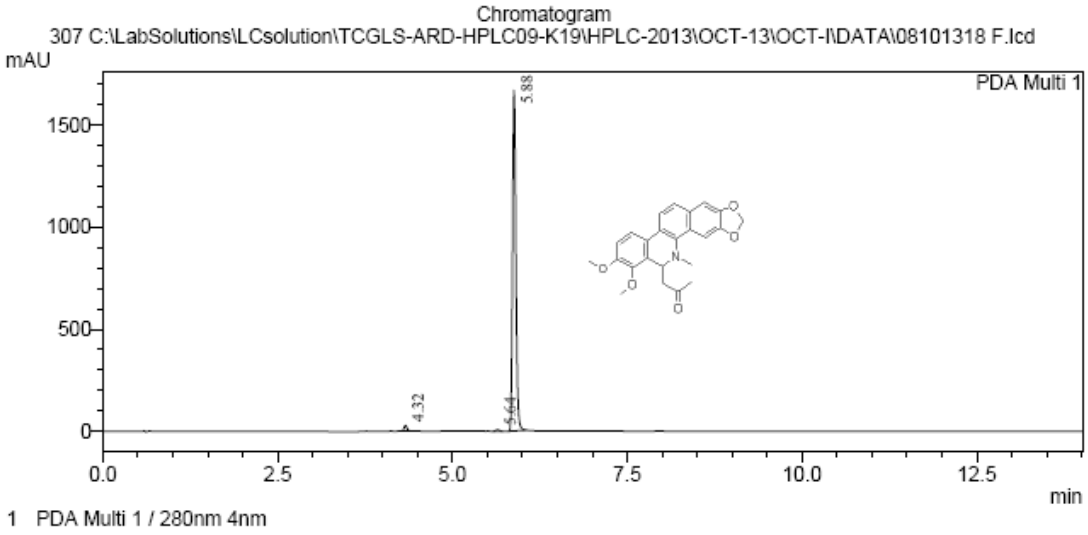

PeakTable

PDA Ch1 280nm 4nm

Peak#	Ret. Time	Area	Area %
1	4.32	78801	1.39
2	5.64	27892	0.49
3	5.88	5569124	98.12
Total		5675816	100.00

Figure S54. HPLC purity of compound (**+)-3**.

```
Column : CHIRALPAK AD-H (4.6x 250mm) 5µ ,
ARD/K/7760 ,
Mobile Phase : EtOH/DEA : 100/0.1,
Flow rate : 0.5 ml/min ,
Solubility : MeOH .

  Injection Date  :Wed, 9. Oct. 20136:00:30 PM    Location   :    Vial 74
                                                  Inj. No.   :         1
  Acq Operator    :NARESH                         Inj. Vol.  :      5 µl

  Last Changed    :Wed, 9. Oct. 2013,

  Acq. Method     :                      08:33:16 pm
                   C:\Chem32\1\DATA\OCT-13\091013 2013-10-09 08-30-23\B.M
```

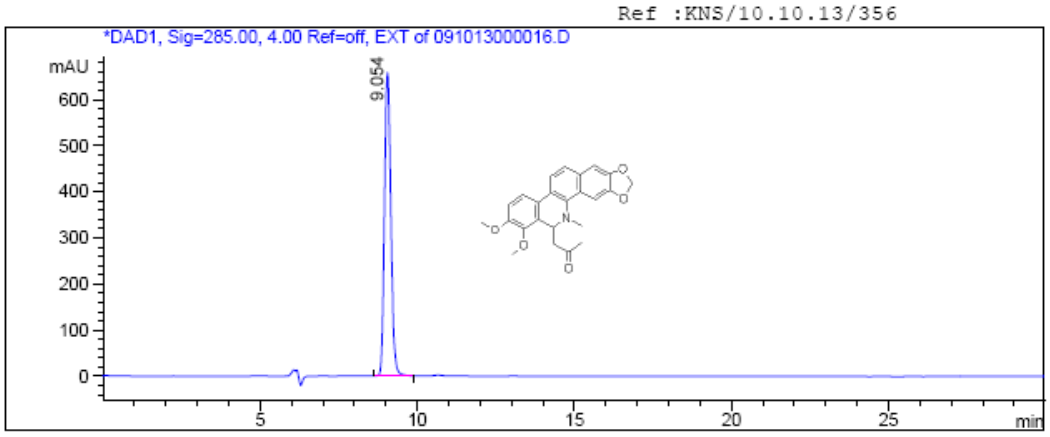


```
Signal  1: DAD1, Sig=285.00, 4.00 Ref=off, EXT

|Peak|   RT    |   Area    | Area % |
| #  |  [min]  |           |        |
|----|---------|-----------|--------|
|   1|     9.05|   9360.60|  100.00|
-------------------------------------
```

Figure S55. Chiral HPLC of compound (**+**)**-3.**

C:\LabSolutions\LCsolution\TCGLS-ARD-HPLC08-K18\HPLC-2013\OCT-13\OCT-II\DATA\16101312 F.lcd

Method File Name	: POLAR50-AA.lcm	Sample Name	: CR211-6862-16P-2-B-P
Data File Name	: 16101312 F.lcd	Tray#	: 1
Acquired by	: Sushovan Ghatak	Vail #	: 54
Data Acquired	: 10/16/2013 5:11:11 PM	Inj Volume	: 2 uL
Data Processed	: 10/17/2013 9:43:47 AM	Column	: GEMINI NX-C18(50x4.6mm)3u,
Ref.No	: SG/17.10.13/495	Mobile phase-A	: ACN
		Mobile phase-C	: 10mM NH4OAC in water
		Diluent	: MEOH

<Chromatogram>

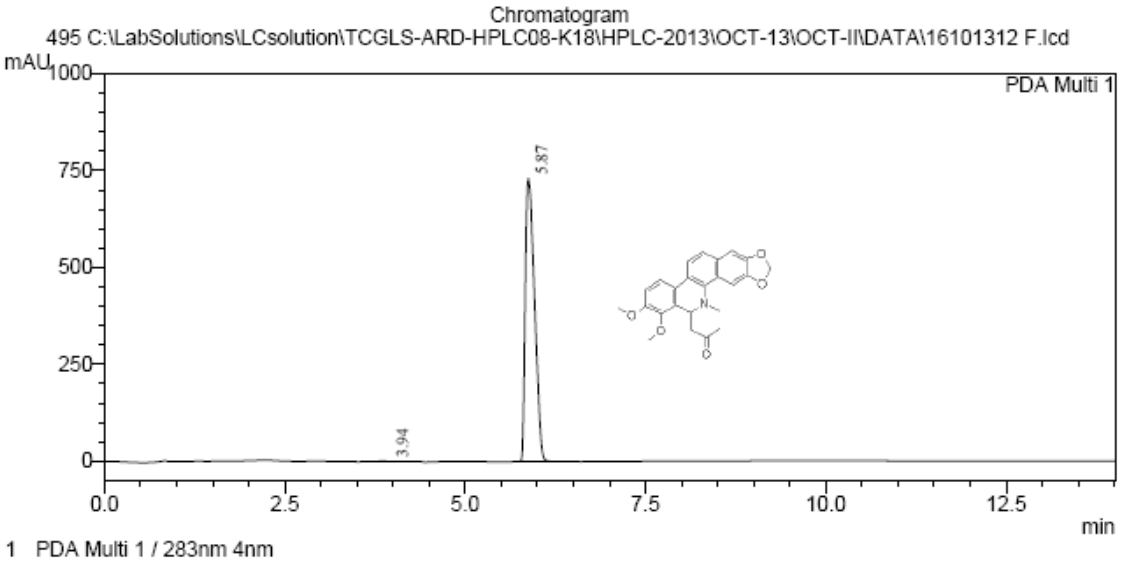

PeakTable

PDA Ch1 283nm 4nm

Peak#	Ret. Time	Area	Area %
1	3.94	6691	0.10
2	5.87	6538215	99.90
Total		6544906	100.00

Figure S56. HPLC purity of compound **(-)-3.**

```
Column : CHIRALPAK AD-H (4.6x 250mm) 5µ ,
ARD/K/7760 ,
Mobile Phase : ETOH/DEA : 100/0.1,
Flow rate : 0.5 ml/min ,
Solubility : MeOH .


  Injection Date  :Tue, 15. Oct.  ->3:15:54 PM    Location   :    Vial 91
                                                  Inj. No.   :         1
  Acq Operator    :NARESH                         Inj. Vol.  :       8 µl

  Last Changed    :Tue, 15. Oct. 2013,

  Acq. Method     :                       02:35:05 pm
                   C:\Chem32\1\DATA\OCT-13\151013 2013-10-15 14-39-44\C.M
```

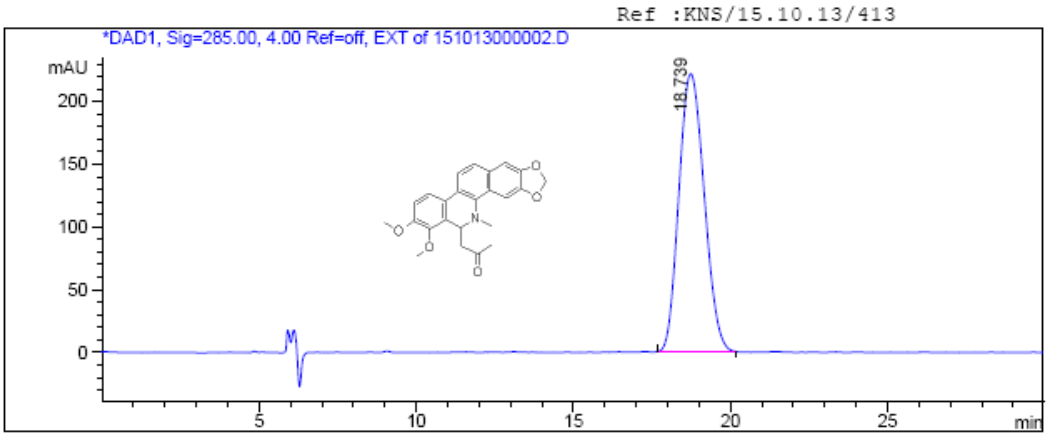


```
Signal  1: DAD1, Sig=285.00, 4.00 Ref=off, EXT

|Peak|   RT    |   Area    | Area % |
| #  |  [min]  |           |        |
|----|---------|-----------|--------|
|   1|    18.74|  12439.04|  100.00|
-----------------------------------
```

Figure S57. Chiral HPLC of compound **(-)-3**.